# ENGINEERING CONTRACTILE MYOCARDIAL TISSUE USING EXTRACELLULAR MATRIX SCAFFOLDS

by

Nathaniel Thomas Remlinger

Bachelor of Science in Bioengineering, Pennsylvania State University 2008

Submitted to the Graduate Faculty of the

Swanson School of Engineering in partial fulfillment

of the requirements for the degree of

Doctor of Philosophy

University of Pittsburgh

2013

UNIVERSITY OF PITTSBURGH

SWANSON SCHOOL OF ENGINEERING

This dissertation was presented

by

Nathaniel Thomas Remlinger

It was defended on

June 18, 2013

and approved by

Sanjeev Shroff, PhD, Professor and Associate Chair, Department of Bioengineering

Alejandro Soto-Gutierrez, MD, PhD, Assistant Professor, Department of Surgery and Pathology

Kimimasa Tobita, MD, PhD, Assistant Professor, Department of Developmental Biology and Bioengineering

William Wagner, PhD, Professor, Department of Surgery and Bioengineering, Director of the McGowan Institute for Regenerative Medicine

Committee Co-Chair: Peter Wearden, MD, PhD, Assistant Professor, Department of Cardiothoracic Surgery

Dissertation Director: Thomas Gilbert, PhD, Vice President of Research and Development, ACell, Inc., Adjunct Assistant Professor, Department of Bioengineering

ENGINEERING CONTRACTILE MYOCARDIAL TISSUE USING EXTRACELLULAR MATRIX SCAFFOLDS

Nathaniel Thomas Remlinger, PhD

University of Pittsburgh, 2013

There is currently an overwhelming need for functional replacement of diseased or damaged cardiac tissue. Biologic based scaffolds are an attractive tissue engineering approach to cardiac repair because they avoid sensitization associated with homograft materials and theoretically possess the potential for growth in similar patterns as surrounding native tissue. A strategy that has been investigated previously is the use of cardiomyocytes seeded onto collagen based scaffolds in order to engineer a contractile tissue. However, in order for this approach to be effective, the cardiomyocytes must be aligned and maintain contractility after seeding onto biologic scaffolds. UBM collagen fiber organization and cyclic mechanical stretch have each been shown to induce cell alignment while maintaining normal cell phenotype. In theory, a combination of these methods should yield a contractile tissue that may perform well when used to reconstruct myocardial tissue.

It was previously shown that a cardiac-derived ECM patch provides beneficial effects when compared to synthetic cardiac patch materials. Acellular UBM and C-ECM patches were directly compared in the present work as scaffolds to repair a full thickness defect in the RVOT of rats. By 16 weeks, only the UBM patches had degraded and were replaced with areas of new muscle tissue, which was in direct contrast to the integration response observed with C-ECM patches. Next, UBM scaffolds were seeded with cardiomyocytes and cyclically stretched *in vitro*. Cells preferentially aligned in the direction of stretch, showed intracellular free calcium transients, expressed contractile cardiac markers, and were visibly contractile. Cell-seeded UBM patches possessed the

ability to repair the RVOT of rats and support the infiltration of cells. Cardiomyocyte seeded patches were also able to develop an endothelial lining and integrate into the surrounding native tissue. In addition, stretched scaffolds appeared to show preliminary indications of communication with the surrounding native tissue. Future studies are necessary to investigate translation to a clinically applicable model, but the methods described herein show that contractile tissue can be generated from ECM scaffolds and may also aid in functional restoration to myocardial tissue when used as a cardiac patch material.

## TABLE OF CONTENTS

## LIST OF TABLES

## LIST OF FIGURES

## PREFACE

During my time at the University of Pittsburgh, I have had the opportunity to work with some extremely talented and wonderful colleagues. The knowledge that I have gained through my experiences in both the classroom and laboratories has been invaluable toward my personal and professional growth, and without the help and guidance from a number of people, this would not have been possible. I would first like to thank Dr. Thomas Gilbert for accepting me into his lab as his first graduate student and providing me with the guidance, advice, and drive necessary to succeed. I would also like to thank Dr. Peter Wearden for his advice and clinical perspective, as well as his help in maintaining the laboratory at Children's Hospital of Pittsburgh. I would also like to thank my committee members for the time that they have dedicated to meeting with me and advising on specific projects: Dr. Sanjeev Shroff, Dr. Alejandro Soto-Gutierrez, Dr. Kimimasa Tobita, and Dr. William Wagner. I would also like to thank Dr. Stephen Badylak for giving me my first opportunity in tissue engineering with his lab as a summer student.

I would like to thank everyone that has helped me with my studies in the Gilbert lab. Caitlin Czajka for helping with trachea experiments and helping to get the lab set up smoothly. Mark Juhas and Michael Kopecki for assisting with bioreactor design, manufacture, and testing. Brogan Guest and Michelle Weaver for helping out with all of my experiments, staining, animal studies, and data collection. Chris Hobson for helping me with experiments, helping with manuscript and proposal edits, and professional advice. Sarah Luffy for helping with cell culture and bioreactor testing. I would like to thank past and present members of the Badylak lab, Bioengineering department, and

the McGowan Institute for all of their help during my time at Pitt. John Wainwright for his help with experiments, guidance, and advice throughout my graduate career. Scott Johnson for help with ECM production, advice on chimera animals, assistance with mechanical testing, and his perpetual patience during my many visits for advice. John Freund for help with experiments and decellularization techniques. Jolene Valentin for guidance and advice while I was a summer student. Bryan Brown for his assistance with macrophage staining and professional advice. Sam LoPresti for help with macrophage immune staining. Chris Carruthers for his advice with cardiac ECM, cell culture, and analysis of cell alignment. Chris Medberry for help with classes and advice on projects. Neill Turner, Hongbin Jiang, Janet Reing, Li Zhang, Chris Dearth, and Matthew Wolf for advice and help with different projects. Jocelyn Runyon, Eve Simpson, Carole Stewart, Jason Vey, Lynette Spataro, Lisa Nickel, Dawn Roberts, and Marie Allie for all of their help and patience with my training grants, funding questions, scheduling, and advice with everything. Jennifer DeBarr and Deanna Rhoads for their patience and help with histology preparation. You have all made my time at the University of Pittsburgh easier and more enjoyable and I appreciate the time taken out of busy schedules to help me.

I would also like to thank all of the collaborators who helped me throughout my time and contributed to the work and data presented in this dissertation. Masahiro Yoshida and Ryotaro Hashizume for their time and help with performing the difficult RVOT surgeries throughout all of my studies. Sebastian Gilbert for his assistance in performing tracheal surgeries. Jason Tchao for help with calcium imaging and analysis. All of the people at the animal facilities around campus for their help with animal care and assistance with projects: Joe Hanke, Teri Horgan, Buffie Kerstetter, Shawn Bengston, Shayne Cooley, Kara Kracinovsky, and Lacey Mock.

I would also like to thank everyone who helped me outside of the laboratory. Mark Gartner for giving me the opportunity to be a teaching assistant for senior design, as well as for his time and continual career advice. To Andy Holmes, for helping with machining components for all of the bioreactors and other parts around the lab. To Rick Schaub, Don Severyn, and Doug Lohmann at the Artificial Heart Program, for accepting me to the program and providing me with valuable clinical experience and perspective. I would like to thank my funding sources from the NIH-NIBIB training grant number T32EB001026-06 and the CATER program, as well as grant number NIH-NHLBI T32-HL76124 entitled "Cardiovascular Bioengineering Training Program." In addition, I would like to thank the directors of CATER and CBTP, Dr. Satdarshan Monga and Dr. Sanjeev Shroff for accepting me to these training programs and their advice during my time at Pitt.

I would like to thank my family for their support over the past few years. To my wife, Lindsay Remlinger, for her love, support, and unwavering understanding during the long, inconsistent hours and many nights and weekends spent in the lab. To my parents, Donald and Janet Remlinger, for their love and understanding of my strange schedule, which often included abbreviated visits and holidays. And to my mother in law, Maryann Shook, for her love and support throughout my graduate career.

# 1.0 INTRODUCTION

There is currently an overwhelming need for functional replacement of diseased or damaged cardiac tissue. Congenital heart defects (CHDs) are the most prevalent birth defect, while heart disease remains the most common cause of death in the United States [1, 2]. Treatment options for patients suffering from heart disease replace injured or missing tissue with synthetic patches rather than restore native function. Biologic based extracellular matrix scaffolds are an alternative tissue engineering approach to cardiac tissue repair, and provide distinct advantages to the current clinical standards. ECM scaffolds are associated with constructive remodeling into site-appropriate tissue [3-5]. It was recently shown that functional, pulsatile muscle could be generated in esophageal tissue repair using an unseeded ECM scaffold derived from the bladder [6]. ECM scaffolds have served as suitable mechanical patches for cardiac repair, but scaffolds alone have shown limited cardiac tissue regeneration [7, 8].

Traditionally, tissue engineering has utilized a combination of biologic scaffolds and cells to direct the host response and generate functional site-appropriate tissue. Therefore, many studies have opted for pre-seeded scaffolds or investigated cell therapeutic options for repair of damaged or diseased tissue [9-12]. However, there has been limited success toward the development of a robust engineered tissue that possesses the ability to contract *in vitro*. Cardiomyocyte cell sheets and seeded ECM gels have both exhibited the ability to produce contraction, but do not provide the mechanical support necessary to reconstruct a full thickness defect in the myocardial wall [9, 13-16]. An ECM patch with seeded cells would therefore logically provide a solution to myocardial repair.

The alignment of a contractile cell line on ECM scaffolds through means of contact guidance and mechanical stretch would theoretically produce a robust engineered tissue with the ability to withstand the forces in a cardiac location and contract with the surrounding tissue.

## 1.1 HISTORY OF CARDIAC ANATOMY AND SURGERY

During the 2nd century, the Greek physician Galen postulated that the heart was responsible for delivery of blood and air to the body through separate arterial and venous circuits. It was initially believed that the heart did not pump blood, but rather sucked blood from the venous system during diastole and that blood moved by the pulsation of arteries. These ideas were widely believed until the mid-seventeenth century and were generally reaffirmed during the Renaissance revival of anatomy. Early illustrations and conceptualizations of the heart and vascular system were perpetuated by Leonardo da Vinci in the 15th and early 16th centuries, and it was not until English physician William Harvey published "On the Circulation of Blood" in 1628 that an alternative to Galen's theory became widely accepted. While Harvey supported the notion of the heart as the principal organ of the body, he believed that the heart was actively working to expel and fill with blood; thus creating the notion of systole and diastole. Understanding of cardiac function continued to develop throughout the following centuries, although surgical techniques to repair damages to the heart in living patients were widely unsuccessful.

The earliest successful heart surgery was performed on September 7, 1896 in Germany, when a stab wound to the right ventricle was repaired [17, 18]. In its early stages, invasive heart surgery was limited to patients in shock, as anesthesia methods were crude. Cardiac surgery was primarily utilized to repair critical traumatic injury throughout the early 20th century and even

through World War II. It wasn't until 1952 when the first successful intracardiac open heart surgery was performed on a congenital heart defect, that open heart surgery became common practice. Since the 1950s, surgeons have developed a number of methods to increase patient survival both intra- and post-operatively, such as hypothermia, ECMO, and cardiac bypass. In addition, an improved understanding of the developmental processes of the heart and the progression of heart diseases has aided in more appropriate care of patients requiring treatment.

## 1.2 CONGENITAL AND ACQUIRED HEART DISEASE

While the anatomical, functional, and corrective methods of the heart have been well documented, the mechanisms behind the development, progression, and resolution of cardiovascular disease remain a growing body of literature and are not yet fully understood. Many forms of congenital and acquired heart disease exist, and all are presented through varying symptoms. Approximately 84 million Americans are currently living with one or more forms of cardiovascular disease (CVD), accounting for nearly 33% of all deaths in the United States [2, 19]. In addition, approximately 20 in every 1,000 births are reported to express a form of congenital heart defect (CHD) that will require cardiologic care [1, 20].

### 1.2.1 Congenital Heart Defects

Congenital Heart Defects (CHDs) are the most common form of birth defect, accounting for greater than 29% of all birth defect related deaths in the United States annually [21]. It is estimated that over 1 million Americans are currently suffering from or were born with a form of CHD [19]. Additionally, over 5 in 1000 infants will require surgical cardiologic intervention within the first

year of life [20]. Many forms of CHDs exist, ranging from mild to severe, and each is associated with specialized care and operative procedures. Many congenital malformations are resolved spontaneously or with minimal surgical intervention. However, some CHDs require complex surgical procedures or multiple procedures to resolve abnormal heart function. The most common complex forms of intracardiac CHD include Tetralogy of Fallot (ToF), transposition of the great arteries (TGA), atrioventricular septal defects (AVSD), and Hypoplastic Left Heart Syndrome (HLHS) [1, 19, 22].

### 1.2.2 Cardiovascular Disease and Congestive Heart Failure

Cardiovascular disease (CVD) continues to be the leading cause of death in adults, accounting for more than 33% of all deaths in the United States annually [2]. CVD has accounted for more deaths than any other major cause of death in nearly every year since 1900, including more than 800,000 deaths in 2008 alone [2, 23]. According to the National Center for Health Statistics, if all forms of major CVD were eliminated, the national average life expectancy could rise up to 7 years. Acute cardiac events such as myocardial infarction (MI) and stroke are the most lethal results from the progression of CVD to congestive heart failure (CHF). Nearly 800,000 people will experience a new MI every year and an additional 470,000 will have a recurrent attack. The estimated hospital costs associated with treatment and care for patients suffering from CVDs in the United States alone are over $155 billion each year; more than any other diagnostic group, including cancer ($116 billion) [2]. The natural progression from CVDs to CHF is marked by a reduction in the efficiency of the myocardial tissue, eventually leading to cardiac dilation, hypertension, ischemia, or necrosis [24]. Following MI, in particular, the region of ischemic myocardium will evade the entire thickness, leaving behind necrotic or scar tissue [25]. A number of treatment options are available

for patients suffering from CHF including pharmacological management, mechanical assist devices, surgical correction, and heart transplantation. Nearly 6 million Americans are diagnosed with heart failure annually, and the growing number of patients requiring hospitalization is increasing the demand for alternative treatments.

## 1.3 CLINICAL TREATMENTS

Patients suffering from congenital defects, cardiovascular disease, or who have recently experienced an adverse cardiac event have a variety of treatment options depending on their age, history, current medications, and the urgency and severity of symptom presentation. Intervention and treatment of CHDs typically require surgical reconstruction or repair of malformed hearts and related defects. Many corrective procedures require surgical mesh, cryopreserved tissue, or cadaveric donor material to repair defects, but such products do not restore function. Reconstruction of adult myocardium with these materials is more difficult due to size restrictions, and often results in an area of the heart that is non-contractile, similar to the fibrotic tissue which develops after infarction. Therefore, a material capable of repairing myocardial defects while restoring function in a cardiac location is highly desirable. The restoration of function to an area of fibrotic or necrosed tissue would theoretically increase surgical success rates and reduce the risk for additional patient surgeries.

### 1.3.1 Congenital Heart Defect Treatment

Treatment for patients suffering from CHDs can range from simple monitoring of conditions to a series of complex surgical procedures. Many CHDs spontaneously resolve over time, but some CHDs are diagnosed *in utero* or upon birth and require immediate surgical intervention. Atrial and ventricular septal defects are the most common form of intracardiac CHD and are presented in nearly half of patients diagnosed, although many do not require surgery. The severity of each type of CHD is based on defect size or the degree to which the heart and related vessels are malformed, and each CHD is associated with a specialized operation. Patients exhibiting complications from initial corrective surgeries will normally require additional surgery to repair or replace the implanted material. The use of homograft materials for cardiac repair is also associated with an immune sensitization, eliminating a significant percentage of donor tissues and making future orthotopic transplantation of heart tissue difficult.

Tetralogy of Fallot (ToF) is observed in approximately 400 per million patients, and is an ultimately fatal disease if left untreated [26]. Recent advancements in corrective surgery have allowed for over 85% of patients diagnosed with ToF to survive into adulthood. Corrective surgery includes the implantation of a Blalock-Taussig shunt to reroute blood, which must be oversized to accommodate for patient growth, as well as a cardiac patch material, typically composed of Gore-Tex or homograft material. However, there are a number of complications that patients encounter as they grow and age. As patients progress into adulthood, many suffer from valve incompetence, RV outflow tract obstruction, or RV dilation, leading to heart valve replacement or, in severe cases, heart transplantation [22].

Transposition of the Great Arteries (TGA) is presented in patients when the morphological right side of the heart, typically connected to the pulmonary trunk, gives rise to the aorta, and vice

versa [27]. Incidence of TGA is estimated to be 1 per 3,500 to 5,000 live births, or approximately 6% of all CHDs, with approximately 50% of TGA patients expressing additional cardiac malformations such as ventricular septal defects (VSD) or outflow tract obstructions. Diagnosis of TGA can be confirmed *in utero* and surgical correction typically occurs immediately after birth. Preferred treatment of TGA is surgical correction of the malformation by arterial switch, and this procedure has been associated with a low mortality rate. However, even after surgical correction, patients diagnosed with TGA have severe complications resulting from surgery [22]. In many cases, patients will develop coronary arterial problems, often leading to myocardial infarction and the requirement for further surgical correction or cardiac assist devices.

Atrioventricular septal defects (AVSD) are a severe form of CHD arising from a deficiency in, or the lack of a septal wall to separate the cardiac chambers. However, AVSDs are typically presented alongside other cardiac malformations, making treatment more difficult. While not immediately fatal in some instances, surgical intervention is typically required upon the first indication of lung distress, critically low blood oxygen content, or heart failure. Ultimately, a cardiac patch material, typically composed of Gore-Tex or homograft must be implanted to close the intracardiac gap [26]. As stated previously, currently available patch materials are associated with multiple complications and many patients will require additional corrective surgery following initial correction of the heart.

Hypoplastic Left Heart Syndrome (HLHS) is considered to be among the most severe forms of congenital heart defects due to a high mortality rate and complex surgical correction of the disease. Over the past few decades, improvements and modifications to the three stage Norwood procedure have increased the long term outcomes for patients exhibiting HLHS. However, conversion of the diseased vascular system to a univentricular physiology is assolciated

with a mortality rate of approximately 30% through the first three stages of surgery; a rate that is among the highest for any pediatric cardiac surgery [28]. Survivors of the surgery are now entering their early 30s, and it has been observed that these patients are exhibiting severe or fatal heart, lung, and gastrointestinal problems. Therefore, even with successful completion of the Norwood procedure, patients can expect lifelong complications, eventually culminating in the requirement of orthotopic heart transplantation.

### 1.3.2 Congestive Heart Failure Management and Treatment

If diagnosed in the early stages of heart failure, patients can be advised to make lifestyle changes. However, if the disease has progressed to the point that intervention is necessary, administration of pharmacologic drugs, implantation of mechanical assist devices, and eventually surgical reconstruction or heart transplantation may be necessary. Each treatment course has significant advantages if successful, although many have drawbacks if relied upon for long term intervention.

Pharmacological intervention has distinct advantages if heart failure is diagnosed early. However, management of pharmaceuticals may be ineffective in prevention of disease progression if not prescribed quickly. Naturally, the prescribed treatment plan is highly dependent on patient demographics and the extent to which cardiac function is compromised. As a first line of defense, patients are frequently given Aspirin, Coumadin, Warfarin, or other anticoagulants to lower the risk of acute cardiac events such as myocardial infarction (MI) or stroke [29]. Additionally, ACE inhibitor therapy is recommended for almost all patients diagnosed with a mild to moderate form of heart failure [30, 31]. ACE inhibitors are able to slow or reverse the deterioration of cardiac function through the reduction of afterload, thereby reducing the amount of work the heart must perform.

Other pharmacological agents such as diuretics, β-blockers, and positive inotropic agents are also used, albeit less often than both anticoagulants and ACE inhibitors, and on a more specialized basis [32-34].

Beyond pharmacological intervention, mechanical devices such as pacemakers or ventricular assist devices (VADs) are able to provide assistance to the heart. Patients exhibiting a widened QRS complex of longer than 120ms, with a reduction in ejection fraction of less than 35% have been shown to benefit greatly from implantable cardioverter defibrillators and pacemaker devices, with a significant reduction in mortality at 1 and 3 months after implantation [35]. However, there is debate whether such devices are able to prolong life or if the devices simply contribute to an improvement in quality of life. Therefore, if conditions worsen for patients with heart failure, ventricular assist devices are the next therapeutic option to prolong life [36].

Many types of VAD devices exist, and are designed to assist the left ventricle (LVAD), right ventricle (RVAD), or both ventricles (BiVAD). VADs provide active support to weakened or failing ventricles, reducing the demand placed on the myocardium and allowing the heart to recover following heart failure. Originally, all VADs were designed for left ventricular assistance and were pulsatile in nature, with a synchronized timing mechanism to mimic the normal filling and ejection of blood from the heart. Early devices were very large and required continuous monitoring of patient conditions, impacting overall quality of life. In recent years, VADs have improved significantly in their design and survival outcomes, often providing continuous flow assistance to patients, lowering the risk of thrombogenesis within VAD components [36-39]. Improvements in VAD design have allowed for much smaller and more portable devices to be implanted, improving the quality of life for patients receiving devices and making pediatric ventricular assistance possible [40-43]. While the initial reports from pediatric devices are promising,

there are still a number of complications associated with VADs, including coagulation, infection, and device failure, which prevent extended long-term use [44-47]. Significant anticoagulation therapy is necessary following implantation in all cases due to the non-biologic nature of VADs. The risk of infection is also very high, despite aggressive antibiotic treatments and immunosuppressive therapy. Therefore, many VADs are used as a bridge-to-transplantation or destination therapy and are not a permanent solution to heart failure.

The final option for patients suffering from CHF who are unable to benefit from pharmocologics or mechanical assist devices is corrective surgery and orthotopic heart transplantation. Approximately 35% of patients are placed on a VAD as a bridge to heart transplantation [48]. However, the number of patients requiring heart transplantation far outnumbers the quantity of organs available for transplant. Approximately 4,000 heart transplants are performed annually worldwide, while nearly 57,000 patients die from heart failure [2]. Donor-recipient matching requires extensive immune typing, size and age matching, patient history analysis, and the minimization of donor tissue ischemic time prior to transplantation [49]. In addition, many of the complications associated with VAD implantation are more prevalent in heart transplantation, reducing the quality of life in patients receiving heart transplants and limiting the post-operative survival of patients to approximately 11 years [50]. Ventricular reconstruction is a growing alternative to transplantation due to the lack of available donor tissue. However, similar to the observations within pediatric patients, the currently used cryopreserved and synthetic grafts do not restore function to the damaged heart, and are often associated with a number of complications requiring additional surgeries. Therefore, a patch material or therapy that is capable of reconstructing myocardial tissue, while restoring function to weakened or damaged areas is highly desirable and would provide benefits to currently used materials.

## 1.4 INVESTIGATIONAL TREATMENTS

It is widely believed that tissue engineering and regenerative medicine strategies may be able to improve surgical outcomes for patients suffering from CHDs or CHF. Regenerative medicine takes a multidisciplinary approach to the generation of new therapies through the combination of cellular therapies, tissue engineering and biomaterials, as well as medical devices and artificial organs. The ultimate goal of tissue engineering is to develop clinically translatable devices to improve surgical outcomes and patient quality of life. Tissue engineering is a rapidly developing field of research and many groups have shown success in preclinical studies using a wide array of techniques. The prevalence and severity of heart disease and cardiac defects has led to a large division of the tissue engineering community dedicated to developing strategies for cardiac related injuries. However, the wide array of cardiac injuries and procedures have resulted in an enormous variety of theories and approaches regarding the repair and regeneration of diseased or damaged cardiac tissue.

### 1.4.1 *In Vitro* Techniques and Cell Therapy

Many groups have tried to identify key design characteristics for functional cardiac tissue engineering through *in vitro* studies. While the results are not directly translatable to *in vivo* performance, these studies are able to isolate variables and determine individual effects in order to optimize an implantable material. The maintenance of cell contraction within isolated heart tissue in culture has been a topic of interest for decades [51-53]. Until recently, research conducted on beating cardiac tissue has been limited to 2-dimensional culture, which has further limited the

applicability in an *in vivo* environment and the ability to control culture conditions. Even with successful experiments that are able to maintain normal contractile function, a significant drawback of 2D culture is the detachment of tissue from culture plates. Recently, Shimizu et al. have developed a technique to coat culture plates with a temperature responsive polymer, poly-n isopropylacrylamide (PIPAAm) [13]. At physiologic temperatures, the polymer is hydrophobic, allowing cells to attach, proliferate, generate cell-cell connections, and secrete ECM products. When the temperature is lowered to approximately 20°C, the polymer becomes hydrophilic, and the cells are displaced from the surface in a single cell sheet due to the maintenance of intercellular junctions and the newly formed ECM network. However, it was observed that after release from the surface, cardiac cells stopped beating and quickly retracted to a small sheet. These techniques have been improved upon in recent years and have been expanded to include multiple cell types and tissues, but the first experiments stressed the importance of mechanical loading and cell alignment on the generation of engineered cardiac tissue [11, 12, 54-56].

Since the beginning of three dimensional cell culture techniques, significant improvements toward *in vitro* cardiac tissue engineering have been made. Many experiments have stressed the requirement of mechanical loading and cell alignment individually, with varying means of investigating each variable. In 2005, Eschenhagen and Zimmermann discussed the state of cardiac tissue engineering with a particular emphasis on the importance of substrate alignment and mechanical strain on cell health and alignment [57]. In recent years, these ideas have gained traction in experimental design, although the first true experiment to examine both of these effects together on a contractile cell line was performed in the late 1980s, when Vanenburgh et al. were able to generate contractile aligned skeletal myotubes. The cells were coated with a layer of type I collagen to impose a load on the cells, improving the differentiation state of the myotubes [58]. Motorized and

computer controlled devices were then designed to impose cycles of stretch and relaxation on cardiac myocytes and skeletal myotubes. The results had a favorable effect on cell orientation and myotubes were able to perform work, resulting in what some consider to be the first engineered 3D skeletal muscle [58-60]. As stated previously, an established method of aligning cells is through the use of substrate alignment and contact guidance. Multiple substrates have proven to be effective when used in culture with cardiac cells including type I collagen, polyurethane film, small intestinal submucosa (SIS), and urinary bladder matrix (UBM) [61-64]. While many studies have been able to define preferred characteristics of engineered myocardial tissue with moderate success, these studies have been largely limited to *in vitro* investigation.

Numerous studies have sought to isolate and use skeletal myoblasts, bone marrow-derived cells, and cardiac progenitor cells for direct injection *in vivo* to treat a number of cardiac conditions, including heart failure [65]. There are currently a number of preclinical and clinical trials in progress in order to investigate cardiac cell therapies, although the cell preparation and delivery techniques of these trials vary greatly [66-70]. However, the exact benefits of cardiac cell therapy have been debated and the mechanisms behind cardiac improvement and cell interactions following injection are still unclear. Injection-based cardiac cell therapies have had variable results, with cited limitations of low cell retention at the injection site, poor cell survival, and poor cell incorporation with the surrounding native tissue [71]. While cell therapy studies are the first "tissue engineering" approaches to appear in a clinical setting to treat cardiac injury, significant drawbacks still persist. The most prevalent complications currently include patient immune typing, cell isolation, culture, and injection, variations in the type, number, and site of injection for cells, and, ultimately, the heterogeneity between different treatments and studies [72].

### 1.4.2 Implantable Scaffolds for Myocardial Repair

It is believed that cell function and retention can be improved through an improvement in the means of cell delivery and the development of a robust, implantable material for implantation. Preliminary studies have since focused on the development of a material capable of repairing a significant defect in the myocardium. Tissue engineering studies have further attempted to encourage remodeling or regeneration of functional tissue through directing the chemical or structural composition of fabricated scaffolds. In addition, naturally derived extracellular matrix (ECM) scaffolds have gained significant attention recently due to their inherent biocompatibility and ability to degrade and remodel towards site-appropriate tissue in a variety of organ systems.

### 1.4.3 Synthetic Scaffolds

Artificial and synthetic scaffolds have been in clinical practice for years due to low biocompatibility issues and the ability to control the microstructural environment of the materials. Widely used materials such as Dacron™ and Teflon™ (PTFE) have been used for decades for vascular reconstruction in both pediatric and adult patients. However, common complications such as stenosis, aneurysm, and thrombosis exist with such devices [73-79]. Significant advancements in the fabrication of synthetic scaffolds have recently improved surgical outcomes. In particular, electrospun, degradable scaffolds such as polyglycolic acid (PGA) and polylactic acid (PLA) have been used in cardiac and vascular reconstruction with improved outcomes [80-82]. Polymer-based scaffolds have allowed for an increased control of the chemical, structural, and degradation properties, making it easier to tailor a material for individual surgeries. Groups have also shown the ability to design scaffolds to release drugs and growth factors upon degradation [83, 84]. However, recent evidence has suggested that PGA and PLA scaffolds are not appropriate for vascular and

cardiac reconstruction due to their stiffness, and that these materials may be more appropriate for bone and cartilage tissue engineering [85-87]. A softer degradable polymer scaffold such as polyester urethane urea (PEUU) has shown promising results in preliminary studies when repairing a defect in the right ventricle outflow tract [88-90]. PEUU scaffolds have shown the ability to repair a cardiac defect, rapidly degrade, and aid in the formation of fibrous tissue. In 2009, Fujimoto et al. were able to synthesize an injectable copolymer blend for delivery directly to an area of infracted myocardium [91]. No evidence of cytotoxicity or ventricular dilation was observed with small improvements in local contractility. Ultimately, the implantation of many polymer based scaffolds in a cardiac location has resulted in the formation of fibrotic tissue. Results have shown that currently available artificial scaffolds are unable to mimic the chemical and mechanical environment of biologic tissues in the same capacity as biologic based scaffolds.

### 1.4.4 Cryopreserved Tissues and Scaffolds

Cryopreserved homograft tissue is commonly used in pediatric and adult patients to augment and reconstruct vascular structures. Cryopreservation of human tissue is a common clinical practice in order to make surgical material more readily available to surgeons, eliminating the need to harvest and use tissue within a short timeframe. However, the preservation process alters the fiber structure of the materials, thereby changing the host cellular response. Following implantation, homograft tissue expresses a number of failure modes, including rejection, stenosis, aneurysm, or excessive calcification [92-96]. Patients suffering from such conditions may require additional surgical intervention or complete removal of the homograft. In pediatric patients, the use of cryopreserved material is not an ideal solution due to concerns of the surrounding tissue growing disproportionately. The inability of the implanted tissue to grow with the patient requires surgeons

to implant a patch that is oversized in order to accommodate blood flow as the patient grows. Upon implantation, patients will also express an elevated immune response involving HLA antibodies, despite extensive immunotyping and aggressive immunosuppresion [97-99]. Pediatric patients receiving homograft material will nearly always have heart problems later in life, often requiring whole orthotopic heart transplantation. HLA sensitization observed from implanting homograft material eliminates a large majority of potential donor hearts, and options are primarily limited to VAD devices.

Decellularization of cryopreserved tissues has been met with limited success in a clinical setting [100-103]. Decellularization techniques typically eliminate HLA antigens responsible for immune rejection, eliminating a patient's need for immune suppressive drug therapy and maintaining the availability of tissues for future transplantation. The risk of calcification and other failure modes is also significantly lowered due to the complete removal of cellular materials. Further, an underlying extracellular matrix with a fiber structure similar to native tissue can be preserved through the decellularization of homografts. It has been shown that implantation of decellularized homografts have the ability to support small numbers of repopulating host cells, as well as minor tissue remodeling in a cardiac location. However, the limited availability and variety within the tissue source of homograft material is preventative to the development and production of a widely used clinical material.

### 1.4.5 Extracellular Matrix Scaffolds

Biologic based extracellular matrix (ECM) scaffolds are an attractive tissue engineering approach to cardiac repair because they avoid sensitization associated with homograft materials, are inherently biocompatible and bioactive, and theoretically possess the potential for growth in

similar patterns as surrounding native tissue. Naturally occurring extracellular matrix (ECM) scaffolds have been able to successfully repair or replace tissue in a variety of body systems, including cardiovascular tissues, arteries, veins, and myocardium [104-113]. Additionally, ECM scaffolds completely and rapidly degrade upon implantation while being replaced by site appropriate tissue as opposed to scar tissue, an essential characteristic in cardiac tissue engineering [114-116]. The degradation process of ECM scaffolds yields a number of biologic responses within the host that are critical to the regenerative and wound healing processes as well. ECM scaffolds and their degradation products have also been shown to possess natural antibacterial properties [104, 117-121]. Perhaps more importantly, ECM degradation products also change the cell population that participate in wound healing through the recruitment of bone marrow derived cells to the site of ECM remodeling [122-124]. The inherent biochemical and mechanical properties of ECM scaffolds therefore provide numerous potential benefits for both pediatric and adult myocardial reconstructive applications.

Over the past decade, numerous ECM scaffolds have been investigated in a preclinical setting, however the most widely clinically used products are currently derived from porcine small intestinal submucosa (SIS) and urinary bladder (UBM), bovine pericardium, and human dermis [125]. Each scaffold has shown the ability to successfully repair tissue, although studies have tended to prefer SIS and UBM scaffolds due to the availability of tissue and a simpler decellularization protocol. Minimally processed ECM scaffolds can promote one of three distinct host remodeling responses, specifically encapsulation, integration, or remodeling [4]. The encapsulation and integration groups tend to include dermal products that are denser and require more aggressive decellularization protocols. The remodeling group includes SIS and UBM, which undergo a much simpler decellularization process and are derived from organs that experience more rapid turnover.

In addition to the commercially available products, recent efforts have sought to develop site specific scaffolds, including cardiac ECM (C-ECM), which are hypothesized to be preferred scaffold sources since the ECM was deposited by organ specific cells and the morphology matches that of the repair site. However, the process to produce these scaffolds tends to be more similar to the processes used for commercial scaffolds that promote encapsulation or integration responses rather than a constructive remodeling response.

#### 1.4.5.1 Organ Specific Scaffolds

Perfusion-based whole organ decellularization has gained interest in the field of tissue engineering as a means to create organ-specific extracellular matrix scaffolds while largely preserving the native architecture of the scaffold. To date, this approach has been utilized in a variety of organ systems, including the heart, lung, and liver [126-130]. Previous decellularization methods for tissues without an easily accessible vascular network have relied upon prolonged exposure of tissue to solutions of detergents, acids, or enzymatic treatments as a means to remove the cellular and nuclear components from the surrounding extracellular environment [131-133]. However, the effectiveness of these methods hinged upon the ability of the solutions to permeate the tissue via diffusion. In contrast, perfusion of organs through the vascular system effectively reduced the diffusion distance and facilitated transport of decellularization agents into the tissue and cellular components out of the tissue.

Organ specific scaffolds generated through perfusion based decellularization methods have recently shown promise in a variety of tissue engineering applications [134-145], including the heart [146, 147]. Thus, an extracellular matrix scaffold derived from cardiac tissue may be an ideal material

for myocardial reconstruction applications. The inherent architecture of the cardiac tissue may present advantages over an ECM scaffold derived from another organ or an artificial biomaterial. A site-specific scaffold may support host cell infiltration and promote a constructive remodeling response, as opposed to scar tissue formation. To date, cardiac ECM patches have been investigated *in vivo* to reconstruct a defect created in the myocardial wall [148]. C-ECM, UBM, and SIS scaffolds have each been investigated individually as potential materials for myocardial repair, but all have shown limited success [107, 110, 111, 149-151]. In addition, a direct comparison of ECM scaffolds has not been performed in a cardiac location.

#### 1.4.5.2 Cell and Scaffold Engineering

Thus far, the choice of implanted material alone has been ineffective at repairing and replacing myocardium with functional tissue, although ECM scaffolds have provided the most promising results in preclinical studies to date. While scaffold choice is paramount to success *in vivo*, the well-documented requirements of generating contractile tissue *in vitro*, such as mechanical conditioning and cell alignment cannot be ignored. It is believed that cell function and retention can be increased through an improvement in the means of cell delivery. As such, studies have investigated the addition of a cellular component to various ECM scaffolds prior to implantation in studies in an effort to elicit a favorable *in vivo* response [10, 152-154]. The utilization of cell alignment techniques and mechanical conditioning are two guidelines prevalent in studies developing a cell-seeded scaffold for implantation.

The beneficial effects of mechanical conditioning on ECM composition, fiber and cell alignment, and cell behavior have been well documented [63, 64, 155-157]. Cyclic stretch has been shown

to align the collagen fibers of UBM and SIS scaffolds in the direction of stretch *in vitro*. In addition, the introduction of cyclic strain to cells attached to ECM scaffolds has had significant effects on gene expression and cell alignment [157]. The addition of cyclic mechanical strain to cardiac cells seeded onto ECM scaffolds would therefore theoretically maintain a contractile cell phenotype and align cells in the direction of stretch.

Substrate alignment and contact guidance are also well-established and widely accepted means of aligning cells in culture. Turner et al. recently showed the ability to maintain cardiomyocyte phenotype on hyaluronan acid (HA) gel-coated UBM scaffolds [153]. Microchannels were created on the surface of UBM scaffolds to aid in the maintenance of cell-cell contacts and align cells in an effort to generate a contractile, implantable material. Groups have also attempted various fabrication techniques to mimic an aligned ECM fiber network with seeded endothelial and smooth muscle cells [153, 158, 159]. Alignment of the topographic collagen fiber network of naturally occurring ECM scaffolds prior to seeding cells may provide additional assistance in generating an aligned network of contractile cells.

Extensive research has been conducted to investigate contractile tissue development *in vitro*. Previous studies have shown the ability to develop contractile constructs from cells embedded within ECM gels [9, 14, 15, 160]. However, an engineered contractile tissue constructed from contractile cells and a robust, biologic scaffold capable of repairing a critical myocardial defect has remained elusive. *Therefore, the goal of the present study is to generate an implantable, contractile tissue from extraceulluar matrix (ECM) scaffolds.* This goal will be accomplished through the successful completion of three specific aims.

## 1.5 APPROACH AND RESEARCH AIMS

**SPECIFIC AIM 1:** To determine whether an organ-specific extracellular matrix scaffold (C-ECM) or a heterotopically derived scaffold (UBM) better contributes to the formation of new host cardiac tissue.

**Subaim 1:** Determine whether bone marrow derived cells play a role in the long-term remodeling response of either ECM scaffold.

**Rationale:** The differences in host response to two ECM scaffolds, C-ECM and UBM, will be compared in vivo. To date, each scaffold has been investigated individually and in various surgical models. The generation of a GFP(+) chimera rat population will allow for a detailed investigation of the host cellular response and origins of repopulating cells. A well-established surgical model also allows for a direct comparison of the ability for each material to repair a full thickness myocardial defect.

**Hypothesis:** The UBM repair group will contain the largest cellular infiltration into the patched area, as well as express a more complete endothelialization. Remodeling of the C-ECM patch will be slow, with limited cell infiltration and matrix turnover; however, the UBM patch will show faster penetration of bone marrow derived cells to the area as well as the ability to support cardiac cells and contract with the surrounding tissue, as evidenced through MRI examination.

**SPECIFIC AIM 2:** Determine the role of contact guidance and mechanical stretch in the development of contractile tissue with cardiomyocytes seeded onto an ECM scaffold.

**Rationale:** The scaffold for investigation will be selected based upon results obtained after completion of Aim 1. Substrate alignment, contact guidance, and mechanical stretch have all been

well documented means of aligning cells and promoting cell health. A combination of these techniques would therefore be a logical approach toward generating a contractile tissue from cells and ECM scaffolds. The development of a bioreactor will allow for culture and mechanical conditioning of constructs, and contractility will be verified through the measurement of calcium transients, measurement of force generation, and immunofluorescent examinationof contractile markers.

**Hypothesis:** Cardiomyocytes will retain a contractile phenotype and align on uniaxially scraped UBM scaffolds and subjected to cyclic stretch. By utilizing a combination of these techniques, an actively contractile tissue with highly aligned cells in one direction will be generated.

**SPECIFIC AIM 3: Evaluate the efficacy of an engineered cardiac tissue construct for myocardial reconstruction.**

**Rationale:** Survival of implanted cells and maintenance of appropriate phenotype are significant hurdles in cardiac tissue engineering. Various means of cell delivery have been previously investigated, but none have shown the ability to repair a full thickness defect in a cardiac location. A healthy, robust, and contractile engineered tissue may be a viable option to deliver contractile cells to the heart and repair a full thickness defect.

**Hypothesis:** Cardiomyocytes cultured on ECM sheets will spontaneously contract and will lead to improved regeneration of the RVOT in rats with a more uniformly distributed cell population within the remodeled area, as well as increased expression of contractile markers. The presence of aligned cells within the engineered tissue patch will also enhance the functional restoration of cardiac tissue beyond the scaffold alone.

# 2.0 URINARY BLADDER MATRIX PROMOTES SITE APPROPRIATE TISSUE FORMATION FOLLOWING RIGHT VENTRICLE OUTFLOW TRACT REPAIR

## 2.1 INTRODUCTION

In recent years, there has been an increasing demand for functional replacement of diseased or damaged cardiac tissue. Congenital Heart Defects (CHDs) are the most common form of birth defect, accounting for greater than 29% of all birth defect related deaths in the United States annually [21]. It is estimated that over 1 million Americans are currently suffering from or were born with a form of CHD [19]. Additionally, over 5 in 1000 infants will require surgical cardiologic intervention within the first year of life [20]. Many congenital malformations are resolved spontaneously or with minimal surgical intervention. However, some CHDs require complex surgical procedures and the implantation of reconstructive materials to resolve abnormal heart function. There are currently a number of commercially available products that have the ability to patch defects without offering the capability of restoring function to the damaged myocardium [7, 8] Traditionally used cardiac patch materials include cryopreserved homograft tissue, bovine pericardium, and synthetic materials- all of which are commonly associated with multiple failure modes, including rejection, stenosis, aneurysm, thrombosis, and calcificiation [92-95]. An “off the shelf” material capable of repairing damaged myocardial tissue and restoring native function would therefore be ideal in a clinical setting and would provide benefits to currently used materials.

Naturally derived extracellular matrix (ECM) scaffolds have been shown to serve as adequate patch materials in a variety of body systems in both preclinical and clinical trials [161-165]. ECM scaffolds have gained significant attention recently due to their inherent biocompatibility and ability to degrade and remodel towards site-appropriate tissue in a variety of organ systems. Among the most widely investigated ECM patch materials for myocardial repair include small intestinal submucosa (SIS), urinary bladder matrix (UBM), decellularized pulmonary artery, and cardiac-derived ECM products. Currently, CorMatrix SIS is one of the only clinically available products for myocardial repair, having been successfully used in dozens of pediatric patients to correct a variety of CHD malformations [166]. The material has been able to repair both cardiac and vascular related defects with no evidence of calcification at 2 years after implantation. Urinary bladder matrix (UBM) scaffolds have not yet become available in a clinical setting, but have been investigated as a cardiac patch material in several preclinical applications [107, 111, 149, 150, 167]. UBM scaffolds have shown the ability to rapidly and completely degrade in a cardiac environment. Preliminary studies have also shown the ability of UBM scaffolds to support the deposition of small areas of cardiac specific cells as well as minor indications of mechanical support and electrical communication with surrounding native cardiac tissue.

In recent efforts to preserve and mimic the natural biochemical and mechanical environment of organs requiring repair, organ-specific scaffolds have recently shown promise in a variety of tissue engineering applications [135-145], including the heart [146, 147, 168]. Repair of many CHDs requires the reconstruction or augmentation of malformed or underdeveloped vessels. Decellularization of the aorta and pulmonary artery is thought to provide the most appropriate material to facilitate host tissue integration and growth with pediatric patients. However, this approach has been met with limited success in preclinical and clinical studies with primary failure

modes of calcification and occlusion [169] [170, 171]. In the case of myocardial tissue repair, an organ-specific cardiac ECM is thought to provide the most appropriate platform for a cardiac patch material. Singelyn et al. have recently developed an injectable form of C-ECM with the ability to support cardiac specific cells within the matrix after injection [168, 172]. The matrix is able to self-assemble and support neovascularization in highly localized areas within the myocardial tissue. However, a significant drawback of this approach is the inability to repair a full-thickness defect in the myocardium. It has recently been shown that an intact porcine heart can be fully decellularized to generate C-ECM patches [173, 174]. C-ECM patches generated in this manner have shown the ability to support cardiac function as well as the infiltration of small areas of cardiac specific cells [146].

Urinary bladder matrix (UBM) and cardiac ECM (C-ECM) have each been investigated individually as scaffolds for myocardial repair, but have shown limited success [107, 110, 111, 149, 150]. To date, a direct comparison of the scaffolds has not been performed in a cardiac location, due to variations in the animal and surgical models used to investigate each scaffold. However, recent studies have developed an effective surgical model to evaluate materials for repair of full-thickness defects in rat hearts [89, 146]. Previous studies have been able to evaluate functional and histological outcomes within repaired hearts, but did not investigate the origin of repopulating cells at the site of repair. In the present study, UBM and C-ECM patches were directly compared for repair of a full thickness defect created in the right ventricle outflow tract (RVOT) of rats. As a secondary objective, the role that bone marrow derived cells play in the remodeling of an ECM scaffold in a cardiac location will be investigated through the use of a chimera rat model in which the bone marrow cells express green-fluorescent protein (GFP).

## 2.2 MATERIALS AND METHODS

### 2.2.1 Study Design

Animals with confirmed chimerism (GFP+ bone marrow) were anesthetized and intubated for right ventricle outflow tract reconstruction surgery as previously described [89, 146]. A small (2-5 mm) defect was created in the RVOT of chimera rats and subsequently patched with one of the test materials (C-ECM, UBM, n=5 for each material at each time point). The animals were monitored for 4, 8 and 16 weeks. MRI examination of the reconstructed area took place at 4, 8, and 16 weeks in all available animals for functional analysis. At the predetermined time points, animals were euthanized by injection of 1M KCl directly into the heart. The hearts were then removed and prepared for frozen histologic processing for staining with cardiac, endothelial, and macrophage specific cell markers.

### 2.2.2 Bone Marrow Transplantation

Female Sprague Dawley rats were placed in a small box for whole body irradiation. An X-Ray Irradiator (XRad 320, Rangos Research Facility, Pittsburgh, PA) was set to maximum amperage (12.5 amp) and voltage (320 kV) and recipient animals were lethally irradiated (10Gy at 1Gy/min). Following irradiation, animals were transferred to an immune compromised animal room for the remainder of the study. A GFP + transgenic Sprague Dawley male donor rat was then euthanized, and the tibias and femurs from both legs were removed and placed in DMEM/F12 media containing 10% FBS, 1% PS, and 10,000 units of Heparin. Bone marrow was isolated by flushing the bones with media using a 23 gauge needle. Marrow and media isolate was centrifuged at 1500rpm for 7 minutes and resuspended in 10mL of RBC lysis buffer for 10 minutes. The cell

suspension was centrifuged again and resuspended in media, filtered through a 70μm cell strainer, and a cell count was performed. A cell population of greater than 6 $x10^7$ was confirmed and cells were then resuspended in 1mL of media. The cell suspension was divided into two 1mL syringes and placed on ice until ready for injection.

Irradiated rats were then rescued by injection of a minimum of 6 $x10^7$ bone marrow cells after primary isolation. Animals were anesthetized and maintained at 2-3% Isoflurane at 1L/min of $O_2$ and a 25 gauge needle was inserted into the tail vein. Each rat received 0.5mL of bone marrow cell suspension directly into the tail vein, and 0.2g of Cefazolin was injected intramuscularly into the hind leg. Antibiotics were injected every other day for the ten days after bone marrow transfer, alternating injection sites between hind legs. At 30-60 days post-irradiation, a small sample of blood was taken from the tail vein and a blood smear was performed on a slide and less than 0.5mL of blood was mixed with culture medium. The slide was observed under fluorescence for presence of GFP(+) cells, and the tube containing blood was centrifuged at 1500rpm for 7 minutes. The supernatant was aspirated and the cells were resuspended in RBC lysis buffer for ten minutes. The cells were centrifuged a second time and resuspended in a small volume of media for flow cytometry analysis. Cell suspensions were analyzed for both GFP presence and front and side scatter plots to identify GFP(+) WBC percentages. Chimera creation was verified by a GFP(+) WBC percentage above 93%.

### 2.2.3 Preparation of ECM Patches

Whole pig hearts were obtained and subjected to a previously described method for decellularization [173, 175]. Following decellularization, the ventricular walls were separated and a

small portion of the right ventricle near the apex was removed. This portion of the ventricle is much thinner than the surrounding myocardium and is most suitable for rat heart reconstruction. The ventricular wall was lyophilized overnight and 6mm diameter circular patches were cut from the tissue. The patches were packaged individually and sterilized using ethylene oxide gas prior to implantation. UBM sheets (Matristem™ Wound Sheets) were obtained from ACell, Inc. (Columbia, MD) and were removed from sterile packaging, cut to 6mm diameter patches, and re-sterilized in a similar manner as the C-ECM patches.

### 2.2.4 Surgical repair of RVOT

After verification of chimerism, animals were prepared for RVOT reconstruction surgery as previously described [89, 146]. Anesthesia was induced by placing the rats in a small container with 3% Isoflurane in 2 L/minute of $O_2$. A 16G x 2" angiocatheter sheath was inserted in the trachea. Proper insertion of the intubation catheter was ensured through inflation of lungs with a small ambubag. A rodent ventilation system (SAR-830/P) was set at approximately 75 breaths per minute and approximately 700 cc air/minute. Hair was removed from the chest of the rat and the site was sterilized with Iodine. An initial injection of 10mg/kg lidocaine was delivered locally, and the Isoflurane was reduced to 1.5%-2%. A 5cm incision was made in the chest with a #10 scalpel, and a thoracotomy was performed to expose the heart. The ribs were held open with an Alm retractor. A purse-string suture (with diameter of 5.0 – 6.0 mm) was placed in the free wall of the right ventricular outflow tract (RVOT) with 7-0 polypropylene sutures. Both ends of the stitch were passed through a 22-gauge plastic vascular cannula, which was used as a tourniquet. The tourniquet was tightened and the bulging part of the RVOT wall inside the purse-string stitch was resected. The tourniquet was then briefly released to verify a transmural defect was created in the

RVOT as indicated by severe bleeding. One of the proposed patches was then sutured along the margin of the purse-string suture with over-and-over sutures with 7-0 polypropylene to cover the hole in the RVOT. After completion of suturing, the tourniquet was released and the purse-string stitch removed. The muscle layer was then closed with approximately 8 interrupted sutures (5-0 Surgipro). Prior to closure of the chest, the lungs were inflated to full capacity using a pediatric ambubag attached to the ventilator. Approximately 8 interrupted sutures were placed to close the skin and a local injection of 10mg/kg lidocaine was delivered. Additionally, a dose of 200mg/kg/day cefazolin was delivered to the thigh muscle, as well as 0.1mg/kg buprenorphine (buprenex), subcutaneously. Doses of cefazolin were delivered once daily for 3 days post-operative and buprenorphine was delivered twice daily for the same time period.

### 2.2.5 Cardiac MRI

Cardiac MRI (Horizontal bore 7-T MRI system, Bruker Biospin 70/30) was performed for detailed assessment of cardiac function of all hearts treated with ECM. Animals were anesthetized with 1.5 to 2% Isoflurane in oxygen gas via nose cone during MRI imaging. Animal body temperature, heart rate, respiratory rate, and arterial oxygen saturation were continuously monitored using a vital monitoring system. The total scanning time for each animal was approximately 45 to 60 minutes. Under electrocardiogram and respiratory gating, right (left lateral image plane) and left ventricular (long and short axis image planes) wall motions were recorded by a FLASH cine image sequence. Cardiac MRI was performed at 4, 8 and 16 weeks after ECM patch implantation and images were compared to those taken from a native heart. All videos detailed a minimum of one full cardiac cycle so that distinct measurements could be taken from the left and right ventricles throughout systole and diastole. Cardiac function was assessed by calculation of ejection fraction

and end diastolic volume from the LV, as well as shortening fraction from RV outflow tract where graft was implanted using OsiriX software. A repeated measures, two-way analysis of variance (ANOVA) was performed on all samples to determine significant differences ($p<0.05$) from native values for ejection fraction, RV shortening fraction, and LV end diastolic volume.

### 2.2.6 Specimen Processing

At time points of 4, 8 and 16 weeks, animals were euthanized by injection of 5mL of 1M KCl directly into the heart. The hearts were then removed and fixed in 4% paraformaldehyde for 24 hours. Hearts were then moved to 30% sucrose for another 24 hours. The hearts were then cut in half through the patched area, frozen in OCT solution at -80°C, and sections were cut at 8µm thickness and placed onto slides for future staining. Masson's Trichrome staining was performed to analyze the collagen and cell presence within each specimen prior to immunofluorescent staining.

### 2.2.7 Immunofluorescent Staining

All specimens were permeabilized with 0.1M glycine, 0.5% Triton X-100 in PBS for 15 minutes. The specimens were then washed five times in 1X PBS and then incubated with 1% goat serum for 1 hour. After the hour, the specimens were again washed three times in 1% BSA. The primary antibodies (α-actinin (Sigma Aldrich, A7811), connexin 43 (Abcam, ab11370), von Willebrand factor (Abcam, ab6994), α-smooth muscle actin (Abcam, ab7817), and GFP (Invitrogen, G10362)) were then added and incubated for two hours at room temperature and then washed five times in 1% BSA. After these washes, the secondary antibodies (AlexaFluor A21125-594 and AlexaFluor

A11008-488, respectively) and Draq5 for nuclear staining were added and incubated for another two hours. Hoechst (1mg/100mL) solution was then added for 30 seconds and then washed five times in 1% BSA. Slides were covered in mounting medium, coverslipped, and sealed until imaging.

### 2.2.8 Macrophage Phenotype Analysis

Macrophage staining was performed on samples in order to describe the immune response of the ECM patches as recently described [4, 176]. Antibodies for CD68 (pan-macrophage), CD86 (M1), and CD206 (M2) were used for an investigation of the M1 and M2 macrophage phenotypes. Prior to staining, samples were submerged in a solution of methanol to quench the GFP signal. After the elimination of GFP signal was verified, slides were washed in PBS and then incubated in a blocking serum consisting of horse serum, BSA, Triton X-100, and Tween 20. Blocking solution was removed and a 1:150 dilution of mouse anti-rat CD68, rabbit anti-CD86, and goat anti-CD206 antibodies in blocking solution was added to the slides at 4°C overnight. The following day, the slides were washed in PBS three times to remove primary antibodies. Secondary antibodies were added to blocking solution at the following concentrations; donkey anti-goat AlexaFluor 488 and donkey anti-mouse AlexaFluor 594 (1:200), donkey anti-rabbit Perp Cy5.5 (1:300). Secondary antibodies were added to the slides and allowed to incubate at room temperature for 1 hour. Slides were washed three times in PBS to remove the secondary antibody. Mounting media with DAPI and coverslips were then added to each slide prior to imaging.

## 2.3 RESULTS

### 2.3.1 Bone Marrow Transplantation and Surgical Outcomes

Prior to RVOT surgeries, a chimera population was created from wild type recipient rats and GFP+ marrow donors. The observed survival rate of bone marrow transplantation was approximately 66%, with complete engraftment achieved between 30-60 days after transplant. Currently accepted rates of chimerism are approximately 95% of the white blood cell population expressing the GFP protein. Blood smear analysis revealed a large GFP+ cell population within peripheral blood samples, and this was verified through flow cytometry analysis. The animals used in this study expressed an average GFP + white blood cell population of 94.9%, confirming the creation of the chimera rats. Both UBM and C-ECM patches measured 6mm in diameter and were implanted with the luminal side of the scaffold on the blood contacting surface.


**Figure 1. Macroscopic photo of UBM and C-ECM patches prior to implantation.**

UBM patches measured approximately 0.25mm in thickness and C-ECM patches measured approximately 0.25-0.4mm in thickness. Intra-operative and post-operative mortality associated with the surgical procedure in both UBM and C-ECM groups was approximately 25%. The patches replaced approximately 25% of the RV wall in both groups and suture lines indicated the original placement of the scaffold up to the 16 week time point.

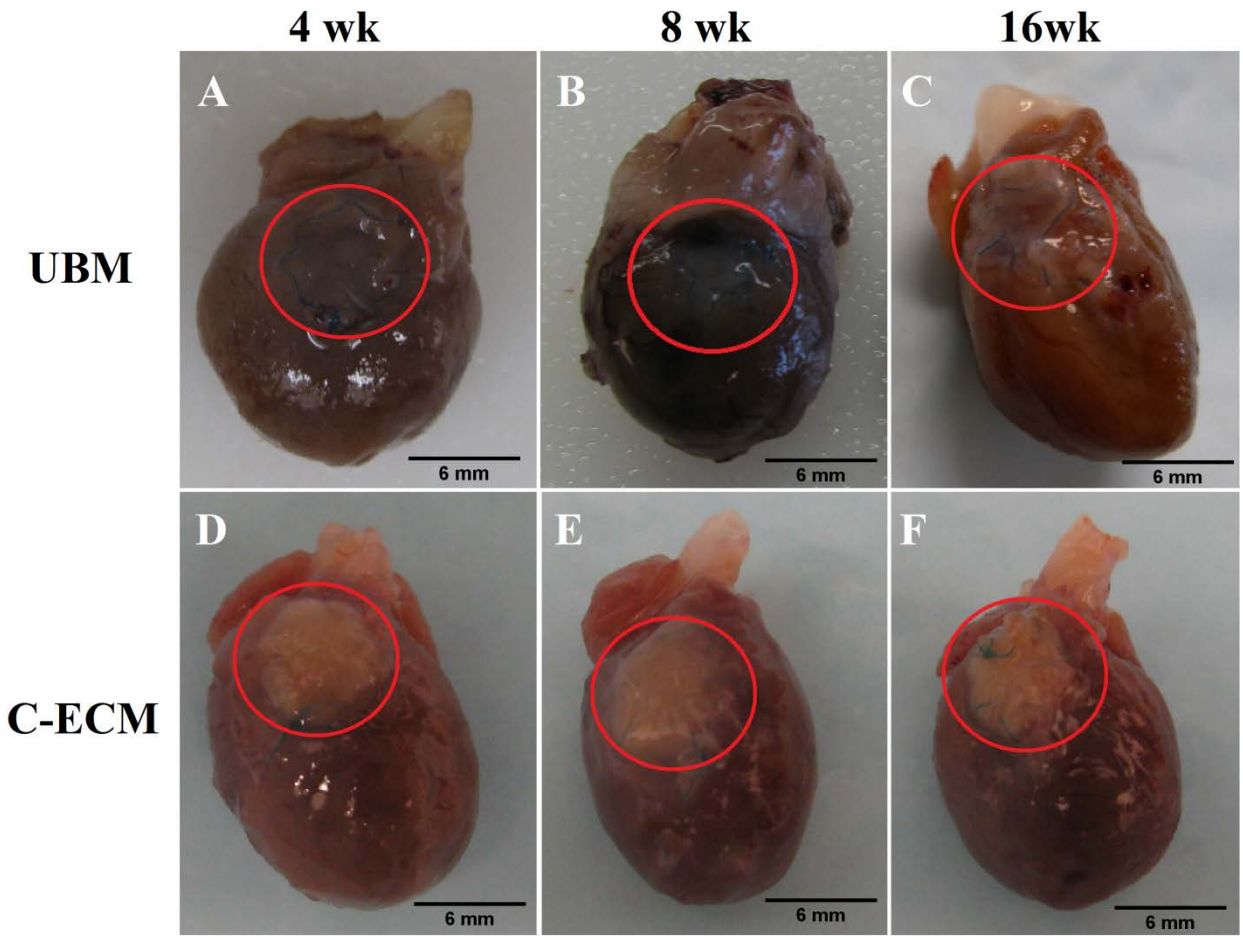


**Figure 2. Macroscopic images of the patched area of rat hearts at 4, 8, and 16 weeks after implantation. UBM patches were incorporated into the native tissue by 4 weeks after surgery. (A) The original white color of the patches were not evident at any time point. (A-C) C-ECM patches retained a whitish appearance and preserved the native thickness of the ventricle wall through the end point of the study. (D-F)**

### 2.3.2 C-ECM scaffolds

The C-ECM patches were incorporated into the native tissue by 4 weeks and the patches retained a whitish appearance through the 16 week time point. (Figure 2) The thickness of scaffolds was not statistically different than native RV wall thickness (0.93 ± 0.07 mm) at all time points with wall thickness values of 1.26 ± 0.14, 0.98 ± 0.1 , and 1.07 ± 0.11 mm at 4, 8, and 16 weeks, respectively. The C-ECM patches were incorporated into the native tissue by 4 weeks. The patches

retained a whitish appearance through the 16 week time point, and the thickness of the scaffold was similar to the thickness at implantation. Cardiac LV ejection fraction of hearts were significantly reduced at 4 weeks after reconstruction ($p < 0.05$), however, a return toward normal ventricular ejection and RV shortening values by 16 weeks was observed.

**Table 1. Left ventricular ejection fraction, right ventricle shortening fraction, and LV end diastolic volume of reconstructed hearts (n=5 for each material at each time point).**

**LV Ejection Fraction %**

| | 4 weeks | 8 weeks | 16 weeks |
|---|---|---|---|
| Native | 68.3 ± 0.8 | 68.3 ± 0.8 | 68.3 ± 0.8 |
| C-ECM | 64.7 ± 1.3* | 65.6 ± 0.1 | 68.4 ± 1.0 |
| UBM | 65.0 ± 4.6 | 66.3 ± 1.4 | 67.9 ± 1.1 |

* denotes statistical difference from Native values ($p < 0.05$)

**RV Shortening Fraction %**

| | 4 weeks | 8 weeks | 16 weeks |
|---|---|---|---|
| Native | 22.9 ± 1.1 | 22.9 ± 1.1 | 22.9 ± 1.1 |
| C-ECM | 31.2 ± 11.0 | 31.2 ± 1.3 | 27.2 ± 2.6 |
| UBM | 32.2 ± 6.4 | 32.5 ± 7.6 | 28.7 ± 7.0 |

**LV End Diastolic Volume ($cm^3$)**

| | 4 weeks | 8 weeks | 16 weeks |
|---|---|---|---|
| Native | 0.21 ± 0.03 | 0.21 ± 0.03 | 0.21 ± 0.03 |
| C-ECM | 0.25 ± 0.04 | 0.18 ± 0.01 | 0.28 ± 0.02 |
| UBM | 0.22 ± 0.06 | 0.19 ± 0.04 | 0.19 ± 0.03 |

No significant differences of LV end diastolic volume were observed following reconstruction. There was no RV outflow tract obstruction observed due to either patch material.

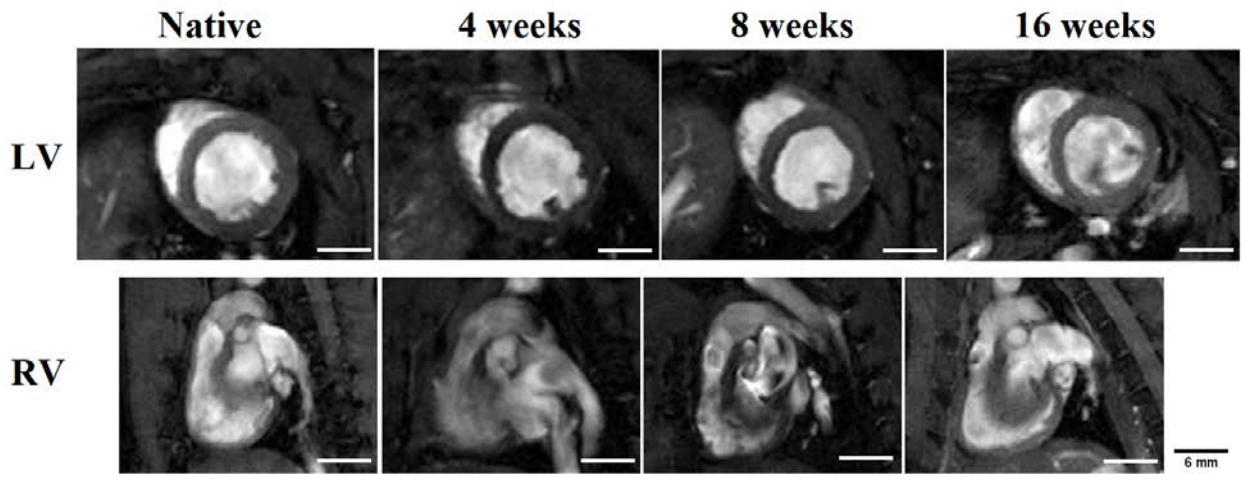


**Figure 3. C-ECM patched hearts showed no geometric changes in the RV and LV when compared with native hearts that had not undergone surgery. The LV cross section of reconstructed hearts maintains its native circular shape, indicating minimal pressure changes within the RV after patch implantation. Scale indicates 6mm.**

Histological examination of C-ECM reconstructed hearts showed that the patches had been incorporated into the native tissue by 4 weeks with cellular presence evident within the scaffold. Masson's Trichrome staining showed that the presence of collagen remained at the site of patch implantation throughout the study.

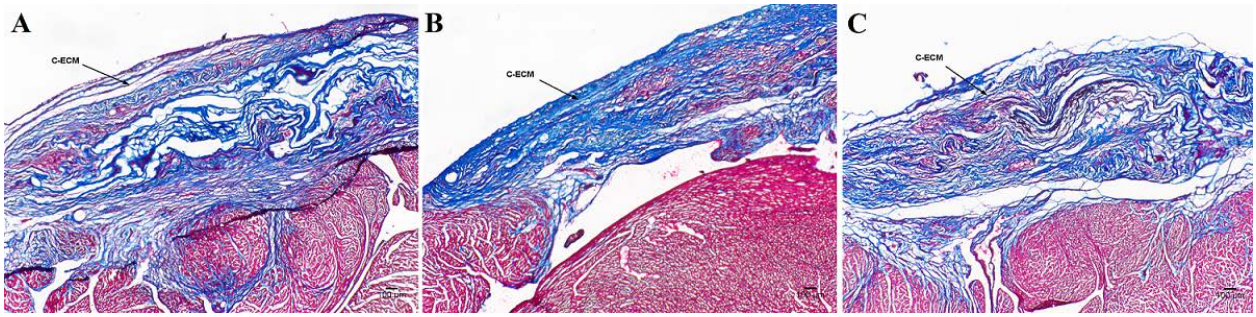


**Figure 4. Histological examination of C-ECM patches using Masson's Trichrome. The patches are incorporated into the native tissue by 4 weeks (A). The scaffold was also easily observed at 8 weeks (B) and 16 weeks (C) with a similar thickness as the surrounding ventricular wall and little evidence of remodeling. Scale indicates 100 µm.**

The scaffold was easily observed at all time points and the reconstructed area of the RVOT remained highly collagenous. The section of the ventricular wall repaired by the C-ECM scaffolds appeared to have a similar thickness as the surrounding native wall at all time points with minimal dilation evident, although a thickening of the surrounding native myocardial wall was observed.

Immunofluorescent examination of cardiac specific markers within the C-ECM patched hearts showed cellular presence in patches by 8 weeks after reconstruction, with a large population of GFP + cells evident in the patch. However, the cells had not completely penetrated the thickness of the scaffold and were localized to the luminal half of the patches. C-ECM patches expressed small areas of α-actinin, commonly evident in the sarcomere structure of cardiomyocytes. However, staining was intermittent and did not show normal striated cells, suggesting that cells within the patch were immature and possessed little contractility. Positive staining within the red channel of Figure 5 was primarily autofluorescence from the C-ECM patch, and was included to illustrate the boundaries of the remaining material with respect to cell infiltration.

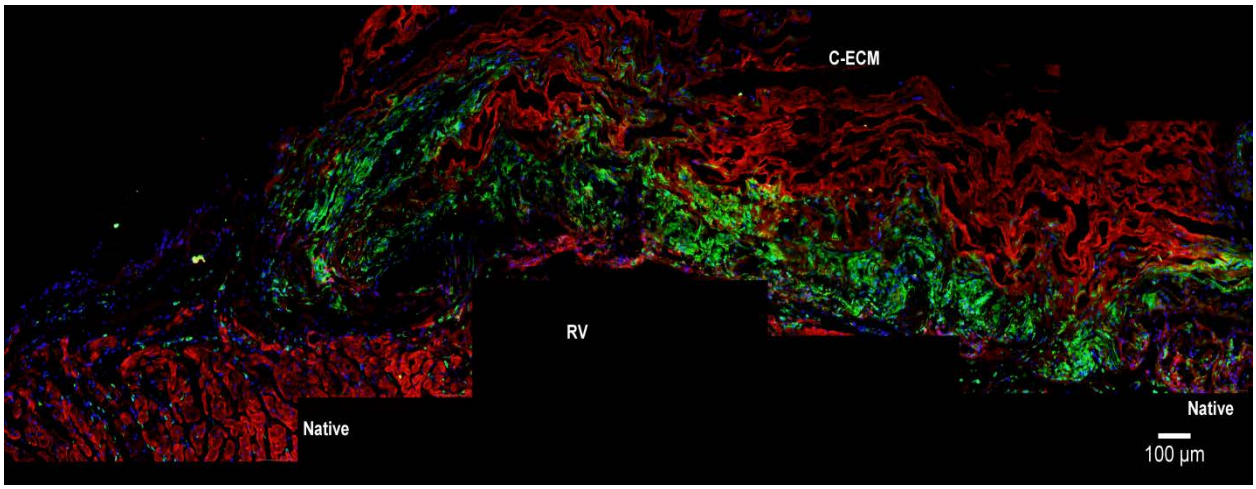


**Figure 5. Immunofluorescent examination of C-ECM patches for α-actinin at 8 weeks after reconstruction. A distinct presence of GFP (+) cells (green) was observed within the C-ECM patches with minimal staining for α-actinin (red, draq 5-blue). Scale indicates 100 µm.**

The C-ECM patches showed positive staining for α-smooth muscle actin (α-SMA) in intermittent areas of the tissue and were not associated with GFP expressing cells.

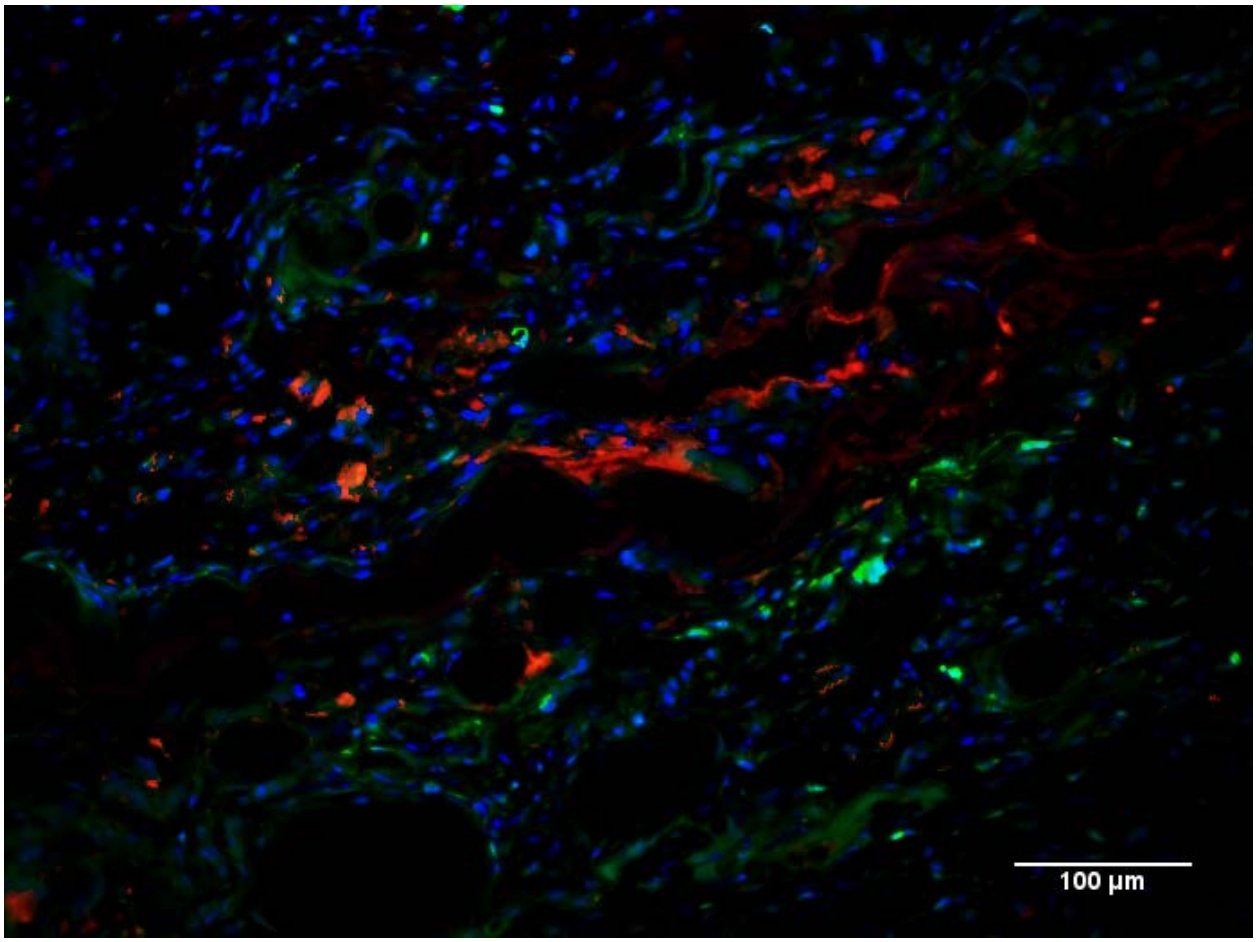


**Figure 6. Positive staining was confirmed for α-smooth muscle actin (red) in C-ECM scaffolds (GFP-green, draq5-blue) Scale indicates 100 µm.**

Cells that had accumulated along the endocardial surface were confirmed as endothelial cells through von Willebrand factor staining.

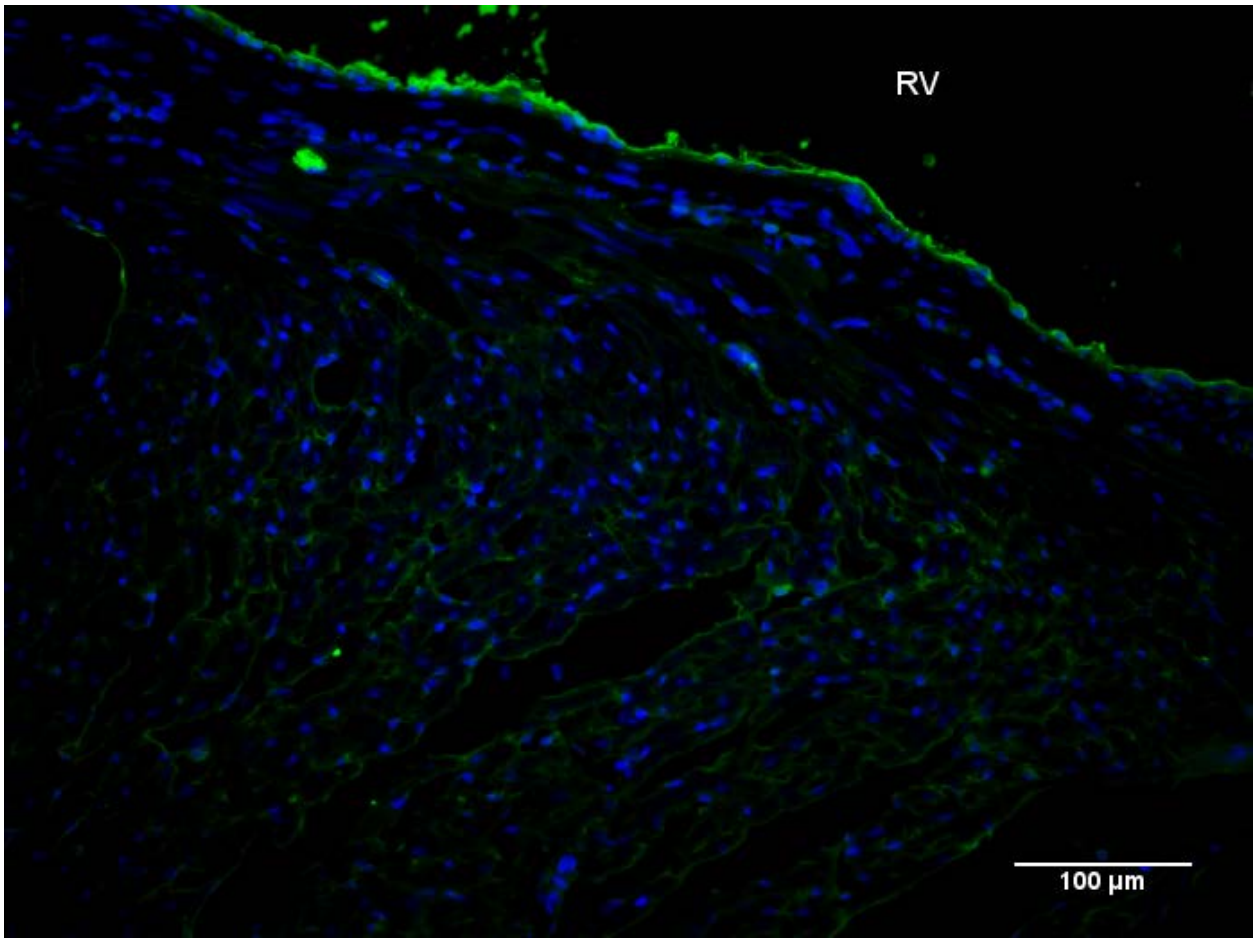


**Figure 7. A continuous endothelial lining along the endocardial surface was observed in C-ECM scaffolds as evidenced by von Willebrand factor (green, draq5-blue). Scale indicates 100 µm.**

Connexin 43 staining was also performed to identify gap junctions and electrical connections between cardiomyocytes, however, there was no observable staining within the patched area, suggesting that the cardiomyocytes present within the scaffolds were immature. (Data not shown) There was also little indication of fibrotic tissue development of the patches at all time points. Few differences were observed in cell staining within C-ECM patches between 8 week and 16 week time points.

C-ECM scaffolds were analyzed for macrophage response at the 4 week time point to determine the acute response to the patches. Macrophages had penetrated the inner half of the patches and expressed a mix of M1 and M2 cells. There were distinct spatial differences in the macrophage response at the interface with native tissue, which consisted of primarily an M1 type macrophage response, and the endocardial surface of the material, which consisted of a predominantly M2 type macrophage response.

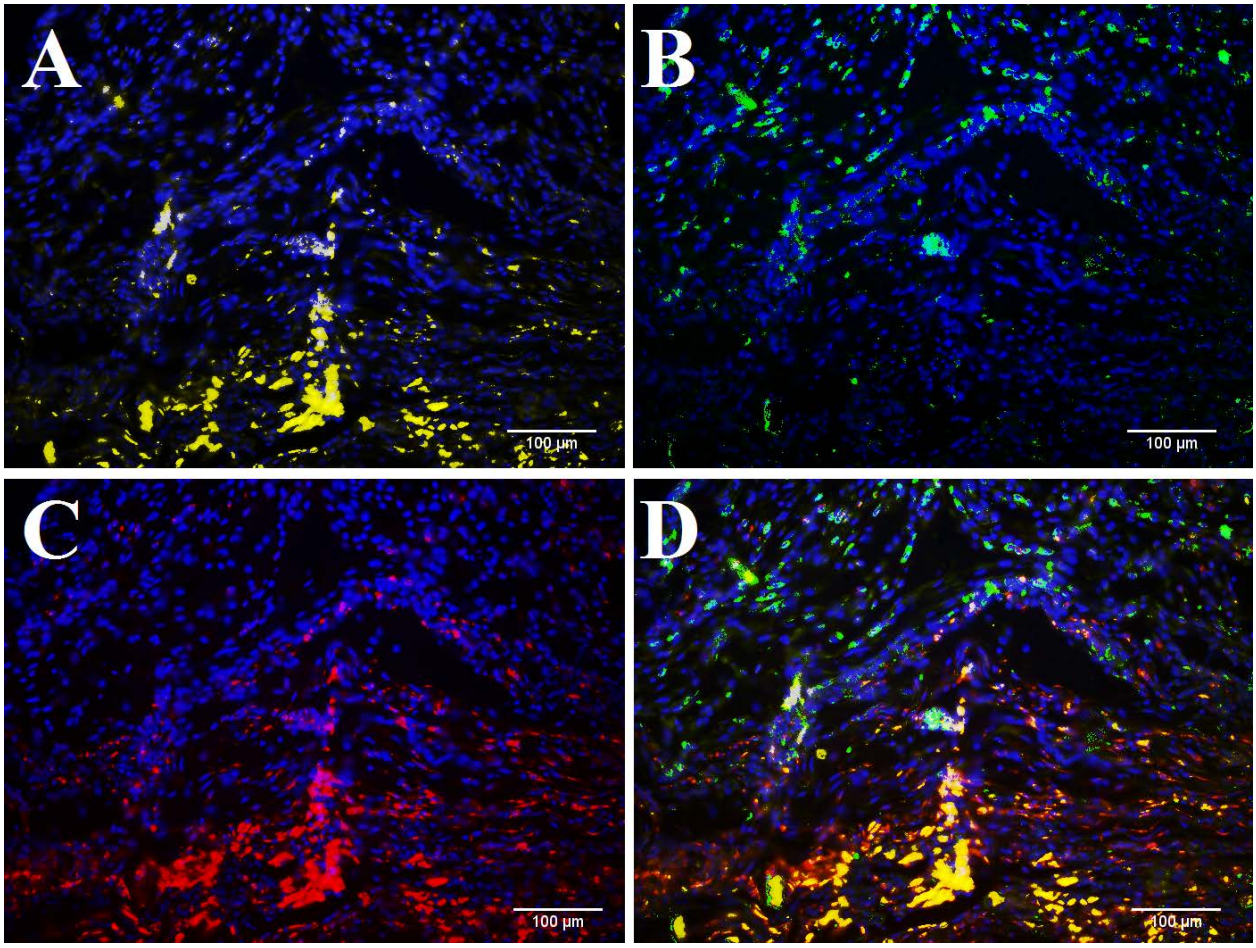


**Figure 8. Macrophage phenotype analysis of C-ECM patches at 4 weeks after surgery. Macrophages had completely penetrated the patches and expressed a mix of M1 and M2 cells. (A) M1 macrophages (CD86-yellow, draq5-blue), (B) M2 macrophages (CD206-green, draq5-blue), (D) combined image. Scale indicates 100 µm.**

### 2.3.3 UBM scaffolds

The UBM patches were completely incorporated into the native tissue by 4 weeks after RVOT repair surgery and the original white color of the patch was not evident upon explant at any of the time points of the study, which was a preliminary indication that the patch supported host cell infiltration and revascularization. The thickness of UBM scaffolds was not statistically different than native RV wall thickness (0.93 ± 0.07 mm) at 4 and 16 weeks after surgery with wall thickness

values of 1.02 ± 0.13 and 1.06 ± 0.16 mm, respectively. However, at 8 weeks after surgery, the RV wall thickness (0.35 ± 0.12 mm) was significantly thinner than native values. Cardiac LV ejection fraction was reduced at 4 weeks after implantation, however, by 16 weeks a complete return toward native ventricular ejection values was observed. (Table 1) The RV shortening fraction was minimally compromised, although not significantly, at 4 weeks, and by the end of the study it had also returned to native values. No geometric changes were observed in the LV, as observed from end diastolic volume, or RV of hearts through 16 weeks, suggesting that no RV outflow tract obstruction was seen by patches implantation.

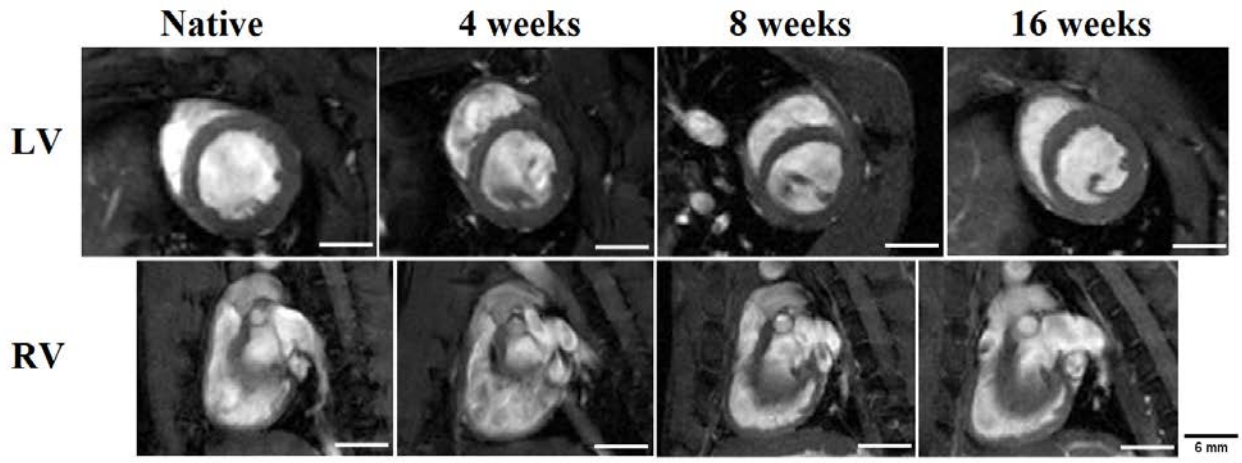


**Figure 9. UBM patched hearts showed no geometric changes in the RV and LV when compared with native hearts that had not undergone surgery. The LV of reconstructed hearts maintains its native circular shape through the end of the study, indicating minimal pressure changes within the RV after patch implantation. Scale indicates 6mm.**

Histological examination of UBM patches showed that by 4 weeks after implantation, there was complete penetration of infiltrating cells. Cellular presence was observed within UBM patches

at all time points. In Masson's Trichrome staining of the hearts, the morphologic presence of the scaffold was observed at 4 weeks after reconstruction.

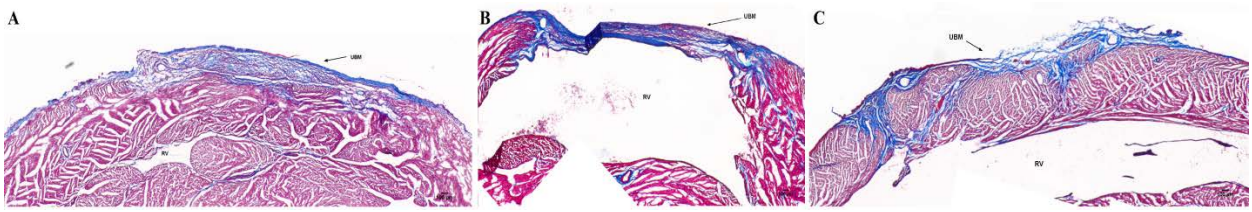


**Figure 10. Histological examination of UBM patches using Masson's Trichrome at 4 (A), 8 (B), and 16 (C) weeks after implantation. Cell presence is evident at all time points. (A-C) The patches had decreased in thickness at 8 weeks, but were similar to surrounding native tissue at 4 and 16 weeks. By 16 weeks, the UBM patches appeared to be completely degraded and replaced with native tissue. (C) Scale indicates 100 µm.**

By 8 weeks, the section of the ventricular wall repaired by the UBM scaffolds appeared to be thinner than the surrounding native wall and there was scattered evidence that the scaffold was still present. There also appeared to be some replacement of the scaffold with small quantities of muscular tissue. However, by 16 weeks after reconstruction there was an observable return to native ventricular wall thickness and the scaffold could not be observed morphologically.

Immunofluorescent examination of the UBM patched hearts showed a uniform cellular distribution throughout the thickness of the patch material by 8 weeks after reconstruction, with a large population of GFP+ cells evident in the patch.

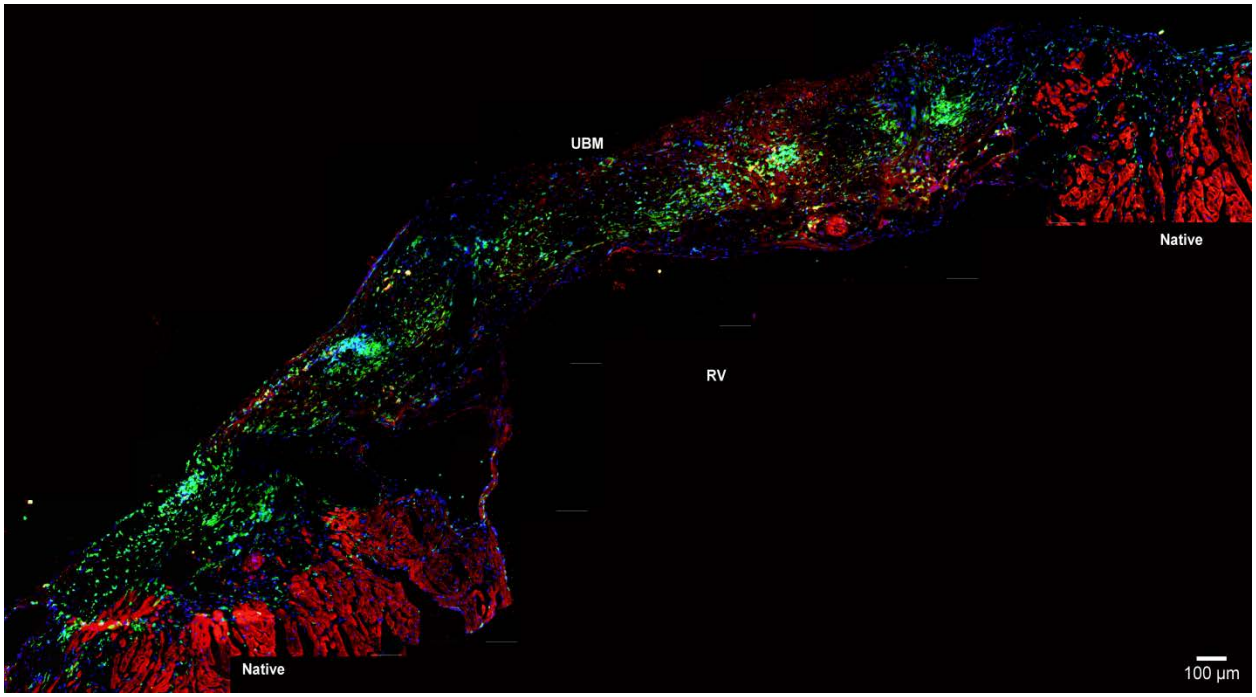


**Figure 11. Immunofluorescent examination of UBM patches for α-actinin at 8 weeks after reconstruction. A distinct presence of GFP (+) cells (green) as well as GFP (-) cells (blue) was observed throughout the thickness of the UBM patches with intermittent staining for α-actinin. Scale indicates 100 µm.**

Cells within the UBM patches also expressed α-smooth muscle actin (α-SMA) in small areas of tissue throughout the patch thickness.

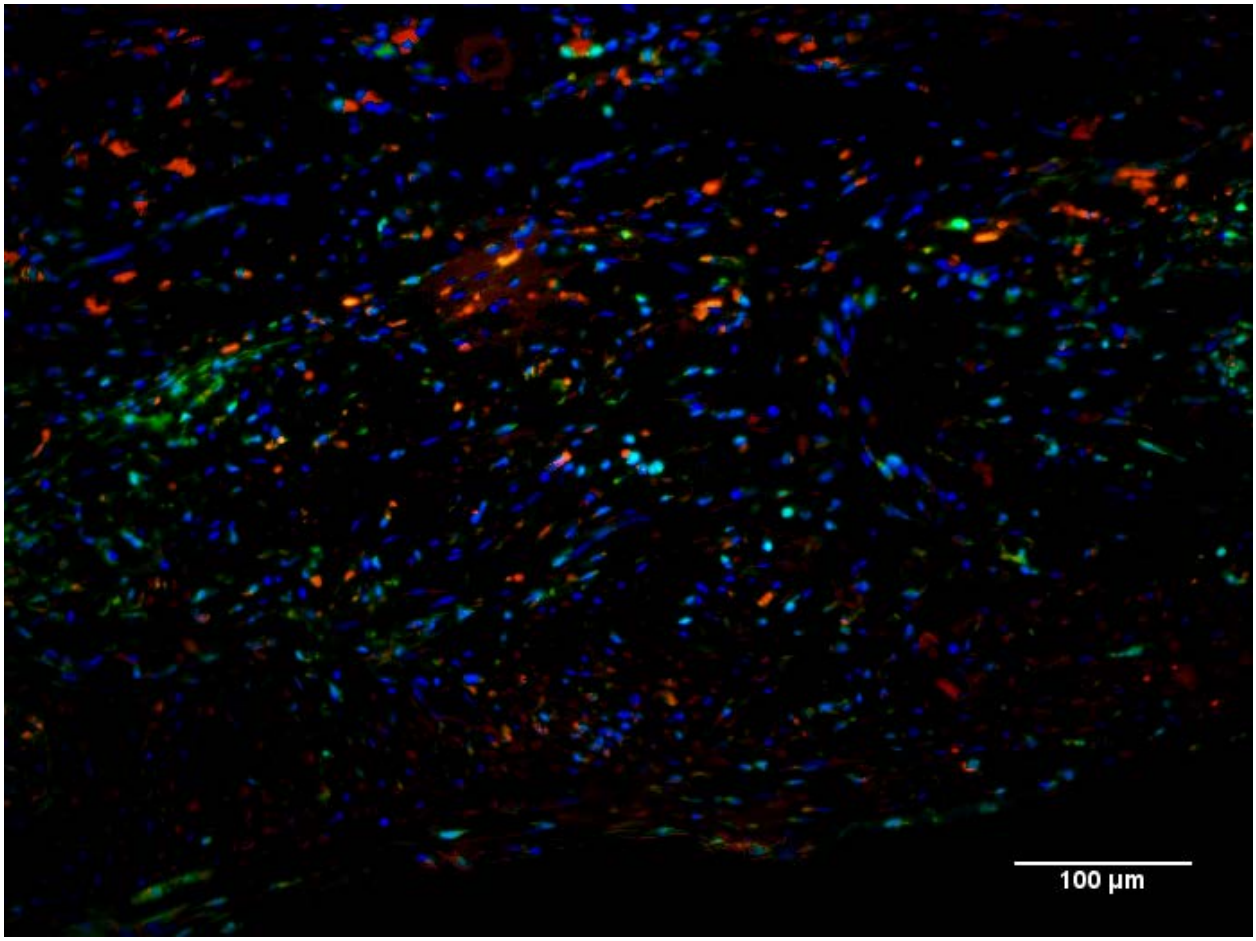


**Figure 12. Positive staining was confirmed for α-smooth muscle actin (red) in UBM scaffolds (GFP-green, draq5-blue) Scale indicates 100 µm.**

There was no indication of fibrotic tissue development on the patches. Cells within the remodeling UBM scaffolds had developed a continuous monolayer along the endocardial surface of the RV by 8 weeks, and no changes were observed at 16 weeks after surgery. Cells accumulating along the endocardial surface were confirmed as endothelial cells through von Willebrand factor staining.

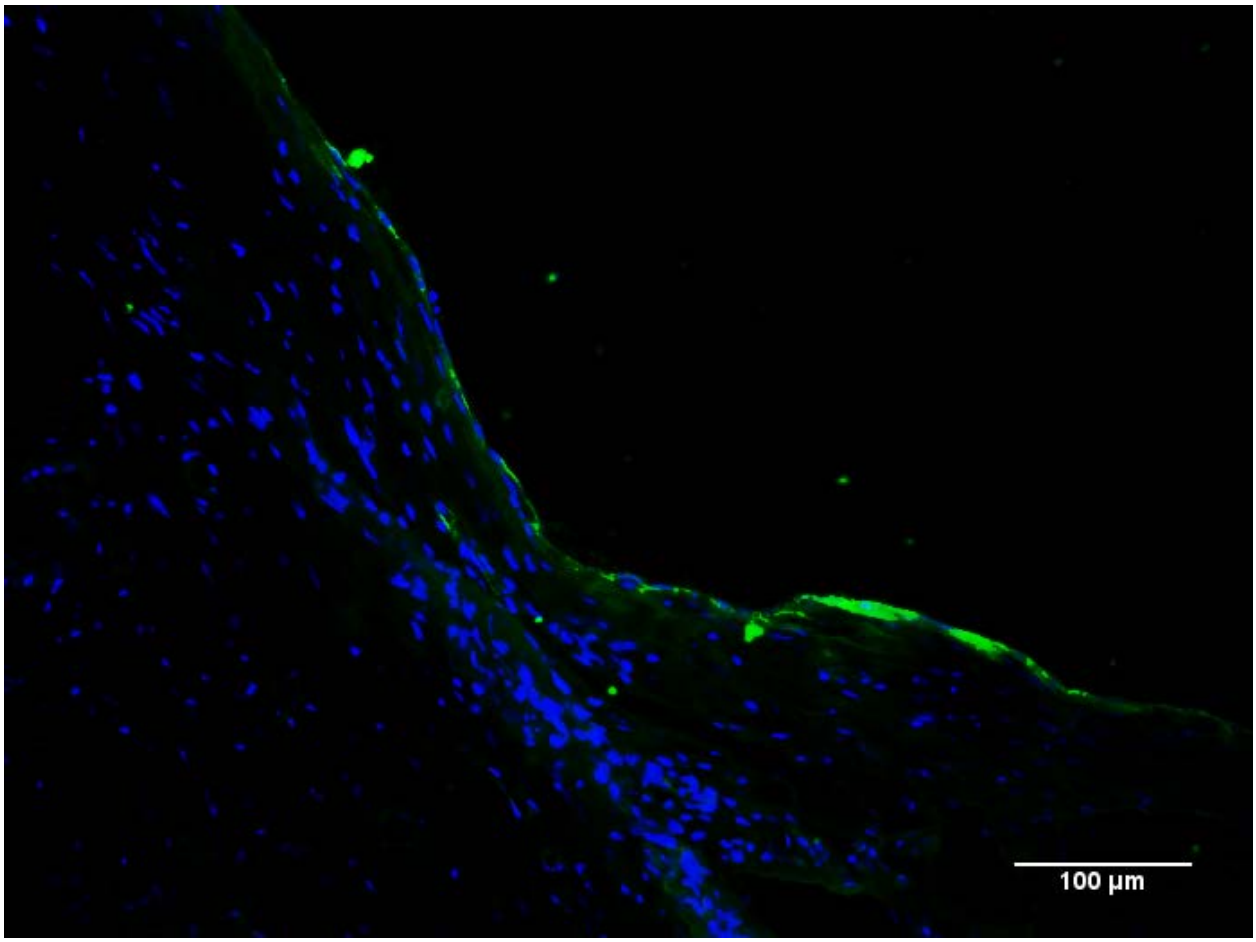


**Figure 13. A continuous endothelial lining along the endocardial surface was observed in UBM scaffolds as evidenced by von Willebrand factor (green, draq5-blue). Scale indicates 100 µm.**

Connexin 43 staining showed no observable gap junctions within the patched area, suggesting that cardiomyocytes present within the UBM patches were immature at this time point. (Data not shown) However, further analysis of α-actinin staining at 16 weeks within UBM reconstructed hearts showed the presence of cardiomyocytes expressing organized striated sarcomere structure. GFP+ cells were present within UBM patches at 16 weeks after surgery, and were located in close proximity to cardiomyocytes, although no co-staining was evident.

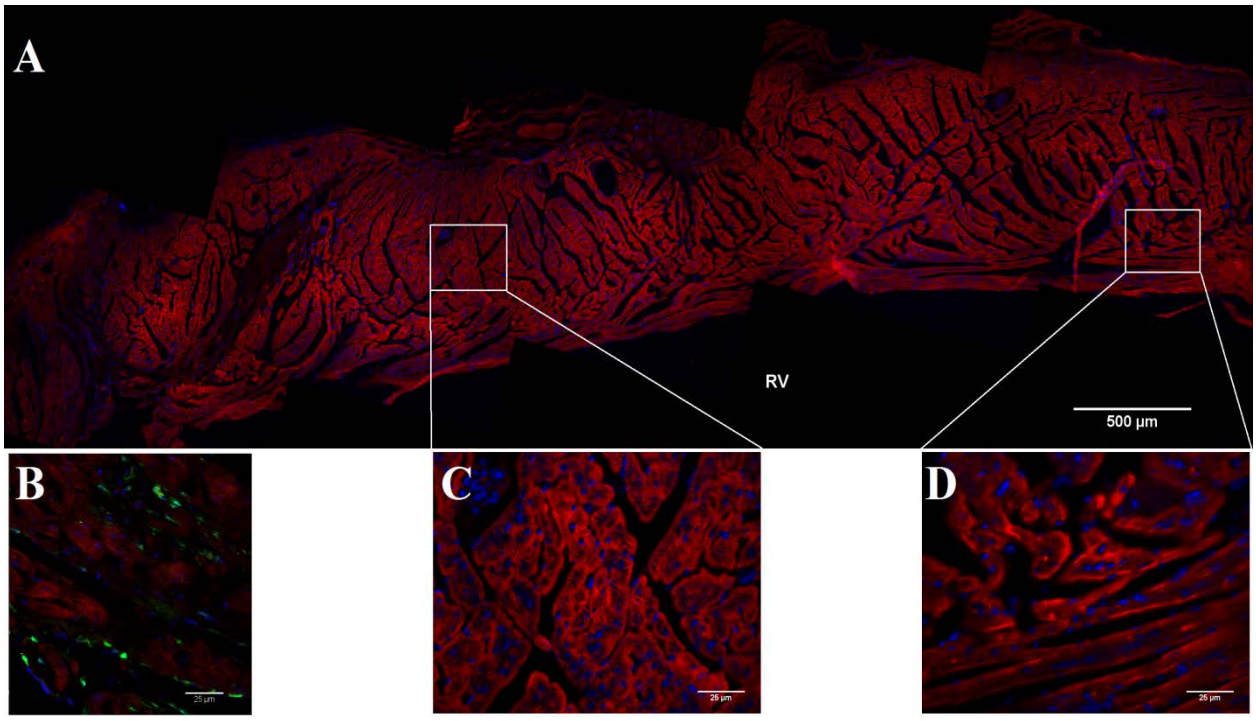


**Figure 14. α-actinin staining of UBM patches at 16 weeks after surgery. (A) The patched area shows evidence of organized sarcomere structure (red) within cardiomyocytes. (B) GFP + cells (green) can be observed within the patch, but are not associated with actinin staining. (C,D) Insets from multiple areas throughout the patch show striated actinin structure within cardiomyocytes. (draq5-blue) Scale indicates 500 µm and 25 µm within insets.**

At the 4 week time point, UBM patches elicited a mixed M1/M2 acute macrophage response. CD206+ (M2) macrophages were primarily localized to the area of the ventricular wall nearest the endocardial wall, while CD86+ (M1) cells were located within the inner portion of the patches, although both populations of cells were observed throughout the thickness of the patches.

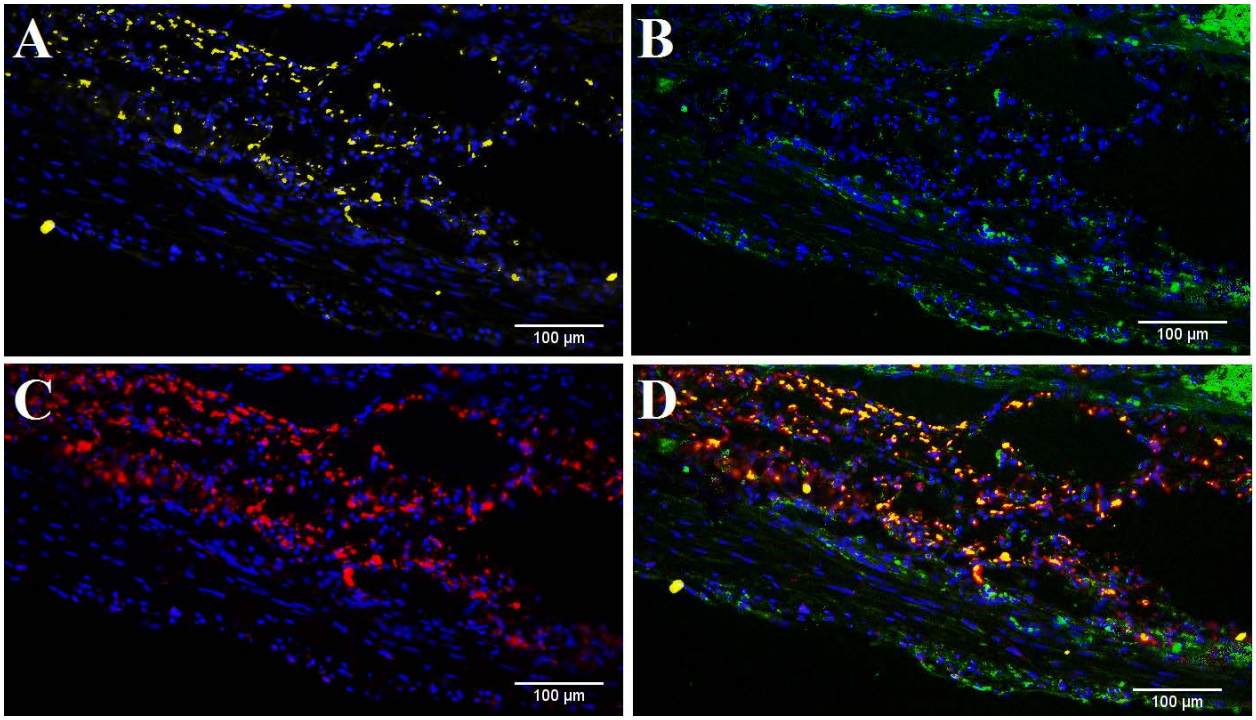


**Figure 15. Macrophage phenotype analysis of UBM patches at 4 weeks after surgery. A mixed M1/M2 response was observed in the patches. Macrophages were primarily localized to the inner half of the patches, with a concentration near the interface with native tissue. (A) M1 macrophages (CD86-yellow, draq5-blue), (B) M2 macrophages (CD206-green, draq5-blue), (C) pan-macrophage (CD68-red, draq5-blue), (D) combined image. Scale indicates 100 µm.**

## 2.4 DISCUSSION

The present study directly compared the ability of UBM and C-ECM patches to repair a critically sized, full thickness defect created in the right ventricular outflow tract of chimera rats. Both scaffolds were able to preserve cardiac performance throughout the study, and both patches were able to support cell infiltration for up to 16 weeks after reconstruction. Neither scaffold showed signs of fibrotic encapsulation, and both scaffolds expressed a continuous endothelial lining along

the endocardial wall of the RV at the site of repair. However, UBM patches were rapidly degraded and remodeled, with the formation of new host tissue in the reconstructed area by 16 weeks. Additionally, cells were able to rapidly infiltrate and fully penetrate the thickness of the UBM scaffolds by 8 weeks, with a significant number originating in the bone marrow. Cardiomyocytes with healthy sarcomere patterns were observed throughout UBM, but not C-ECM, patches by the end of the study. The results from the present study suggest that UBM may be a more viable option than organ-specific ECM as a patch for myocardial repair.

It has been previously hypothesized that organ-specific ECM scaffolds are a more attractive option than heterotopically derived scaffolds in many tissue repair applications. The ECM from site specific origins is deposited by cells that are desired to repopulate the scaffold, and, for more geometrically complex organs, the structure of the scaffold can be preserved through perfusion decellularization [147, 175]. This hypothesis is supported by studies that have shown that liver ECM preserves the phenotype of liver specific cells better than heterotopic ECM, and studies with decellularized lung that show the ECM can promote site-appropriate differentiation of mouse embryonic stem cells [142, 177]. However, there are other examples that show that heterotopic ECM from the urinary bladder and small intestine can promote the formation of site appropriate tissue, sometimes with greater efficacy than the organ-specific ECM. For example, vacuum pressed UBM was equivalent to hydrated decellularized tracheal matrix for patch tracheoplasty, and was superior to a lyophilized form of the same [178]. UBM has also been shown to promote site-appropriate remodeling in the esophagus, thoracic wall, and body wall [3, 4, 6]. Both UBM and C-ECM have been evaluated independently for myocardial repair, but variations in the model have made comparisons difficult.

Following implantation, minimally processed ECM scaffolds can promote one of three distinct host remodeling responses, specifically encapsulation, integration, or remodeling [4]. The encapsulation and integration groups tend to include dermal products that are denser and require more aggressive decellularization protocols. The remodeling group includes small intestinal submucosa (SIS) and urinary bladder matrix (UBM), which undergo a much simpler decellularization process and are derived from organs that experience more rapid turnover. In addition to the commercially available products, recent efforts have sought to develop organ-specific scaffolds, including cardiac ECM (C-ECM), which are hypothesized to be preferred scaffold sources since the ECM was deposited by organ specific cells and the morphology matches that of the repair site. However, the process to produce these scaffolds tends to be more similar to the processes used for commercial scaffolds that promote encapsulation or integration responses rather than a constructive remodeling response. In the present study, UBM patches could be observed throughout the remodeling process at 4 and 8 weeks after implantation, but had been degraded and replaced by host tissue by 16 weeks. In contrast, C-ECM patches showed little evidence of remodeling. After implantation, C-ECM patches were integrated into the host myocardium were visible through the end of the study.

In recent years, there has been an increasing clinical demand for a biomaterial that has the ability to restore function to damaged myocardium. The emergence of the regenerative medicine field has provided a number of biologic based materials that have shown the ability to repair and integrate into native tissue, as well as materials that are able to remodel and restore function to damaged tissue. In a cardiac location, previous studies have investigated heterotopically derived ECM scaffolds for repair and have been met with moderate success [107, 111, 150]. These studies were able to show local contractility of patches and the presence of small areas of site specific cardiac

cells. However, the primary result of these studies was ultimately the integration of ECM patches into the native tissue with collagenous tissue present at the endpoint of the study. The results of the present study suggest that C-ECM becomes integrated into the adjacent myocardium, while UBM promotes remodeling of cardiac tissue.

Through MRI examination, differences could be observed between groups in the functional analysis of reconstructed hearts throughout the study. Ejection fraction, an indicator of ventricular health, decreased at 4 weeks, but returned toward normal values by the end of the study. A 4% drop in ejection fraction was the largest difference observed between reconstructed hearts and native values, measured in C-ECM hearts at 4 weeks after reconstruction. This value was the only measurement in the study that was significantly different from native values. Maintenance of cardiac performance may be attributed to the cellular presence within both scaffolds, as there was uniform cell distribution throughout each scaffold by 8 weeks after reconstruction. Additionally, UBM scaffolds had been largely replaced with native tissue by 16 weeks, as evidenced through Masson's Trichrome and α-actinin staining.

The present study expanded on previous work by Wainwright et al., where a C-ECM scaffold was directly compared to a currently used surgical patch material in the clinic, Dacron™ [146]. Using a RVOT reconstruction model, Wainwright et al. showed that C-ECM supported localized site-specific cardiac cells and aided in normal cardiac function, while the implantation of Dacron™ patches resulted in fibrous encapsulation through the end point of the study. The results of the present study, however, showed that C-ECM patches were unable to support the infiltration of site-specific cells and a significant decrease in ejection fraction was observed at 4 weeks after surgery. By the end of the study, C-ECM patches had been incorporated into the surrounding myocardium. The major difference between the C-ECM in the two studies was that

the C-ECM in the present study was subjected to a longer decellularization process to more effectively remove cellular debris. This potentially adds support to the idea that processing may be a stronger predictor of outcome than tissue origin [179]. The present study also sought to compare UBM and C-ECM scaffolds as they are currently produced, and did not account for differences in processing techniques between the scaffolds to ensure that each material is fully decellularized through previously optimized protocols. Obvious changes to the mechanical and chemical constituents of the scaffolds are expected if the production methods are altered, and future studies are necessary to examine the effects of controlling for such differences.

The exact cell populations involved in the host response to ECM patch implantation in a cardiac location has not previously been investigated, but it is hypothesized that bone marrow derived cells play a role. Previous mouse studies have suggested that bone marrow cells are recruited to the site of ECM implantation and participate in the remodeling response, although the specific role is not fully understood [122, 123, 180-182]. However, the surgical complexity of cardiac repair in mouse models prohibits their use, and larger animal models do not offer the capability to label bone marrow cells and track the origin of resident cells.

In the present study, bone marrow derived cells were among the first to infiltrate both scaffolds through observation of GFP expression. As the scaffolds were repopulated, an increasing number of non-GFP expressing cells could be observed up to 8 weeks after reconstruction. Non-GFP cells appeared to be primarily localized near the periphery of the scaffolds and near the interface with native tissue. By 16 weeks, there was little indication that cells were still migrating from the bone marrow to the site of implantation and a large reduction of GFP expressing cells was observed in both scaffolds. Although the present study did not quantify the exact number of GFP expressing cells, similar expression levels were observed at each time point. In UBM

reconstructed hearts, cardiomyocytes could be easily observed throughout the area and were not associated with GFP staining. However, in C-ECM reconstructed hearts, cardiomyocyte presence was absent and GFP expressing cells did not associate with site-specific cell markers.

GFP expression tended to be associated with the presence of macrophages within the scaffold. Recently, macrophage phenotype at early time points (<1 month) have been shown to be predictive of downstream encapsulation or site-appropriate tissue remodeling [4, 183]. Briefly, the persistence of increased pro-inflammatory, M1 type, macrophage populations within implanted ECM scaffold materials has been associated with encapsulation of the material or degradation without downstream formation of site-appropriate tissues. Conversely, increased M2 populations have been associated with a more rapid resolution of the inflammatory response and improved site-appropriate tissue formation. In the present study, a qualitative assessment of macrophage phenotype was performed, showing that both samples elicited a mixed M1/M2 macrophage population. However, the spatial location of these cells within the implanted samples was observed to differ. C-ECM implants were characterized by a predominance of the M1 phenotype at the interface with native tissue and M2 cells towards the endocardial surface of the remodeling samples. UBM implants were characterized by a mixed M1/M2 population which was located within the area closest to the native tissue. The superficial portion of the remodeling implant was populated with cells at the 4 week time point, however these cells did not stain positive for macrophage markers. This may indicate that bone marrow derived cells may influence remodeling through the differentiation of macrophages with respect to the ECM. It should be noted that macrophage phenotype occurs along a spectrum between M1 and M2 phenotypes and cells may express markers of both M1 and M2 phenotypes concurrently [184, 185]. Cells expressing both CD86 and CD206 concurrently were observed in both C-ECM and UBM implants. The exact

implications of these cells in the process of cardiac tissue remodeling are largely unknown and a subject of significant interest.

An important question remains regarding the origin of the cells found in the remodeled UBM after 16 weeks. It has long been believed that resident cardiac cells are non-migratory and that there is little turnover within adult myocardium. However, there has been recent evidence that cardiac cells can migrate to areas of injury [186, 187]. In the present study, cardiomyocytes observed within remodeled UBM patches did not express GFP, indicating that the cells did not originate in the bone marrow. Preliminary hypotheses for the origin of these cells include cardiac progenitor cells or pre-existing cardiomyocytes within the surrounding tissue; however, future studies are required to determine the exact origin.

The primary limitations of this study stem from the use of a small animal model for cardiac tissue repair. The smaller size and lower pressures observed in the rat model do not provide an adequate prediction to the potential performance in a human setting. The current models for investigation of myocardial reconstruction and vascular treatments are juvenile sheep or piglets due to the similarities in the size, growth rates, and calcification issues as humans. However, the primary focus of this study was the differences in the cellular infiltration, distribution, and overall remodeling responses of the scaffolds as they are currently produced. The use of rat-derived ECM may have provided a more appropriate control for material performance, however, rat ECM scaffolds would not be feasible as a clinical material and the means of generating these scaffolds would not be applicable. Obvious differences exist between the mechanical structure and environment of the porcine organs of origin and the ultimate site of repair as well. However, the development of a chimera population allowed for more complete analysis of cell origin. Additionally, the use of a well-established RVOT surgical model for rats allowed for direct

comparison to previous studies. Future experiments are necessary to investigate the performance of ECM patches in larger animals to more closely mimic the native environment of human hearts.

## 2.5 CONCLUSION

ECM scaffolds provide distinct advantages to currently used biomaterials for myocardial reconstruction. The ability to restore function in a cardiac location, however, is paramount to the long term success of the scaffold. Previous studies have shown that artificial materials are completely encapsulated with fibrotic tissue and do not develop an endothelium. Wainwright et al. showed that C-ECM avoided fibrotic encapsulation, was integrated into the native tissue, and was able to support small areas of contractile cells with the development of an endothelial lining [146]. In contrast with previously held hypotheses, the results of the present study showed that UBM scaffolds may provide a more viable option for myocardial reconstruction than a scaffold derived from a cardiac location. The ability for the UBM patches to completely and rapidly degrade, while being replaced with newly formed site-appropriate tissue is a significant finding. These results are in direct contrast with results from the C-ECM patches, which showed integration into the cardiac tissue with little evidence of remodeling or presence of cardiomyocytes at the end of the study. Additional studies are needed to investigate both scaffolds on a more physiologically relevant scale, but this study provides evidence that the use of an organ-specific patch material in a cardiac location may not be the most appropriate approach in future studies.

# 3.0 *IN VITRO* EVALUATION OF ENGINEERED CONTRACTILE CELL-SCAFFOLD CONSTRUCTS

## 3.1 INTRODUCTION

As observed in the previous chapter, the microstructural environment of ECM scaffolds is a primary determinant of the overall cellular response. As such, UBM scaffolds may provide more appropriate mechanical and chemical cues than C-ECM scaffolds when used for myocardial reconstruction. The ultimate goal of cardiac tissue engineering is the development of an engineered patch through a combination of cardiac specific cells embedded within a scaffold material. While scaffold choice is paramount to success *in vivo*, well-documented requirements of generating contractile tissue *in vitro*, such as mechanical conditioning and cell alignment cannot be ignored. It is believed that cell function and retention can be increased through an improvement in the means of cell delivery. Previous studies have investigated the addition of a cellular component to various ECM scaffolds prior to implantation in studies in an effort to elicit a favorable *in vivo* response [10, 152-154]. However, many studies have ignored important characteristics of healthy myocardial tissue such as uniform cellular distribution and alignment.

The utilization of cell alignment techniques and mechanical conditioning are two guidelines prevalent in studies developing a cell-seeded scaffold *in vitro*. However, the application of these techniques has been largely implemented individually thus far, and studies have had limited success in engineering a robust contractile tissue with the capability of repairing myocardial tissue. It has been previously shown that UBM scaffolds can be processed in such a way to align the collagen fiber architecture in a preferential direction [64]. An aligned collagen

structure within a potential scaffold material would theoretically provide a means of contact guidance to align seeded cells. The beneficial effects of mechanical conditioning on ECM composition, fiber and cell alignment, and cell behavior have also been well documented [63, 64, 155-157]. Uniaxial cyclic stretch is able to align the collagen fibers of UBM and SIS scaffolds in the direction of stretch *in vitro*, and the introduction of cyclic strain to cells attached to ECM scaffolds has had significant effects on gene expression and cell alignment [157]. Therefore, the goal of the present study is to engineer a robust contractile tissue from UBM scaffolds and cardiomyocytes *in vitro*.

## 3.2 MATERIALS AND METHODS

### 3.2.1 UBM Scaffold Processing

Urinary bladder matrices were prepared in a similar manner as previously described [64, 188]. The urinary bladder from market weight pigs was harvested immediately upon euthanasia. External connective tissues were removed, and the bladder was rinsed with tap water to remove residual urine and frozen at -80°C until ready for processing. Bladders were thawed by submersion in Type I water at room temperature for up to two hours. Once thawed, the apex of the bladder was removed and a longitudinal incision was made to expose the luminal surface of the bladder in a flat sheet. The luminal side of the bladder was placed face down and the external muscle layers (tunica serosa, tunica muscularis externa, tunica submucosa, and most of the muscularis mucosa) were removed through mechanical delamination. Physical delamination of the muscle layers was performed in a single direction along the longitudinal axis of the bladder to align the collagen fibers of the resulting UBM [64]. The UBM was thoroughly rinsed in Type I water to lyse any remaining cells

and clean the surface of the scaffold. UBM sheets were disinfected using 0.1% peracetic acid in 4% ethanol (v/v) and thoroughly rinsed in phosphate buffered saline (pH = 7.4) and Type I water.

### 3.2.2 Isolation of Cardiomyocytes

Day 0-4 neonatal rat pups were first sterilized by cleaning off excess bedding and debris from skin and soaking in 70% ethanol. Hearts were removed from the pups using sterile forceps and scissors and transferred to chilled RCGM (Lonza media/bullet kit) supplemented with 1% Penicillin-Streptomycin and 1% Fungizone immediately. Aortas and atria of the hearts were removed to limit the population of fibroblasts in culture. The remaining heart was squeezed to remove excess blood, and tissue was minced under sterile conditions. Cardiac tissue was then washed in 1x KG solution containing 51.8g Glutamic Acid/Potassium salt (Sigma G1149), 35.6 mL Sodium Bicarbonate solution (7.5%w/v Gibco 25080-094), 0.12g Sodium Phosphate (Sigma S3264), 50mL HEPES Buffer, 1M (Sigma H0887), 5.94g D-Glucose (G7021), and pH tested to 7.4. Tissue was placed in a 50mL tube containing approximately 10mL of Collagenase Type II (3mg/mL) and a small stir bar was rotated at 1 rev/sec. The 50mL tube was then placed in a 37°C water bath on a heated stir plate for 20-30 minutes. Collagenase solution was then removed and tissue was rinsed with 1x KG solution. 15mL Trypsin solution (4mL Trypsin (10x, 2.5%) in 96mL 1x KG) was then added to cardiac tissue and incubated in the water bath for approximately 7 minutes, stirring at 1 rev/sec. Supernatant was removed and filtered through a 100μm strainer into a 50 mL tube filled with 20mL of RCGM chilled in an ice bath. Fresh Trypsin solution was added to the remaining tissue in the heated bath and triturated at 3mL/sec 4-5 times. The Trypsin solution was then harvested and replaced 5-6 times. Trypsin harvests 1, 2, 3-4, and 5-6 were all collected in each of four separate 50mL tubes containing DMEM. Each tube had a final volume of approximately 40mL. The cell

and media mixtures were removed from the ice baths and centrifuged at 200G for 5 minutes. Media was replaced with fresh RCGM complete and cell suspensions were added to plasma treated petri dishes and incubated for one hour to allow for fibroblast attachment. Preplating of cell suspensions was performed a second time for Trypsin collections 1 and 2, due to the higher fibroblast population. Suspensions were removed from dishes and cell counts were performed using a Coulter Counter. Cells were centrifuged at 200G for 5 minutes and resuspended in fresh RCGM (Lonza CC-4515) complete.

### 3.2.3 Cardiomyocyte Cell Sheets

Cardiomyocytes cultured on temperature responsive poly-n-isopropylacrylamide (PIPAAm) surfaces have been shown to maintain cell contractility while producing an extracellular matrix and establishing cell-cell connections [13]. Upon release from the surface, cell sheets have a uniform distribution of contractile cells, and have been investigated for cardiac implantation. Cardiomyocytes were plated on temperature-responsive dishes at a density of approximately 5 $x10^5$ cells/$cm^2$ and placed at 37°C, 5% $CO_2$ for 24-48 hours for attachment. After a total of 96 hours in culture on temperature responsive dishes, cell sheets were harvested by placing on ice for 25-35 minutes until release from polymer surface. Sheets were transferred to UBM pieces in a separate 6-well dish, secured under a culture ring, and submerged in media. Media was changed as needed for the following 6 days in culture, at which time cell-scaffold constructs were cut in half. One half was fixed in formalin and submitted for histologic staining and the other was fixed in 4% Paraformaldehyde for 30 minutes and washed in PBS.

### 3.2.3 Mechanical Conditioning of Cardiomyocytes on UBM Scaffolds

A second group of cells were also seeded directly onto Urinary Bladder Matrix (UBM) scaffolds that had been scraped in the longitudinal direction as a single cell suspension ($5 \times 10^5$ cells/$cm^2$). UBM scaffolds were cut into dogbone shaped pieces and placed in a silicone mold prior to cell seeding. Cells were cultured for 5 days on UBM scaffolds and cell-scaffold constructs were then transferred to a custom built cyclic stretching system.

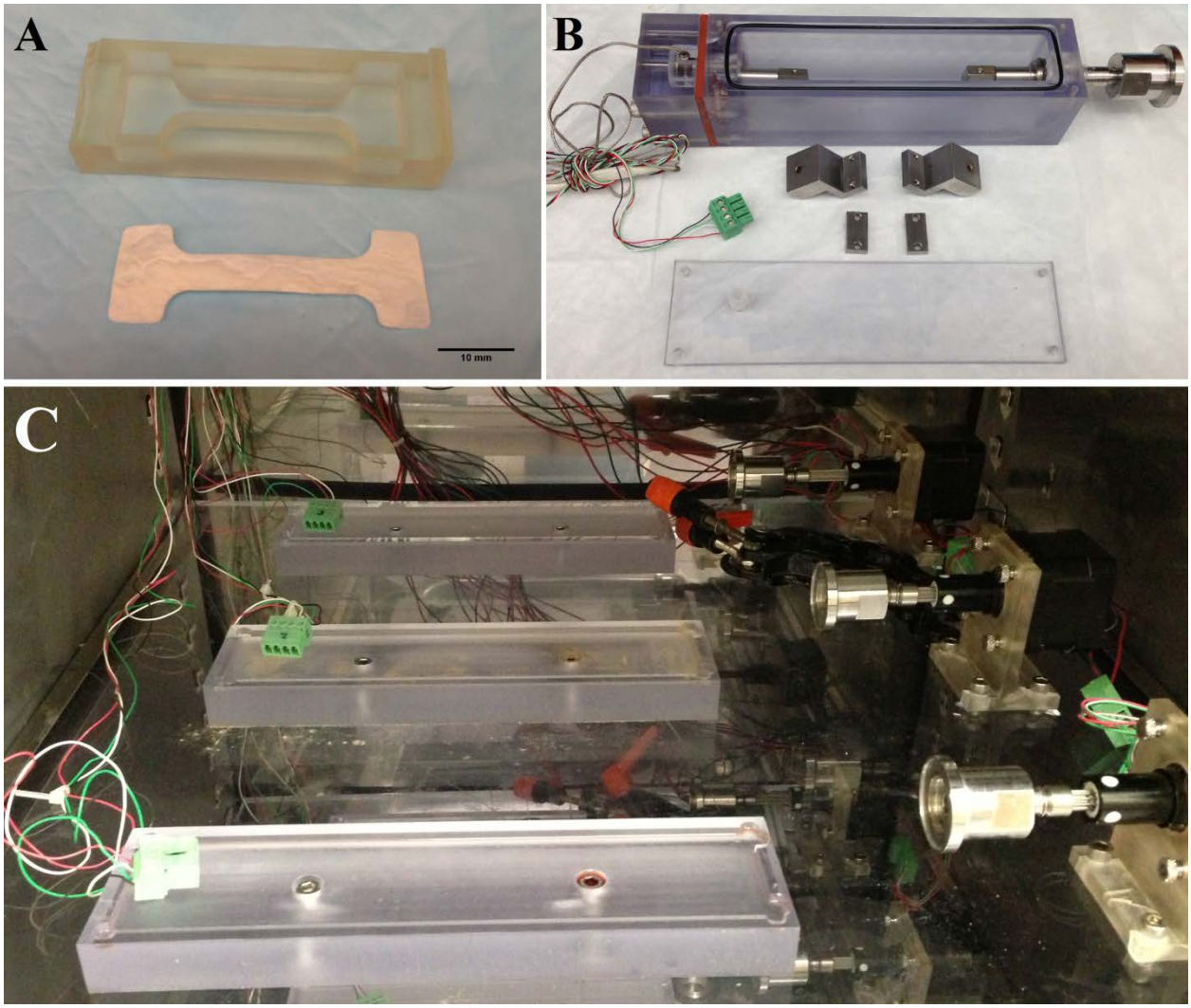


**Figure 16. A) Photograph of (A) a scraped UBM scaffold prior to cell seeding and a silicone culture dish, (B) a single stretch chamber with associated clamps, and (C) the stretch bioreactor system. Each stretch chamber consists of tissue clamps, which are attached to the UBM scaffold on either side, as well as stainless steel rods. The rods are attached to an enclosed load cell on one side and pass through a frictionless bearing and attach to a linear actuator outside the chamber on the other. Self-aligning connectors attach the linear actuator to the stretch chamber and allow for cyclic stretch to be applied to the UBM scaffolds.**

One group was held static at a small (0.05N) tension for the duration of the test, and another group was cyclically stretched (7%, 0.5Hz) for 7 days. Cyclically stretched cells were subjected to preloading conditions (0N- 0.05N) for 5 cycles, held at a small tension for 1 minute, and the full stretch regimen was started. Media was removed after 24-48h and replaced with RCGM supplemented with 200μM BrdU to limit fibroblast proliferation. Media was removed after an additional 24h in culture and fresh RCGM was again added. Media was replaced each 24h period, until cardiomyocyte cells reached a total of 7 days in culture under mechanical loading conditions. Following removal from stretch chambers, cell-scaffold constructs were either fixed and prepared for immunofluorescent staining or prepared for contractility measurements.

### 3.2.4 Cell Contractility Measurements

Cardiomyocyte seeded scaffolds (n=10) and cells in culture (n=10) were analyzed to observe the contractility of cells within UBM scaffolds and determine the ability of cells to produce measurable contractile forces. Constructs were first stained using rhodamine dye to observe the calcium transients within contracting cells. DMEM supplemented with 10% FBS and 1% Penicillin-Streptomycin was warmed to 37°C in a water bath. A stock solution of 1mg Rhod2-AM dye dissolved in 1mL dimexylsulfoxide (DMSO) and 10% Pluronic was previously prepared and frozen. 3mL of warmed DMEM was supplemented with 30μL dye solution and added to constructs within a 30mm culture dish. Cells were incubated for approximately 45 minutes in dye. The media was then removed and replaced with fresh DMEM. After an additional 30 minutes in a humidified incubator, samples were placed on a heated microscope stage for imaging. Small electrical pulses (15-20V, 15ms) were cycled through electrodes placed at opposite ends of the scaffolds. Fluorescent imaging was used to examine the calcium transients within cells through the cycles of

relative light intensity of the fluorescent dye during contraction. Videos were captured over multiple cycles of contraction and were analyzed through a custom designed Matlab program. Brightfield video imaging of cells attached to UBM scaffolds was also used to further examine cell contraction. In addition, a small number (n=2) of scaffolds were selected for contractile force measurements and were tested as previously described [189]. A small segment (~5mm x 2mm) of cell-seeded UBM scaffolds were cut and attached to a custom built force measurement device. Specimens were attached to the device on each end in the direction of stretch through 7-0 Prolene sutures. Small electrical pulses (15-20V, 15ms) were cycled through electrodes placed at opposite ends of the scaffolds, and measurements were recorded.

### 3.2.5 Immunofluorescent Staining

Samples were first permeabilized with 0.1M glycine, 0.5% Triton X-100 in PBS for 30 minutes. Samples were then washed five times in 1X PBS and incubated with 1% goat serum for 1 hour. After the hour, samples were again washed three times in 1% BSA. The primary antibodies [Alpha Actinin (abcam mouse IgG1) and Connexin 43 (abcam rabbit IgG)] were then added and incubated for two hours at room temperature. Samples were then washed five times in 1% BSA, and the secondary antibodies [alexa 21127-555 and alexa 11008-488, respectively] and Draq5 were added and incubated for another two hours. Hoechst (1mg/100mL) solution was then added for 30 seconds and then washed five times in 1% BSA. Samples were stored at 4°C until being imaged.

### 3.2.6 Cell Alignment Analysis

To quantify the cell alignment from the immunofluorescent images, custom image analysis software was applied separately to the actinin (red) channel. The image analysis software was written in Matlab by Courtney, using an algorithm developed by Chaudhuri and modified by Karlon [190, 191]. This algorithm applies a variation of a Sobel operator to obtain the pixel intensity gradient to determine the preferred cell direction for each sub-region. The cell angle from each sub-region was then placed into a histogram to determine the preferred cell direction of the network. In addition, the normalized orientation index (NOI) was calculated from the orientation index (OI) of samples [64]. The OI has been previously defined as an angle about the preferred fiber direction containing 50% of the fibers [192]. In the present study, NOI was defined as (90° – OI)/90° x 100% [156]. NOI ranges from 0-100%, with an NOI of 100% correlating to a perfectly aligned network of cells and an NOI of 0% indicating random alignment. A one-way independent ANOVA was performed to examine the statistical difference ($p < 0.05$) between the alignment of cells in culture and static and stretched cell-scaffold constructs as well as the differences between static and cyclic stretched groups.

## 3.3 RESULTS

### 3.3.1 Cardiomyocyte Cell Sheets

Neonatal rat cardiomyocytes were isolated and successfully cultured on temperature responsive surfaces for up to 10 days in culture. Cells showed the ability to form small “clusters” that were able to spontaneously and synchronously contract at physiologically similar rates. Cardiomyocytes were able to attach to culture surfaces, develop intercellular gap junctions, and secrete their own

extracellular matrix. Upon release from temperature responsive dishes, cells remained attached in a sheet form, although the loss of strain resulted in a reduction in surface area to only approximately 25% of the original size. Following release from the culture dish, electrical stimulation of cell sheets produced visible contraction of the edges. However, the contraction occurred along the complete circumference of the cell sheets and was not in a preferred direction. Immunofluorescent examination of cell sheets showed a healthy, striated sarcomere pattern of cardiomyocytes, as well as abundant gap junctions to facilitate intercellular communication and conduction of electrical signals. Following attachment and culture of cell sheets on UBM scaffolds, cardiomyocytes did not appear to maintain a healthy phenotype. Cells did not express striated sarcomere pattern and did not show gap junction staining.

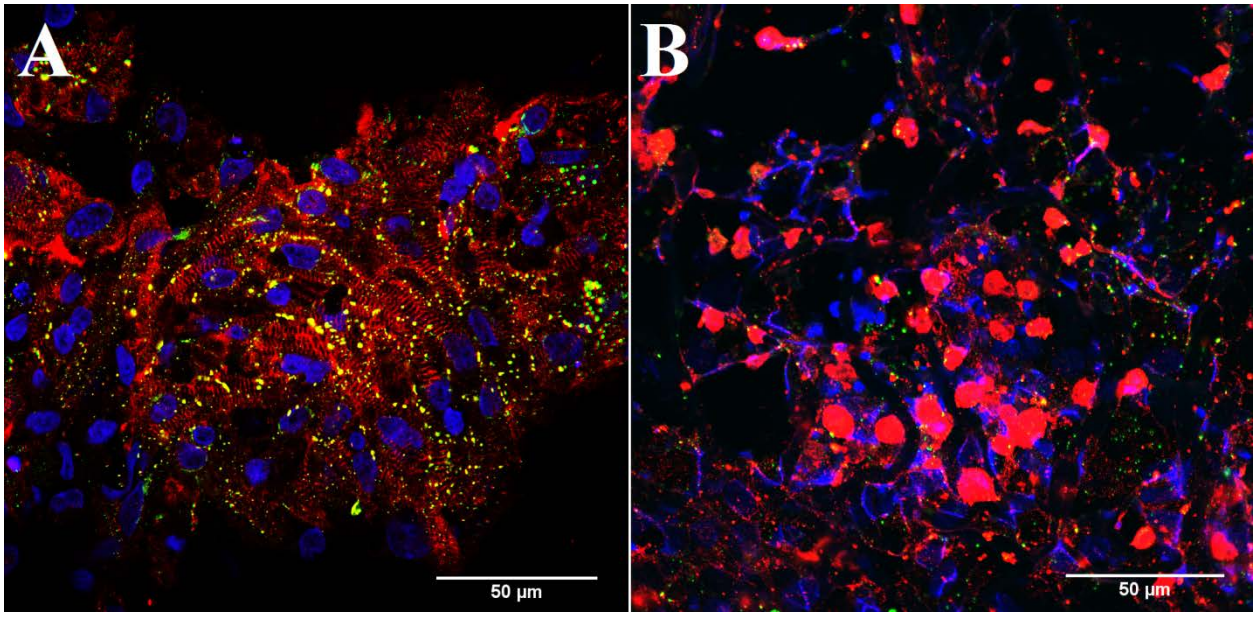


**Figure 17. Immunofluorescent image of cardiomyocyte cell sheets (A) after release from PIPAAm surface and (B) after 4 days in culture on UBM scaffolds. (Red- α-actinin, Green-connexin43, Blue-draq5) Image: 63x. Scale: 50µm.**

### 3.3.2 Cardiomyocytes on UBM Scaffolds

The inability to transfer and culture healthy cell sheets on UBM scaffolds facilitated an alternative approach to attach cells directly to scaffolds following isolation. UBM scaffolds were placed in silicone culture wells, and single cell suspensions were seeded directly onto scaffolds. Following an attachment period, cell-scaffold constructs were placed inside a tissue stretching system and either held under static conditions or cyclically stretched.

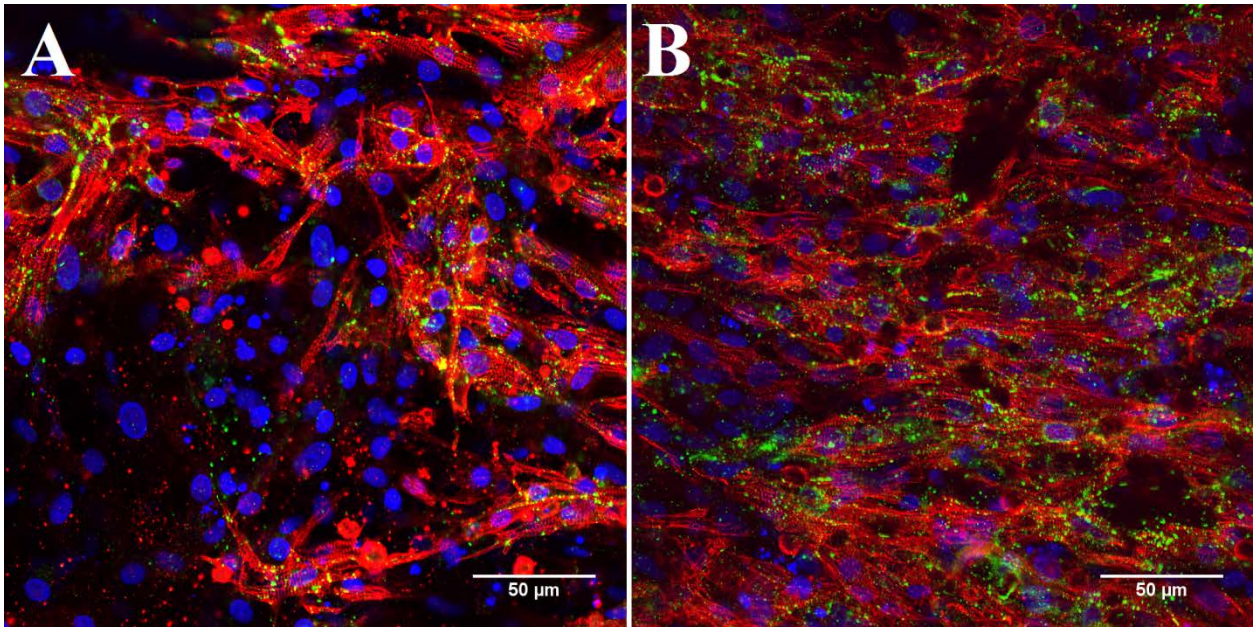


**Figure 18. Immunofluorescent image of cardiomyocytes seeded directly onto UBM scaffolds. Cells were cultured on UBM scaffolds for 4 days and transferred to a uniaxial stretching system, where cells were (A) held under static conditions or (B) cyclically stretched for up to one week. (0.5 Hz, 7%) (Red- α-actinin, Green-connexin43, Blue-draq5) Image: 63x. Scale: 50µm.**

Multiple stretch regimens were tested to optimize culture conditions. (0.1, 0.25, 0.5, 1 Hz; 5, 7, 10, 15% stretch) Cells cultured under static conditions were able to maintain a small degree of contractile characteristics, with small areas of striated sarcomeres and gap junctions. Static cell-scaffold constructs showed random alignment and intermittent staining; indicating that the "tissue" may have contractile cells, but would not produce any functional contraction. However, cells subjected to cyclic stretch (0.5Hz, 7% stretch) showed a large increase in the number of cells expressing a striated sarcomere pattern, as well as uniform expression of gap junctions throughout the tissue. In addition, cells subjected to stretch patterns appeared to preferentially align in the direction of stretch. The expression of contractile markers coupled with the appearance of

alignment within UBM scaffolds indicated that a stretched tissue may have the ability to contract and produce measurable forces.

### 3.3.3 Cell Alignment

A quantitative measurement of the alignment of cellular networks within each group was performed using a MATLAB algorithm to analyze immunofluorescent images ($n \geq 8$). The actinin channel of each image was separated and used to dictate the overall alignment of individual cells.

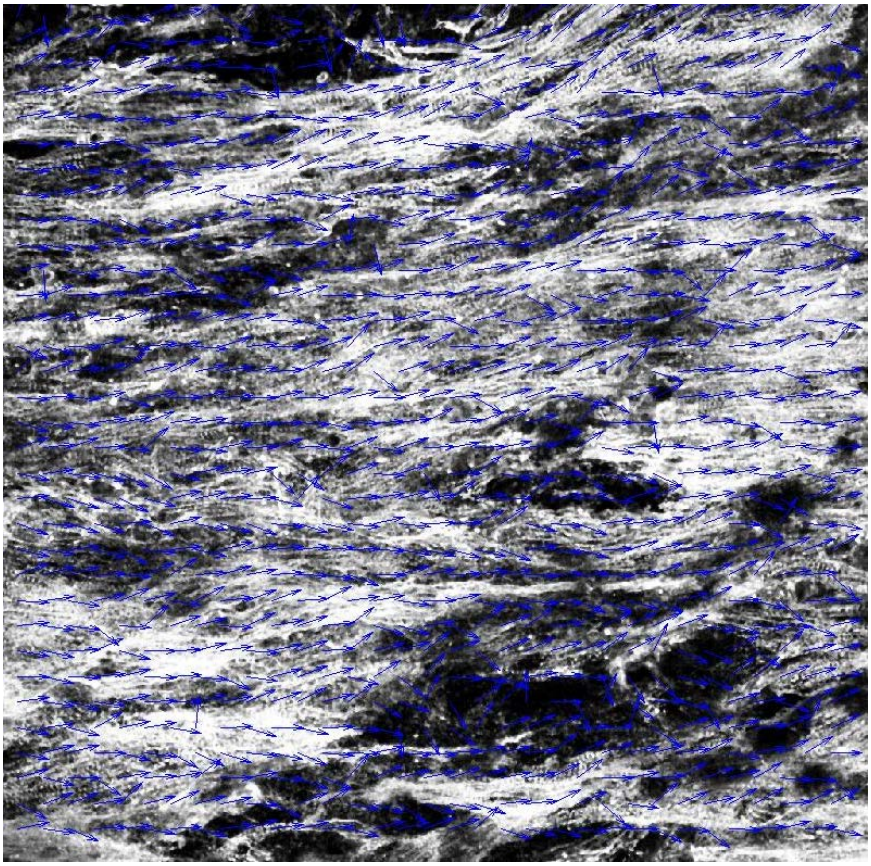

**Figure 19. Representative image of MATLAB analysis within actinin channel of stretched scaffolds.**

A histogram of the individual cell alignments was then plotted for each group of images over a range of 180°.

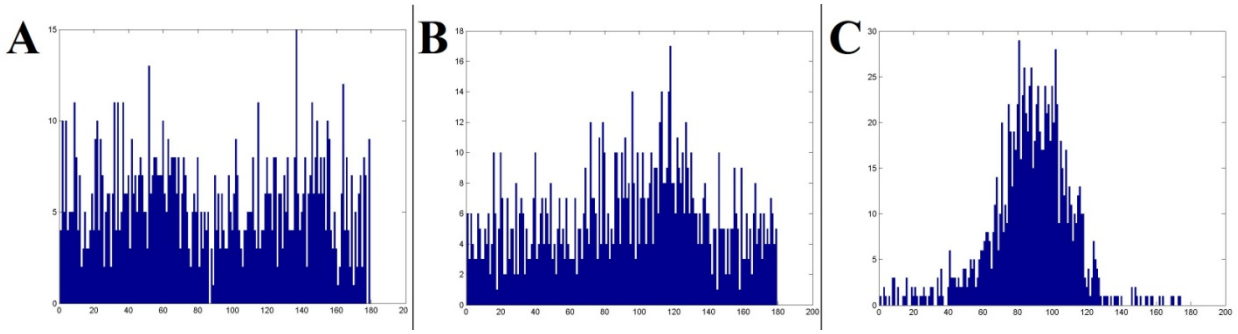


**Figure 20. Histogram plots of the number of (A) cardiomyocytes in culture, (B) cells attached to UBM scaffolds and held under static conditions, and (C) cells attached to UBM scaffolds and cyclically stretched over a range of 180°. The x-axis indicates the major axis angle of cell alignment and the y-axis indicates the number of cells at a particular angle. Cells in culture and held under static conditions appear to be randomly aligned and cells subjected to cyclic stretch are preferentially aligned in the direction of stretch. An angle of 90° signifies perfect alignment in the direction of stretch.**

Additionally, a normalized orientation index was calculated to further quantify the overall degree of alignment within each group.

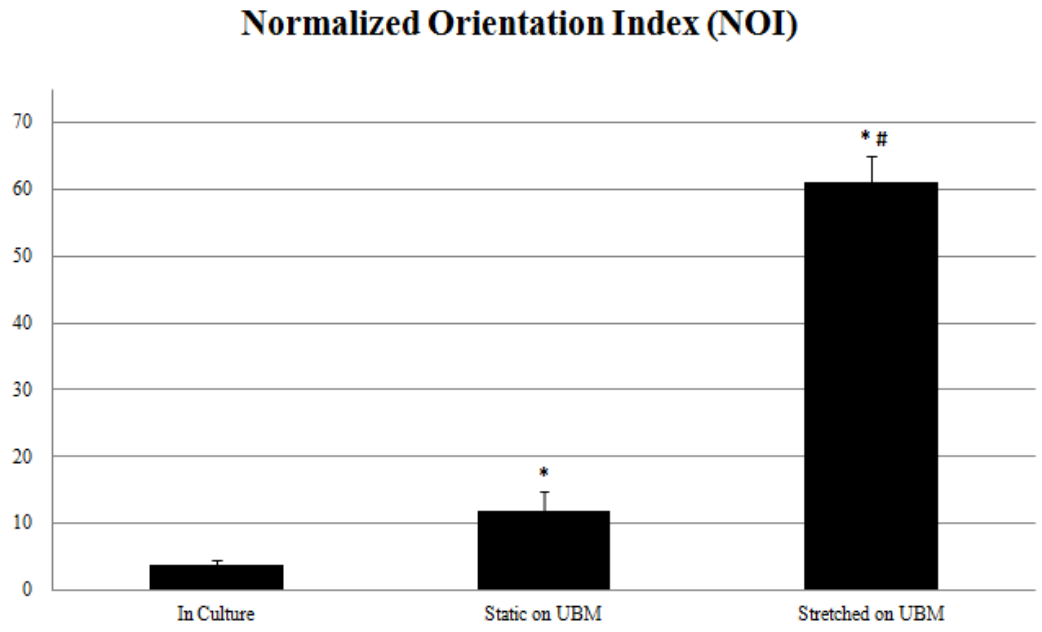


**Figure 21. Graph of normalized orientation index (NOI) for each culture group. Cells in culture had a NOI of 3.7% and statically held cells expressed a NOI of 11.9%, indicating that both populations of cells expressed a fairly random distribution. Cells subjected to cyclic stretch had a NOI of 61.1%, a five-fold increase in alignment when compared to cells under static conditions. *indicates a statistically significant difference when compared to cultured conditions and #indicates statistical difference from static conditions.**

Cells in culture expressed the lowest degree of alignment with a random distribution of cells and a NOI of 3.7 ± 0.7. Cells attached to UBM scaffolds and held under static conditions showed mild improvement in alignment with a NOI of 11.9 ± 3.0. A dramatic increase in alignment was observed within cells attached to UBM scaffolds and subjected to cyclic stretch, with a NOI of 61.1 ± 3.8. A statistically significant increase in alignment was observed in both groups cultured on UBM when compared to cells in culture, as well as a significant increase in alignment of cells subjected to cyclic stretch as opposed to static conditions.

### 3.3.4 Cell Contractility

Further analysis of cell-scaffold constructs was performed to investigate the ability to produce contraction and measureable forces. With limited ability to microscopically view cells attached to a robust scaffold material, fluorescent calcium analysis has been shown previously as a means to verify cell contraction. Cells in culture were easily visible, and showed spontaneous and synchronous beating patterns, albeit in no particular direction. Calcium transients analysis showed a pulsatile nature of light intensity, consistent with visible contraction patterns when stimulated with electrical pulses.

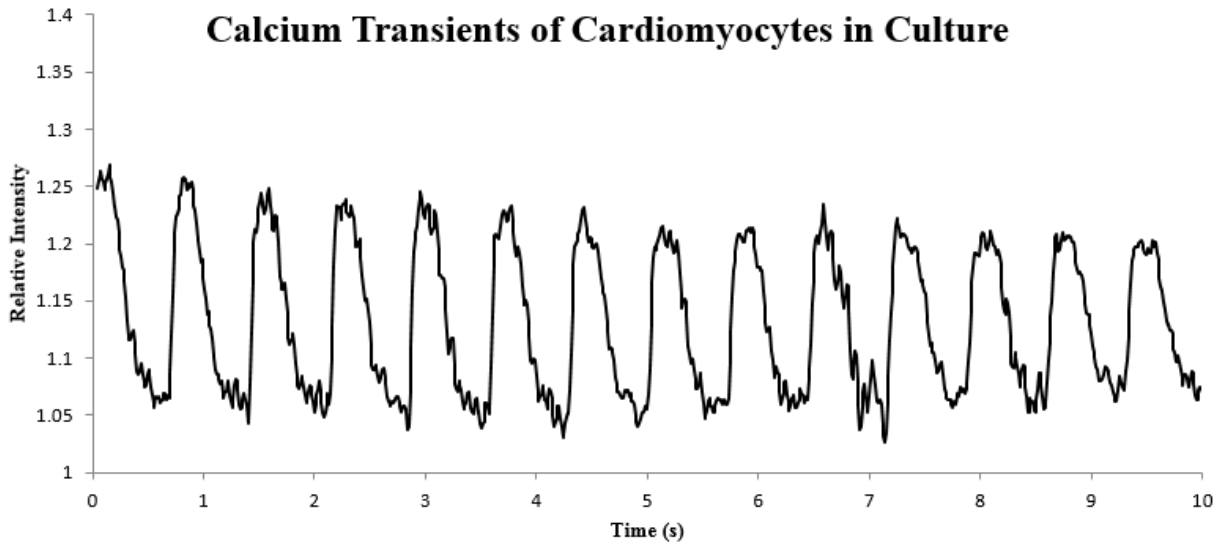


**Figure 22. Relative intensity of calcium fluorescence within cardiomyocytes in culture. Cells exhibited pulsatile calcium transients in culture, an indicator of cell health.**

Cells held under static patterns showed no visible signs of contraction or calcium transients. However, cells subjected to cyclic stretch expressed a similar pulsatile contraction pattern as cells

in static culture without attachment to UBM scaffolds. Calcium transients occurred at a slightly slower rate, and a degree of noise in the fluorescent signal was observed.

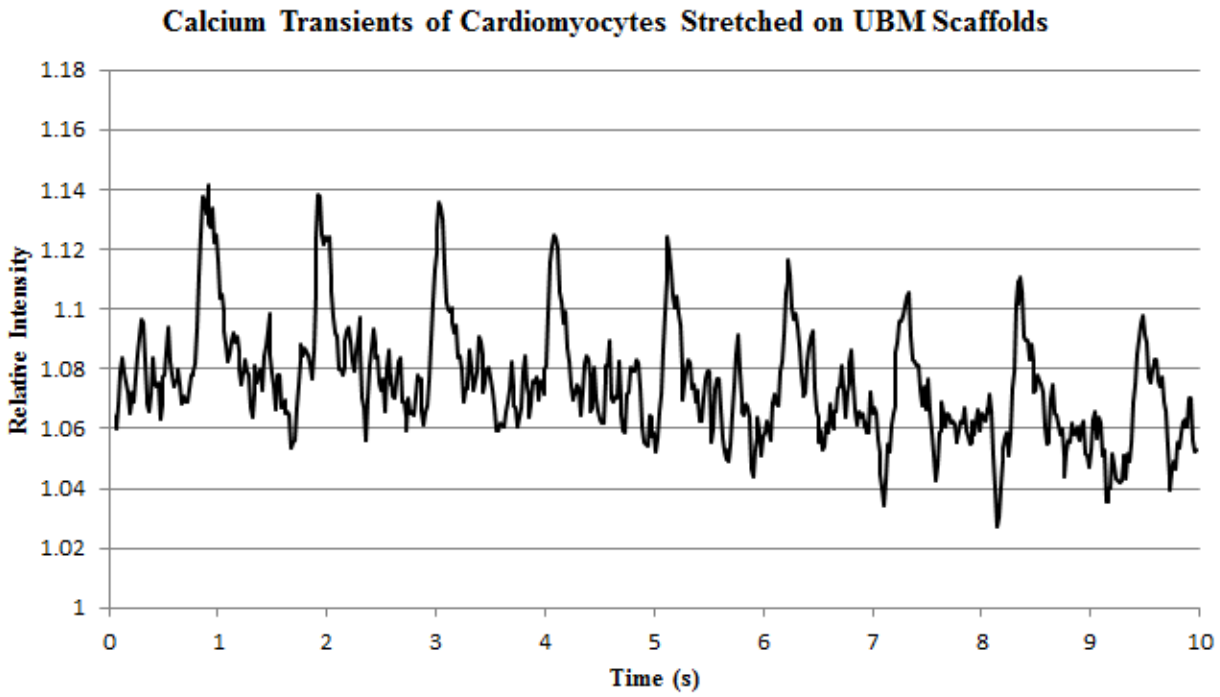


**Figure 23. Relative intensity of Calcium fluorescence within cardiomyocytes attached to UBM scaffolds following cyclic stretch. Cells exhibited pulsatile calcium transients for up to 24 hours following removal from cyclic stretch conditions.**

The level of noise could be attributed to the inability to maintain a constant focus on cells embedded within the UBM scaffolds during contraction. Brightfield microscopy was able to capture videos of cells and UBM scaffolds contracting in the direction of stretch when pulsed electrically. Cell-scaffold constructs were attached to a force measurement system to investigate the ability to produce forces. However, no measurable forces could be observed within any group.

## 3.4 DISCUSSION

The results from the present study show that a healthy, contractile tissue can be engineered using cardiomyocytes seeded onto UBM scaffolds and subjected to cyclic stretch. The resulting tissue expresses a highly aligned network of contractile cells with the ability to contract in a cyclic pattern, as evidenced through calcium transiets examination and brightfield imaging. Engineered tissues generated through the current methods lack the ability to generate measurable forces *in vitro*, although the contractions observed may occur on a scale that was not detectable with the available measurement system. The methods described in this study utilize a robust ECM material that has performed well in myocardial reconstructive applications previously without a cellular component. The addition of an appropriate cell population with an established communication network and the ability to contract may provide an appropriate platform for an engineered cardiac patch material in future studies.

The first approach of the present study investigated the ability to develop cell sheets for uniform surface coverage and easy attachment to UBM scaffolds. It was observed that the culture of cardiomyocytes on a temperature responsive surface supported visible cell contraction and intercellular communication through immunofluorescent staining. However, an effective means to successfully harvest the cell sheets and effectively attach and culture on UBM scaffolds could not be achieved. Upon release from the temperature responsive surface, cell sheets contracted significantly and did not allow for coverage of large surfaces. However, attachment of single cell suspensions directly onto UBM scaffolds yielded a healthier cell population, and the addition of mechanical strain to scaffolds increased the expression of contractile cell markers drastically.

Cells seeded directly onto scaffolds showed the ability to migrate and attach to the scaffold more effectively than in the sheet form. In addition, the cells establish intercellular junctions necessary for proper communication more effectively when attached as single cells. It is believed that cells first attach to the given substrate and subsequently establish intercellular connections. After cell sheets are released from their primary culture substrate and attachment to UBM scaffolds is attempted, cells will become uncoupled in order to attach to the introduced substrate. Further, because UBM scaffolds are comprised of a diverse fiber network that is not arranged in a single plane, cell will migrate to different locations throughout the thickness of the scaffolds. If the cells are introduced to this environment individually, it is thought that the cells are able to migrate as necessary and establish intercellular connections following the natural response to the matrix environment.

Cell alignment is extremely important toward the development of engineered contractile heart tissue. An engineered cardiac patch would be ineffective unless cells are able to align in a single direction and pulse simultaneously to generate force in a single direction. While the latter has shown promising results, methods to consistently produce the former have been ineffective to date. In the present study, a strategy was developed using contact guidance and mechanical strain to induce cellular alignment. Prior to isolation, UBM scaffolds were processed as previously described in order to align the collagen fiber topography and encourage cell alignment. Seeded scaffolds were also placed in a uniaxial stretch bioreactor to introduce mechanical strain, a mechanism that has shown the ability to maintain healthy cell phenotype and align cells unidirectionally. Immunofluorescent examination of cells in culture, cells attached to statically held UBM scaffolds, and cyclically stretched scaffolds showed an incremental increase in the health and alignment of cells.

The results generated in the present study to date suggest that cardiomyocytes are able to attach, align, and produce contraction within UBM scaffolds subjected to cyclic stretch. The present study was limited to *in vitro* culture and only included a primary cell population of cardiomyocytes. The maintenance of contractile nature of cells must be assessed in an *in vivo* setting to determine the efficacy of the current methods to produce an engineered cardiac patch material. Engineered contractile tissues were also unable to produce measurable forces. This observation may be attributed to the inherent stiffness of the UBM scaffolds and the inability of cells to produce contractile forces to overcome the stiffness of the scaffold. In another sense, the cells may have produced isometric contractions, but could not be measured within the UBM matrix. Translation of the described methods to a clinical setting would necessitate an alternative cell source. The present study utilized a well-established contractile cell line as proof of concept, but this cell line would not be available clinically. Future experiments using this technology would ideally utilize a stem cell source with the ability to differentiate toward a cardiomyocyte or smooth muscle cell lineage. This would allow for autologous cell isolation and culture prior to implantation, and would avoid concerns of immune rejection or future complications.

Future experiments are necessary to evaluate the *in vivo* host response and the ability for engineered contractile tissues to reconstruct myocardial tissue. An acellular UBM patch was shown in the previous chapter to support cardiomyocytes and contribute to the formation of newly formed muscle tissue in the right ventricle by 16 weeks after repair. However, it was not clear if function to the area of damaged tissue had been restored by this point. This study was also performed in a small animal model with a small (6mm) defect size. Translation of the results observed in this study to a larger animal model or a clinical application would be difficult, as patch size would play a large role towards the overall success of the study. The introduction of cellular

patches to a cardiac location has also historically resulted in a rapid clearance of implanted cells. Implantation of electrically coupled and contractile cells embedded within a robust patch may avoid this response; however, future work is necessary to determine cell survival within implanted patches.

# 4.0 EVALUATION OF ENGINEERED CONTRACTILE PATCHES IN RIGHT VENTRICLE OUTFLOW TRACT REPAIR

## 4.1 INTRODUCTION

The results observed in the first aim of this study expressed the ability for UBM to repair a full thickness defect in the myocardial wall and remodel into new host tissue by 16 weeks. However, in many preclinical and clinical studies, the choice of implanted material alone has been ineffective at repairing and replacing myocardium with functional tissue. Acellular cardiac patches have been largely unsuccessful due to the large demand placed on the surrounding native tissue to support cardiac function during repair. The success observed in the first aim was performed in a small animal model with a patch size of 6mm. Translation to a clinically applicable material would necessitate a much larger patch, and a cellular component may be necessary to ensure positive host response.

Currently, cell delivery options are crude and lead to low survival, retention, and incorporation into the surrounding native tissue. The ultimate success of an engineered patch material is largely based on the ability to electrically and mechanically couple with the native tissue in order to aid in heart tissue contraction. It has been previously shown that an engineered heart muscle (EHM) can be generated *in vitro* using cardiomyocytes embedded within ECM gels that show the ability to produce measurable contraction and preferential alignment of

cardiomyocytes [9]. EHM grafts were recently generated using the same methods using stem cells differentiated toward a cardiomyocyte lineage [16]. EHM grafts showed the ability to survive implantation and maintain healthy cell phenotype, but the study used a myocardial infarct model and did not show the ability to repair the myocardium.

A healthy, engineered tissue has been developed *in vitro* using a combination of methods to align cells and ensure proper cell health within a robust delivery system in the previous chapter. The previous aim was able to show that engineered tissues expressed the ability to align and contract in physiologically similar patterns. The addition of a healthy cellular component to a biologic scaffold material that has previously shown the ability to repair myocardial tissue may encourage cell survival and electrical coupling following implantation and ultimately allow for larger cardiac patches to be generated in future studies.

The goal of the current aim is to generate cell seeded cardiac patch materials using methods outlined in the previous chapter and evaluate their ability to repair a full thickness myocardial defect. An aligned, contractile tissue was previously developed using cells seeded onto aligned UBM scaffolds and cyclically stretched. Circular patches will be cut from these tissues and implanted to the right ventricle outflow tract (RVOT) of rats. Cardiac patches will also be generated from cardiomyocytes seeded onto UBM scaffolds and held under static conditions to determine the benefits of mechanical conditioning prior to implantation. In addition, a GFP(+) dermal fibroblast cell population will be isolated, seeded onto UBM scaffolds, and held under static conditions to generate a third group of cardiac patches. GFP control cells will be used to evaluate cell survival within the patch, as well as determine the paracrine effects of a non-cardiac cell population in myocardial repair.

## 4.2 MATERIALS AND METHODS

### 4.2.1 Study Design

Animals were anesthetized and intubated for right ventricle outflow tract reconstruction surgery as previously described [89, 146]. A small (2-5 mm) defect was created in the RVOT of chimera rats and subsequently patched with either a statically cultured (SC) or cyclically stretched (CC), cardiomyocyte seeded patch from aim 2, with a GFP+ fibroblast seeded UBM patch (SF) used as a control material (n=4 for cardiomyocyte seeded patches, n=2 for fibroblast seeded). The animals were monitored for 8 weeks following implantation. MRI examination of the reconstructed area took place at 4 and 8 weeks in all available animals for functional analysis. At the predetermined time point, animals were euthanized by injection of 1M KCl directly into the heart. The hearts were then removed and prepared for frozen histologic processing for staining with cardiac, endothelial, and macrophage specific cell markers.

### 4.2.2 Preparation of ECM Patches

Cardiomyocytes were isolated and cultured on UBM scaffolds as described in the previous chapter. UBM scaffolds had been scraped in a single direction prior to seeding and cells were cultured in silicone molds for an attachment period of 5 days. Constructs were inserted into a custom built uniaxial tissue stretching system and either held static or cyclically stretched for an additional 7 days. Following culture of cells, 6mm circular patches were cut from the center of stretched tissue (n=4 for each group), with consideration to the direction of stretch, and prepared for surgical implantation.

As a control group, dermal fibroblasts were isolated from GFP(+) rats as previously described using a primary explant technique [193, 194]. Cells were attached directly onto UBM scaffolds, allowed to attach for 5 days, inserted to a tissue stretch system, and cultured under static conditions for an additional 7 days. GFP(+) fibroblast seeded patches (n=2) were then cut and prepared for surgical implantation in a similar manner as cardiomyocyte seeded scaffolds.

### 4.2.3 Surgical repair of RVOT

Animals were prepared for RVOT reconstruction surgery as previously described [89, 146]. Anesthesia was induced by placing the rats in a small container with 3% Isoflurane in 2 L/minute of $O_2$. A 16G x 2" angiocatheter sheath was inserted in the trachea. Proper insertion of the intubation catheter was ensured through inflation of lungs with a small ambubag. A rodent ventilation system (SAR-830/P) was set at approximately 75 breaths per minute and approximately 700 cc air/minute. Hair was removed from the chest of the rat and the site was sterilized with Iodine. An initial injection of 10mg/kg lidocaine was delivered locally, and the Isoflurane was reduced to 1.5%-2%. A 5cm incision was made in the chest with a #10 scalpel, and a thoracotomy was performed to expose the heart. The ribs were held open with an Alm retractor. A purse-string suture (with diameter of 5.0 – 6.0 mm) was placed in the free wall of the right ventricular outflow tract (RVOT) with 7-0 polypropylene sutures. Both ends of the stitch were passed through a 22-gauge plastic vascular cannula, which was used as a tourniquet. The tourniquet was tightened and the bulging part of the RVOT wall inside the purse-string stitch was resected. The tourniquet was then briefly released to verify a transmural defect was created in the RVOT as indicated by severe bleeding. One of the proposed patches was then sutured along the margin of the purse-string suture with over-and-over sutures with 7-0 polypropylene to cover the hole in the RVOT. An attempt to align

the original direction of stretch of patches with the muscle fiber architecture in the RVOT was also made during implantation. After completion of suturing, the tourniquet was released and the purse-string stitch removed. The muscle layer was then closed with approximately 8 interrupted sutures (5-0 Surgipro). Prior to closure of the chest, the lungs were inflated to full capacity using a pediatric ambubag attached to the ventilator. Approximately 8 interrupted sutures were placed to close the skin and a local injection of 10mg/kg lidocaine was delivered. Additionally, a dose of 200mg/kg/day cefazolin was delivered to the thigh muscle, as well as 0.1mg/kg buprenorphine (buprenex), subcutaneously. Doses of cefazolin were delivered once daily for 3 days post-operative and buprenorphine was delivered twice daily for the same time period.

### 4.2.4 Cardiac MRI

Cardiac MRI (Horizontal bore 7-T MRI system, Bruker Biospin 70/30) was performed for detailed assessment of cardiac function of all hearts treated with UBM seeded patches. Animals were anesthetized with 1.5 to 2% Isoflurane in oxygen gas via nose cone during MRI imaging. Animal body temperature, heart rate, respiratory rate, and arterial oxygen saturation were continuously monitored using a vital monitoring system. The total scanning time for each animal was approximately 45 to 60 minutes. Under electrocardiogram and respiratory gating, right (left lateral image plane) and left ventricular (long and short axis image planes) wall motions were recorded by a FLASH cine image sequence. Cardiac MRI was performed at 4 and 8 weeks after UBM patch implantation and images were compared to those taken from a native heart. All videos detailed a minimum of one full cardiac cycle so that distinct measurements could be taken from the left and right ventricles throughout systole and diastole. Cardiac function was assessed by calculation of ejection fraction and end diastolic volume from the LV, as well as shortening fraction from RV

outflow tract where graft was implanted using OsiriX software. A repeated measures, two-way analysis of variance (ANOVA) was performed on all samples to determine significant differences ($p<0.05$) from native values for ejection fraction, RV shortening fraction, and LV end diastolic volume.

### 4.2.5 Specimen Processing

At 8 weeks after surgery, all animals were euthanized by injection of 5mL of 1M KCl directly into the heart. The hearts were then removed and fixed in 4% paraformaldehyde for 24 hours. Hearts were then moved to 30% sucrose for another 24 hours. The hearts were then cut in half through the patched area, frozen in OCT solution at -80°C, and sections were cut at 8μm thickness and placed onto slides for future staining. Masson's Trichrome staining was performed to analyze the collagen and cell presence within each specimen prior to immunofluorescent staining.

### 4.2.6 Immunofluorescent Staining

All specimens were permeabilized with 0.1M glycine, 0.5% Triton X-100 in PBS for 15 minutes. The specimens were then washed five times in 1X PBS and then incubated with 1% goat serum for 1 hour. After the hour, the specimens were again washed three times in 1% BSA. The primary antibodies (α-actinin (Sigma Aldrich, A7811), connexin 43 (Abcam, ab11370), von Willebrand factor (Abcam, ab6994), and GFP (Invitrogen, G10362)) were then added and incubated for two hours at room temperature and then washed five times in 1% BSA. After these washes, the secondary antibodies (AlexaFluor A21125-594 and AlexaFluor A11008-488, respectively) and Draq5 for nuclear staining were added and incubated for another two hours. Hoechst (1mg/100mL)

solution was then added for 30 seconds and then washed five times in 1% BSA. Slides were covered in mounting medium, coverslipped, and sealed until imaging.

### 4.2.7 Macrophage Phenotype Analysis

Macrophage staining was performed on samples in order to describe the immune response of the ECM patches as recently described [4, 176]. Antibodies for CD68 (pan-macrophage), CD86 (M1), and CD206 (M2) were used for an investigation of the M1 and M2 macrophage phenotypes. Prior to staining, UBM patched hearts that had been seeded with GFP+ fibroblasts were submerged in a solution of methanol to quench the GFP signal. After the elimination of GFP signal was verified, slides were washed in PBS and then incubated in a blocking serum consisting of horse serum, BSA, Triton X-100, and Tween 20. Blocking solution was removed and a 1:150 dilution of mouse anti-rat CD68, rabbit anti-CD86, and goat anti-CD206 antibodies in blocking solution was added to the slides at 4°C overnight. The following day, the slides were washed in PBS three times to remove primary antibodies. Secondary antibodies were added to blocking solution at the following concentrations; donkey anti-goat AlexaFluor 488 and donkey anti-mouse AlexaFluor 594 (1:200), donkey anti-rabbit Perp Cy5.5 (1:300). Secondary antibodies were added to the slides and allowed to incubate at room temperature for 1 hour. Slides were washed three times in PBS to remove the secondary antibody. Mounting media with DAPI and coverslips were then added to each slide prior to imaging.

## 4.3 RESULTS

### 4.3.1 Surgical Outcomes and Gross Examination

Prior to implantation, UBM patches measured approximately 0.25mm in thickness. Intra-operative and post-operative mortality associated with the surgical procedure in all groups was 16.7%. The patches replaced approximately 25% of the RV wall in both groups and suture lines indicated the original placement of the scaffold up to the 8 week time point.

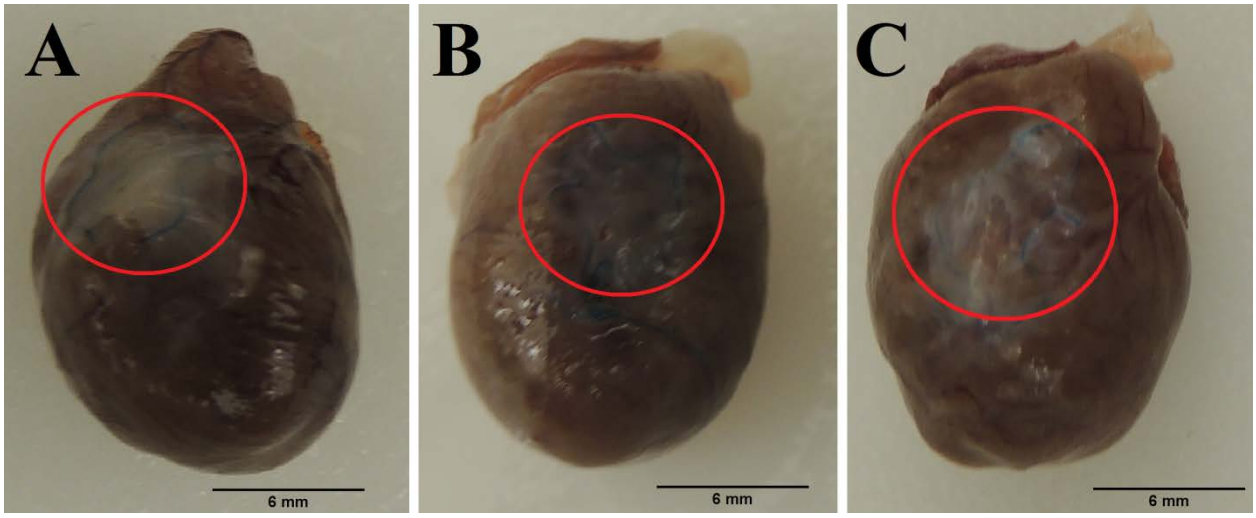


**Figure 24. Macroscopic images of the patched area of rat hearts at 8 weeks after implantation. (A) Statically cultured CM-seeded patches and (C) statically cultured fibroblast seeded UBM patches retained a whitish appearance and preserved the native thickness of the ventricle wall through the end point of the study. (B) Cyclically stretched CM-seeded patches appeared to be incorporated into the native tissue and the original white color of the patches was not evident. Scale: 6mm.**

Statically cultured (SC) cardiomyocyte seeded patches were incorporated into the native tissue by 8 weeks. The patches retained a whitish appearance through the 8 week time point, with minor indications of revascularization based on gross examination. Stretched UBM patches (CC) were completely incorporated into the native tissue by 8 weeks after RVOT repair surgery. The original white color of the patch was not evident upon explant, which was a preliminary indication that the patch supported host cell infiltration and revascularization. Fibroblast seeded patches (SF) retained much of the original white color through the end of the study. The patched area, as indicated by suture lines and tissue color, was larger than the original 6mm size of the patch, indicating that there may be dilation of the RV.

### 4.3.2 MRI and Cardiac Function

Cardiac left ventricular ejection fraction of statically held UBM patched hearts were slightly reduced at 4 weeks after reconstruction, however, LV function was largely maintained throughout the study. RV shortening fraction was significantly different from native values at 4 weeks, however, a return toward normal left ventricular ejection and RV shortening values was observed by 8 weeks.

**Table 2. Left ventricle ejection fraction, right ventricle shortening fraction, and LV end diastolic volume of reconstructed hearts.**

**LV Ejection Fraction**

| | 4 weeks | 8 weeks |
|---|---|---|
| Native | 69.98 ± 0.15 | 69.98 ± 0.15 |
| Fibroblast | 66.15 ± 1.48 | 62.0 ± 0.57* |
| Static | 67.90 ± 0.29 | 68.18 ± 0.05 |
| Stretched | 68.43 ± 0.43 | 69.03 ± 0.67 |

* denotes statistical difference from Native values ($p < 0.05$)

**RV Shortening Fraction %**

| | 4 weeks | 8 weeks |
|---|---|---|
| Native | 35.26 ± 7.96 | 35.26 ± 7.96 |
| Fibroblast | 28.54 ± 3.38* | 34.98 ± 11.41* |
| Static | 41.23 ± 3.80* | 35.99 ± 4.21 |
| Stretched | 33.12 ± 3.36 | 34.77 ± 4.55 |

* denotes statistical difference from Native values ($p < 0.05$)

**LV End Diastolic Volume ($cm^3$)**

| | 4 weeks | 8 weeks |
|---|---|---|
| Native | 0.198 ± 0.25 | 0.198 ± 0.25 |
| Fibroblast | 0.297 ± 0.09* | 0.259 ± 0.04* |
| Static | 0.221 ± 0.04* | 0.204 ± 0.06 |
| Stretched | 0.176 ± 0.04 | 0.177 ± 0.04 |

* denotes statistical difference from Native values ($p < 0.05$)

A significant increase in LV end diastolic volume was observed following reconstruction at 4 weeks as well. There was no RV outflow tract obstruction observed due to patch implantation, however, minor dilation of the LV and RV could be observed at 4 weeks.

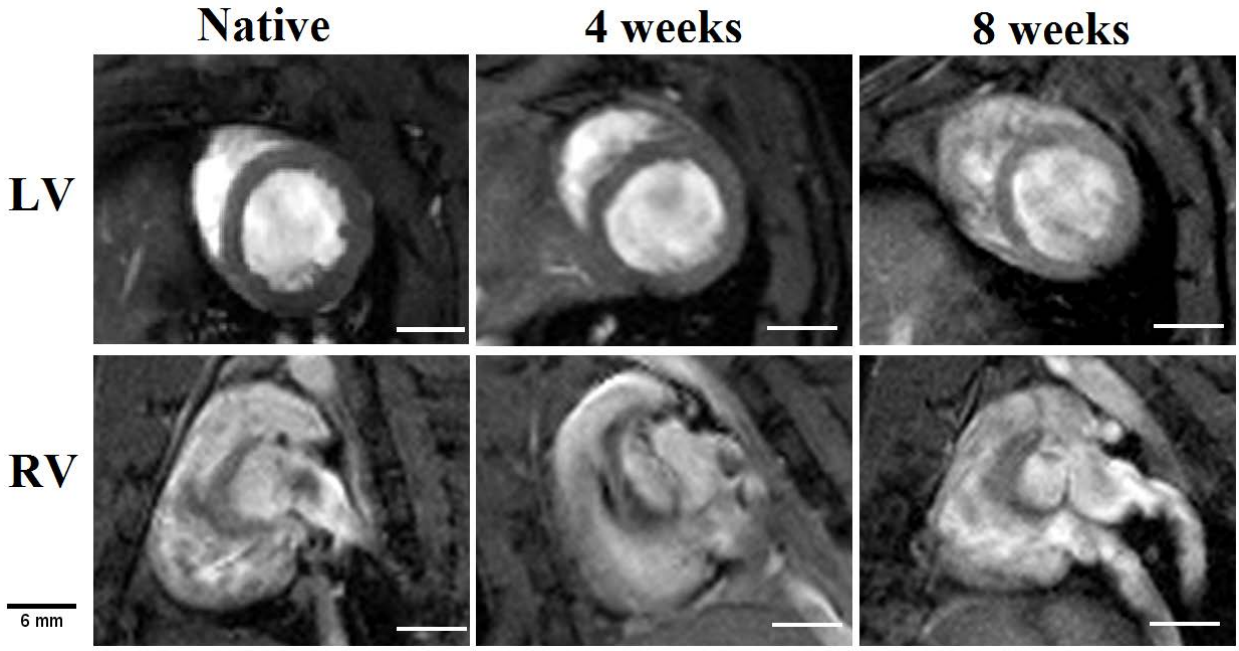


**Figure 25. SC UBM patched hearts showed minimal geometric changes in the RV and LV when compared with native hearts that had not undergone surgery. The LV of reconstructed hearts maintains its native circular shape, indicating minimal pressure changes within the ventricle after repair, and minor dilation of the LV and RV could be observed at 4 weeks.**

Cardiac ejection fraction of CC UBM patched hearts was slightly lower at 4 weeks after implantation. By 8 weeks after repair, a complete return toward native ventricular ejection values was observed. Likewise, the RV shortening fraction was minimally compromised at 4 weeks, and by the end of the study it had also returned to native values. No geometric changes were observed in the LV of hearts, as observed from MRI images and calculated end diastolic volume, as well as the RV, suggesting that no RV outflow tract obstruction or dilation was seen by patch implantation.

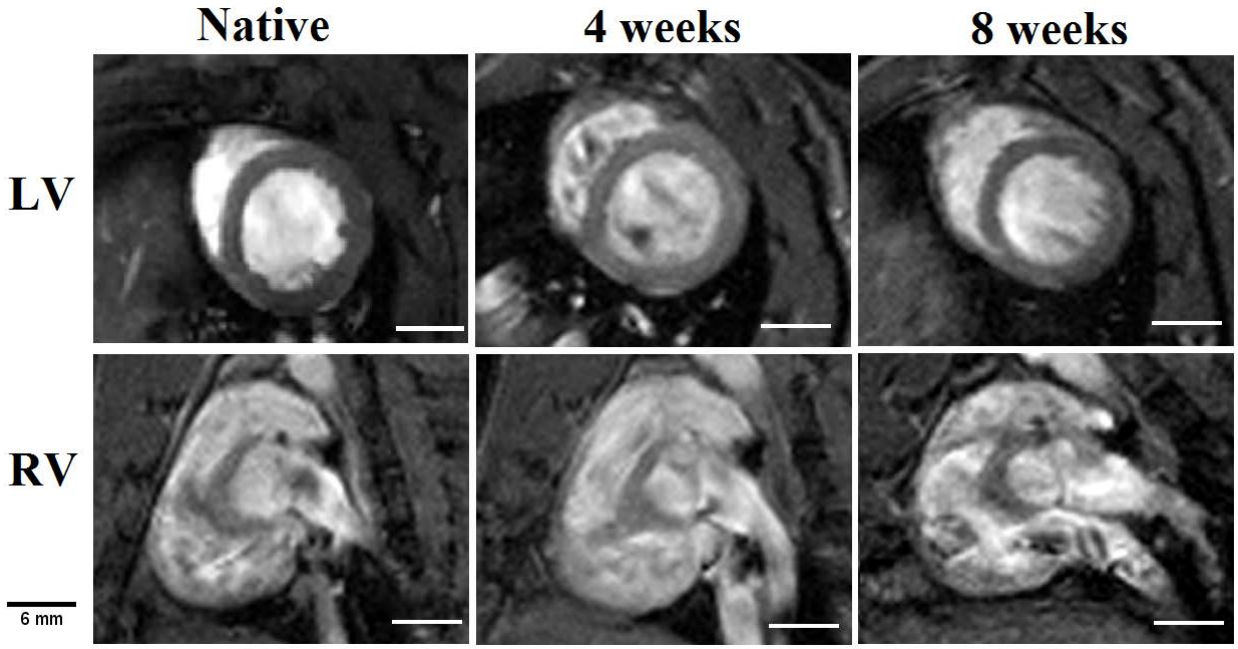


**Figure 26. CC UBM patched hearts showed no geometric changes in the RV and LV when compared with native hearts that had not undergone surgery. The LV of reconstructed hearts maintains its native circular shape, indicating minimal pressure changes within the ventricle after repair.**

A different trend was observed in the functional analysis of the SF patches. LV ejection fraction was lower at 4 weeks after implantation, however, by 8 weeks it had decreased significantly ($p<0.05$) from native values. Likewise, the RV shortening fraction and LV end diastolic volume of hearts were significantly compromised at 4 weeks, although by 8 weeks, the values had slightly returned toward native values. In addition, observation of MRI images indicated a dilation of the RV at both 4 and 8 weeks after implantation.

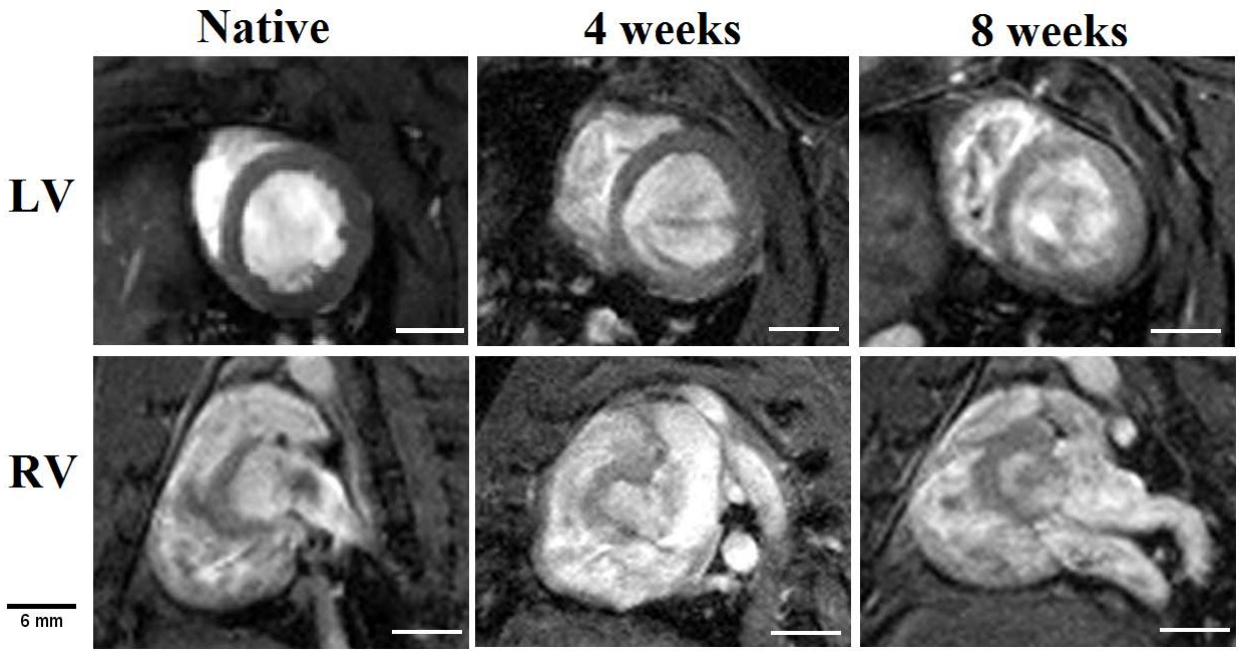


**Figure 27. SF UBM patched hearts showed dilation of the RV and LV at both 4 and 8 weeks when compared with native hearts that had not undergone surgery. The LV of reconstructed hearts dilated to a lesser degree than the RV at both time points, and no RV obstruction could be observed.**

### 4.3.3 Histologic Analysis

Histologic examination of reconstructed hearts was performed using Masson's Trichrome at 8 weeks after repair for all patches. By the end of the study, all patches had been incorporated into the native tissue and the presence of collagen remained at the site of patch implantation throughout the study.

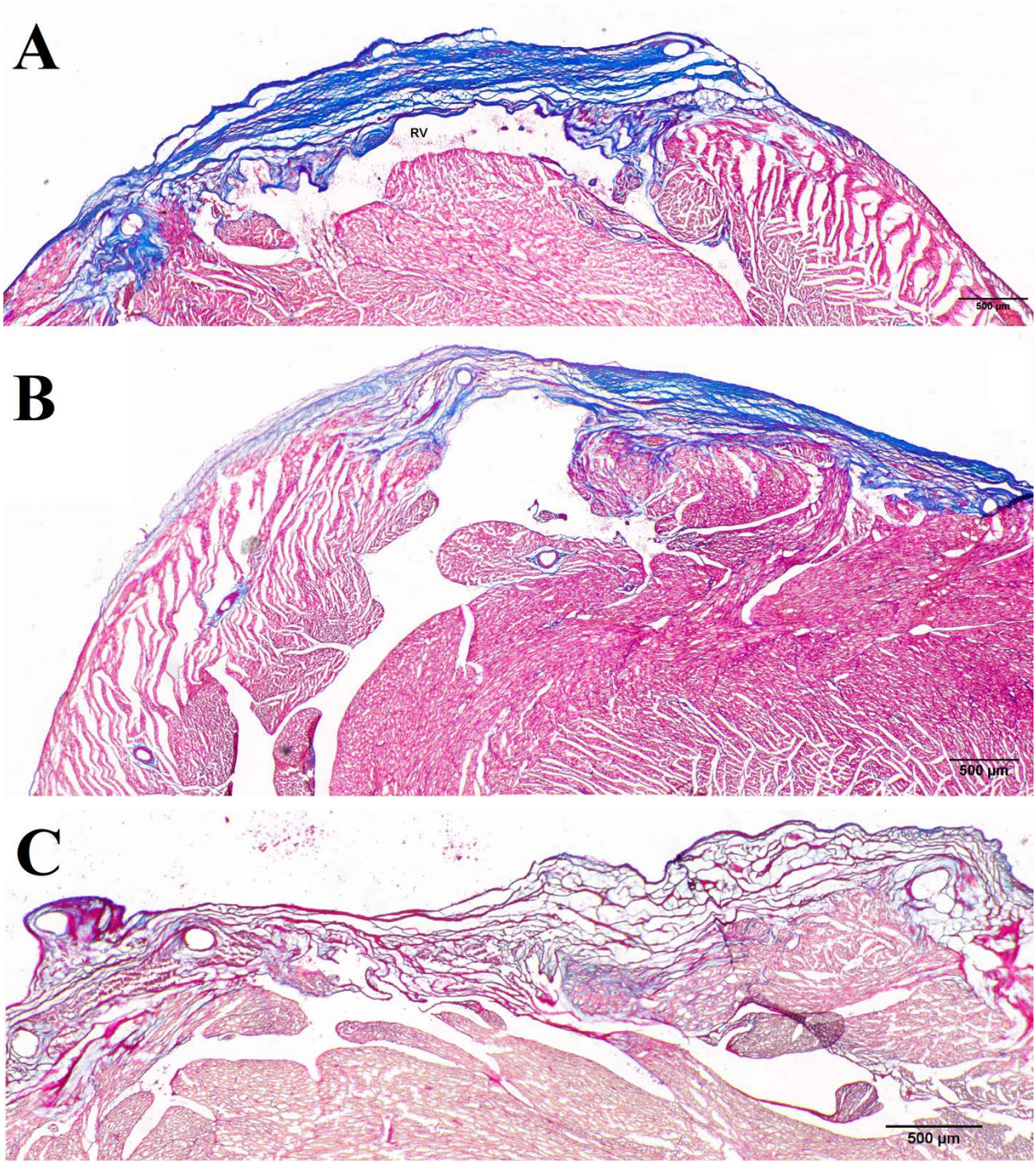


**Figure 28. Histological examination of seeded UBM patches using Masson's Trichrome at 8 weeks. All patches are incorporated into the native tissue by 8 weeks. (A) SC patches, (B) CC patches, and (C) SF patches remained visible at 8 weeks. Scale indicates 500µm.**

The scaffolds were easily observed at and the reconstructed area of the RVOT remained highly collagenous in all groups. The section of the ventricular wall repaired by the scaffolds appeared to be slightly thinner than the surrounding native wall. Minimal dilation was evident in the RV of both cardiomyocyte seeded patches, while fibroblast seeded patches appeared to dilate the RV. In addition, fibroblast seeded patches appeared to contribute to the formation of granulation tissue in the patched area.

Immunofluorescent examination of cardiac specific markers within all hearts was performed to identify the presence of cardiomyocytes and gap junction connections between cells, as well as determine the presence of an endothelial lining along the repaired wall of the RV. In addition, staining was performed to identify the presence of GFP+ cells within fibroblast seeded patches and determine if cells were able to survive implantation. In all patches, cellular presence could be observed by 8 weeks after RVOT repair, although cells within cardiomyocyte seeded patches greatly outnumbered those within fibroblast seeded patches.

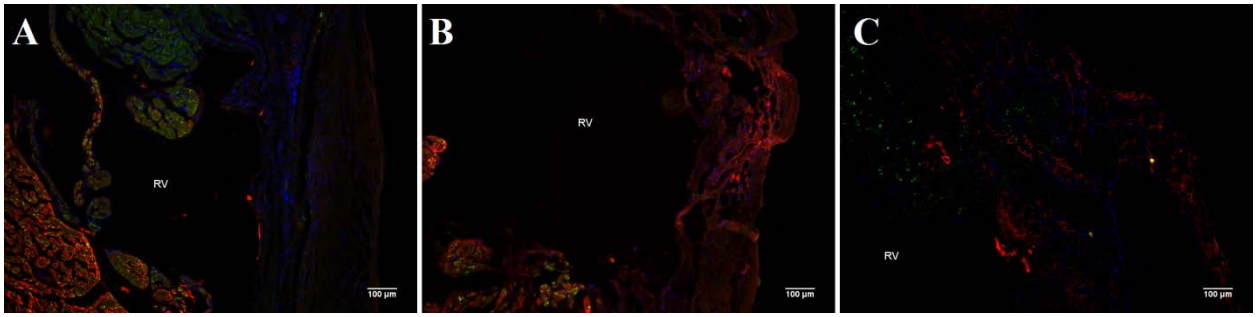


**Figure 29. Immunofluorescent examination of C-ECM patches for cardiac specific markers at 8 weeks after reconstruction. (A) SC and (B) CC patches showed cellular presence (draq5, blue) with intermittent staining for α-actinin (red) and connexin 43 (green). (C) Cells could be observed within SF patches, but no positive staining for cardiac markers was observed. 10x, Scale: 100um.**

SC patches showed minimal staining for α-actinin, as well as no positive staining for connexin 43. CC patches expressed similar levels of cellular presence and minimal staining for both α-actinin and connexin 43. Fibroblast seeded patches did not express either marker and there was a significantly lower presence of cells. In addition, the surrounding native tissue appeared to be affected negatively by patch implantation, with areas of interrupted α-actinin and connexin 43 expression. Cells that had accumulated along the endocardial surface were confirmed as endothelial cells through von Willebrand factor (VWF) staining in both statically cultured and stretched patches.

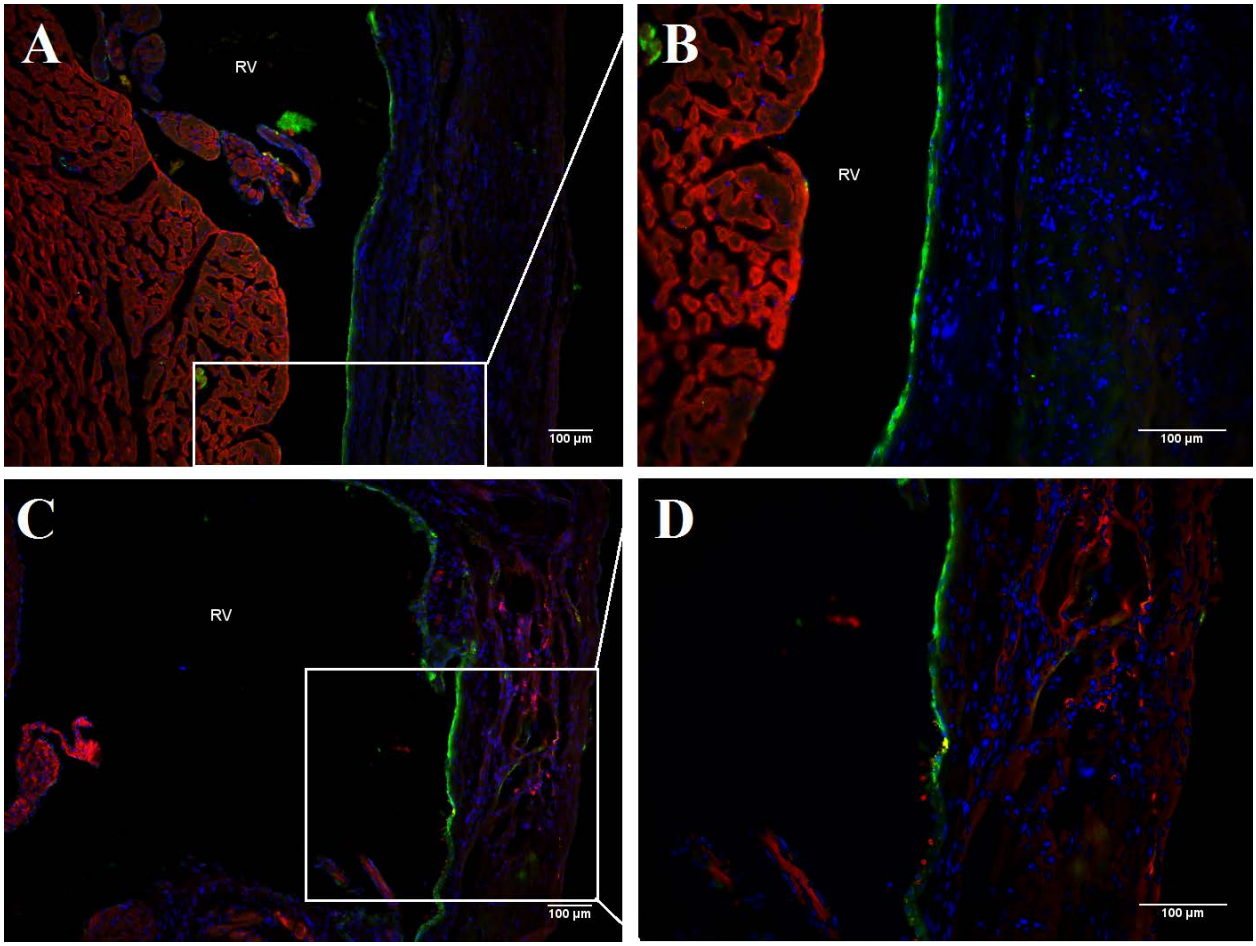


**Figure 30. A continuous endothelial lining along the endocardial surface was observed in statically held UBM patches (A,B) and stretched UBM patches (C,D), as evidenced by von Willebrand factor staining (green). (Blue- draq5, Red- α-actinin) Images A and C: 10x, Images B and D: 20x, Scale indicates 100µm.**

No evidence of an endothelial lining was observable within SF patches. GFP examination of fibroblast seeded patches showed the complete absence of GFP signal at 8 weeks after implantation, suggesting a clearance of implanted cells.

All scaffolds were analyzed for macrophage response at the 8 week time point to determine the host immune response to the patches.

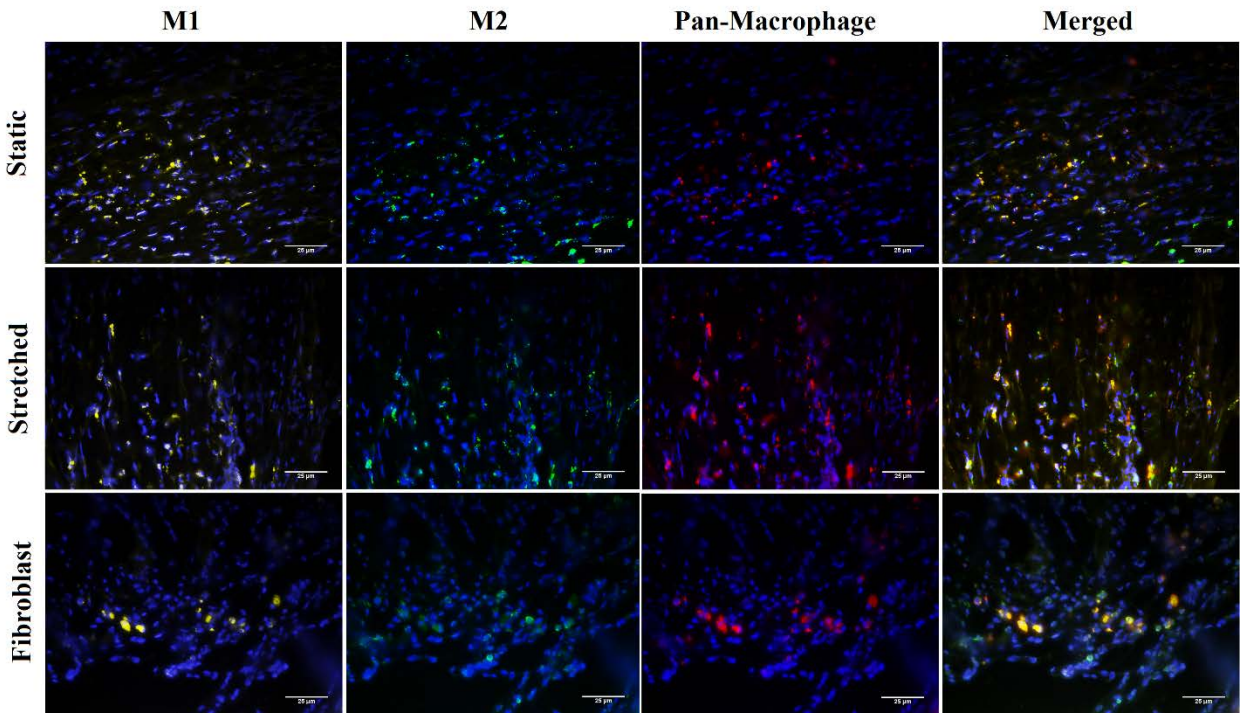


**Figure 31. Macrophage phenotype analysis of seeded ECM patches at 8 weeks after surgery. Macrophages had completely penetrated the patches and expressed a mix of M1 and M2 cells. M1 macrophages (CD86-yellow, draq5-blue), M2 macrophages (CD206-green), pan-macrophage (CD68-red), and combined image. Scale indicates 25 µm.**

Macrophages had penetrated the thickness of all patches and expressed a mix of M1 and M2 cells. Cardiomyocyte seeded patches expressed a uniform distribution of macrophages throughout the thickness of the patches. There were distinct spatial differences in the macrophage response at the interface with native tissue, which consisted of primarily an M1 type macrophage response, and the endocardial surface of the material, which consisted of a predominantly M2 type macrophage response, although both were observed throughout the patches. Fibroblast seeded patches expressed a primarily M1 macrophage response, with a large number of cells localized near the interface with native tissue. However, within the center of patches a mixed M1/M2 response was observed, similar to cardiomyocyte seeded patches.

## 4.4 DISCUSSION

The results from the present study show that cardiomyocyte seeded UBM patches possess the ability to repair a full thickness defect in the RVOT and support the infiltration and presence of cells. Using a primary endpoint of 8 weeks, cardiomyocyte seeded patches were able to develop an endothelial lining and withstand the mechanical environment of the RV. Both groups showed indications of integration into the surrounding native tissue and the restoration of native cardiac function by the end of the study. In addition, stretched scaffolds were able to maintain normal cardiac function throughout the study and appeared to show preliminary indications of communication with the surrounding native tissue. Fibroblast seeded patches did not produce similar results in the present study, exhibiting a deterioration of cardiac function, dilation of the RV, and the formation of granulation tissue. No GFP+ cellular presence could be observed, indicating a rapid cellular clearance from the implanted patch and an inflammatory acute immune response. While fibroblast seeded scaffolds expressed cellular presence by the end of the study, no cardiac markers could be observed and it was likely that the area was fibrotic.

As stated previously, the current methods of cell delivery to an area of damaged myocardial tissue are ineffective and typically result in low cell survival, retention, or incorporation into the surrounding native tissue. Many approaches are focused on direct injection of cells to the area, allowing for a highly localized and accurate distribution of cells. Cellular injection also allows for a large number of cells to be implanted simultaneously. However, in many cases, very few cells are retained within the myocardium after injection, and this approach is unable to repair a critical defect in the tissue itself. Other approaches have attempted to engineer heart tissue for implantation using a more robust delivery system with a cellular component. Many of these studies have been

unsuccessful due to the inability of the scaffold material to degrade and remodel towards functional host tissue following implantation. Another significant challenge has been the development of an appropriate model to investigate the efficacy of engineered tissues. While many studies opt for a myocardial infarct (MI) model, the implantation techniques for tissue tend to be superficial. In many clinical instances, this method may be sufficient, but will not describe the applicability to repair and replace myocardial tissue and respond appropriately to the pressures of the cardiac cycle.

Acellular urinary bladder matrix scaffolds have shown the ability to repair a full thickness defect in the RVOT of rats. By 16 weeks after implantation, UBM patches had been completely degraded and replaced with site-appropriate tissue. However, this was performed with a small (6mm) patch size, and the need to repair larger defects in a clinically applicable model may not produce similar results using an acellular patch. A cellular component may therefore be necessary to speed cardiac recovery time and restore function to the area of repair. However, as previously stated, maintaining adequate cell survival upon implantation has been difficult to date. A healthy, engineered tissue has been developed *in vitro* to ensure proper cell health within a robust delivery system prior to implantation. The present study sought to determine whether cardiomyocytes could survive implantation when embedded within UBM scaffolds, and if there were potential benefits to the implantation of a healthy, contractile tissue.

In order to provide myocardial support after implantation, it is essential that a cardiac patch material is able to maintain contractile structures within cells, as well as exhibit the capacity to couple electrically to the native tissue. The present study used a primary endpoint of 8 weeks, and by the end of the study, cardiomyocyte seeded UBM patches showed results that were similar to acellular patches. While there were few areas of cardiomyocyte presence, scaffolds were

highly cellular with a uniform distribution. In addition, a continuous endothelial lining had developed along the interface with the RV. Following repair with acellular patches, the interface between UBM patches and native tissue was fairly pronounced by 8 weeks. Within the native tissue at the interface with acellular patches, a slight interruption of connexin 43 could be observed, although sarcomere structure was unaffected. In the present study, the native tissue surrounding statically cultured patches showed healthy cardiomyocyte presence, although the connexin 43 expression appeared to be slightly interrupted. Similar to acellular patches, the interface between the native and patched areas was also very distinguished. In contrast, the native tissue surrounding stretched UBM patches maintained healthy sarcomere structure and high levels of polarized connexin 43 staining, with small areas of cells extending into the interface area, making the boundary of the patches unclear and suggesting preliminary patch remodeling. GFP+ fibroblasts were used as a control group to investigate cell retention within implanted patches and determine any potential paracrine effects of a non-cardiac cell line. Fibroblast seeded patches did not express any cardiac markers and resulted in the formation of granulation tissue, which is an indication that cell choice is a strong predictor of the fate of the implanted tissue.

The observations generated in the present study may be attributed to the results from previously performed *in vitro* studies, as well as the mechanical environment of the heart. Based upon the results obtained in Aim 2, cardiomyocytes maintained a normal phenotype to a higher degree when subjected to cyclic mechanical stretch in patterns that mimic normal cardiac contraction. It is logical that a tissue produced by these means would therefore respond to cardiac implantation more appropriately than a scaffold seeded with fibroblasts. If a patch material was desired to repair an organ with a less dynamic mechanical environment, the same results would not have been observed. However, because cardiomyocytes are contractile by nature, they may

have preferentially responded to the cardiac environment over fibroblasts. Conversely, fibroblasts may have performed better in a body wall or a more fibrous tissue repair setting.

While the results observed are promising, the present study was performed as a pilot study with acknowledged limitations and necessitating future experiments. A primary limitation to the present study was the use of a single time point that was unable to observe the acute (4 weeks) and long term (16 weeks) cellular presence within patches. Therefore, a direct comparison to acellular UBM patches could only be made at a single time point. Preliminary indications suggest that stretched cardiomyocyte seeded UBM patches may provide advantages to acellular patches based on MRI data and mild differences in histologic results. However, future studies are necessary to observe differences at 4 and 16 weeks. Another limitation of the present study was the use of GFP labeled cells and the limitation to a single experimental group. While no GFP presence could be observed in fibroblast seeded patches, this observation could be attributed to the cell type and would not necessarily translate to cardiomyocyte seeded patches. It is unclear whether the cells within cardiomyocyte seeded patches were implanted or originated from the host tissue. Future studies are necessary to determine the fate of implanted GFP+ cardiomyocytes within static and stretched UBM patches.

As stated previously, translation of the described methods to a clinical setting would necessitate an alternative cell source, as autologous cardiomyocytes are not easily acquired or cultured. Previous studies have shown the ability to differentiate stem cells toward a cardiomyocyte or smooth muscle cell lineage [16]. The use of an autologous stem cell source would avoid concerns of an adverse immune response when used in a clinical setting. However, future studies are necessary to investigate the ability to isolate, differentiate, and culture stem cells under similar conditions as cardiomyocytes in the present study.

The results generated in the present study to date suggest that cardiomyocyte seeded UBM patches are able to repair a full thickness defect in the RVOT for up to 8 weeks. Stretched patches were observed to provide mild benefits over statically held patches, although both groups showed functional and histologic advantages over fibroblast seeded patches. Cardiomyocyte seeded patches were able to incorporate into the surrounding tissue by 8 weeks, with the restoration of cardiac function and the presence of an endothelial lining. The ability of a seeded UBM patch to maintain normal cardiac function and avoid a fibrotic response is not a trivial observation. Following implantation, ECM scaffolds are either encapsulated, become incorporated into the surrounding tissue, or follow a remodeling response. The fate of implanted ECM materials is primarily dictated by the host acute immune response. Cell-seeded scaffolds traditionally elicit an inflammatory response, directing the scaffolds toward a fibrotic response or initiating foreign body encapsulation. In the present study, fibroblast seeded UBM patches expressed the formation of granulated fibrotic tissue by the end of the study. However, cardiomyocyte seeded patches appeared to be incorporated into the surrounding native tissue, with preliminary indications of remodeling in stretched scaffolds. Further studies are necessary to investigate the long term host response to seeded patches, but the present study was able to show that the previously anticipated adverse host response could be avoided in a cardiac location.

# 5.0 DISSERTATION SYNOPSIS

## 5.1 MAJOR FINDINGS

The present work described efforts towards engineering contractile tissue from extracellular matrix scaffolds for use as a cardiac patch material. The approach taken in the current study began through choosing an appropriate acellular platform with the ability to repair cardiac tissue as a basis for a contractile tissue. Previously held beliefs that organ specific C-ECM patches provided the most appropriate scaffold for cardiac tissue repair were tested against a commonly used, clinically available, and heterotopically derived UBM patch. C-ECM and UBM patches were used to repair a full thickness defect in the right ventricle outflow tract of GFP chimera rats to identify the role of the bone marrow and the source of repopulating cells. The culture of a cardiac-specific contractile cell line was tested on UBM scaffolds *in vitro*, and the effects of contact guidance and mechanical stretch were investigated as a means to align cells and promote cell health. Contractility markers were identified and cell-scaffold constructs were characterized *in vitro*. Finally, engineered contractile tissues were tested *in vivo* for their ability to enhance the functional restoration of repaired cardiac tissue as well as promote mechanical and electrical coupling with surrounding native tissue.

The following are the major findings of the present work:

**Specific Aim 1**

- GFP chimera rat population was generated through bone marrow transplantation.
- UBM and C-ECM patches able to support mechanical function up to 16 weeks.
    a. Minor impact was observed on LV and RV geometry.
    b. Few differences observed in functional assessment of hearts.
- Repopulating cells are derived from bone marrow, but are not only cells to infiltrate both patches.
- UBM patches exhibit remodeling response.
    a. Replacement with muscle tissue and striated cardiomyocytes by 16 weeks after repair.
    b. Cardiomyocytes within patched area not associated with GFP cells.
- C-ECM patches are integrated into surrounding tissue but do not remodel.

**Specific Aim 2**

- Cyclic mechanical stretch and contact guidance can promote a robust engineered contractile tissue *in vitro*.
- Cyclic stretch of cells attached to UBM scaffolds promotes cell alignment.
- Direct seeding of single cell suspensions onto UBM scaffolds maintains healthy cell phenotype better than cell sheets.

**Specific Aim 3**

- Cardiomyocyte seeded patches can maintain normal ejection fraction, ventricular geometry, and heart function after implantation.
- Cardiomyocyte seeded patches express a continuous endothelial lining within the right ventricle by 8 weeks after repair.
- UBM patches are evident at 8 weeks and minimal positive staining was observed for cardiac specific cells.
- Fibroblast seeded patches are able to repair a defect in the RVOT, but result in the formation of granulation tissue and compromise overall cardiac function.

## 5.2 OVERALL CONCLUSIONS

A full thickness defect was created in the RVOT of GFP chimera rats and repaired using UBM and C-ECM patches. Both UBM and C-ECM patches each were able to support rapid cell infiltration with a large GFP(+) cell presence. By 16 weeks, UBM patches had degraded and were replaced with areas of new muscle tissue. In contrast, C-ECM scaffolds did not show indications of newly formed muscle tissue and was incorporated into the surrounding native myocardium.

Cardiomyocyte seeded UBM constructs were cyclically stretched for up to 8 days in culture and cells preferentially aligned in the direction of stretch, showed calcium transients pulsations in similar patterns to cells in culture, and expressed striated actinin phenotype and healthy cell-cell connections. Cell seeded UBM patches possessed the ability to repair a full thickness defect in the RVOT and support the presence and infiltration of cells. Cardiomyocyte seeded patches were able

to develop an endothelial lining and withstand the mechanical environment of the RV, as well as integrate into the surrounding native tissue. In addition, stretched scaffolds appeared to show preliminary indications of communication with the surrounding native tissue.

Future studies must be performed in order to provide sufficient evidence that the methods described herein can be translated to a clinically applicable model, such as ovine or porcine, but the current research provides preliminary indications that both acellular and cell-seeded extracellular matrix scaffolds may allow for structural and functional restoration to the surrounding myocardium when used as a cardiac patch material.

# APPENDIX A

## PROCEDURE FOR DECELLULARIZATION OF PORCINE HEART BY RETROGRADE CORONARY PERFUSION


## ABSTRACT

A method to rapidly and completely remove cellular components from an intact porcine heart through retrograde perfusion is described. This method yields a site specific cardiac extracellular matrix scaffold which has the potential for use in multiple clinical applications.


## INTRODUCTION

Herein, we describe a method to fully decellularize an intact porcine heart through coronary retrograde perfusion. The protocol yielded a fully decellularized cardiac extracellular matrix (c-ECM) scaffold with the three-dimensional structure of the heart intact. Our method used a series of enzymes, detergents, and acids coupled with hypertonic and hypotonic rinses to aid in the lysis and removal of cells. The protocol used a Trypsin solution to detach cells from the matrix followed by Triton X-100 and sodium deoxycholate solutions to aid in removal of cellular material. The

described protocol also uses perfusion speeds of greater than 2L/min for extended periods of time. The high flow rate, coupled with solution changes allowed transport of agents to the tissue without contamination of cellular debris and ensured effective rinsing of the tissue. The described method removed all nuclear material from native porcine cardiac tissue, creating a site-specific cardiac ECM scaffold that can be used for a variety of applications.

## METHODS

### 1. Tissue Preparation and Experiment Setup

1.1 Harvest porcine organ immediately after euthanasia from an abattoir or research facility and rinse off excess blood. Trim the heart of excess fat and tissue, keeping the atria and aorta intact. Trim away fat to separate the pulmonary artery from the aorta. If there are any cuts in the tissue, discard appropriately.

1.2 Wrap each heart individually in freezer paper and store all tissue in a -80ºC freezer for at least 24 hours to ensure complete freezing.

1.3 When ready for use (usually less than 3months), thaw one intact frozen porcine heart in Type 1 water overnight submerged in a 4L beaker at 4°C.

1.4 After the heart is completely thawed, pat the heart dry, weigh the heart, and record the weight. The heart of a market weight pig should weigh between 375-450 grams.

1.5 Connect size 18 Masterflex tubing to the ¼" end of a barbed reducer. Insert the barbed reducer and tubing inside the aorta. Place 2 hose clamps or secure zip ties around the aorta, just below the brachiocephalic trunk. The reducer and tubing must remain above the aortic valve, so the coronary arteries can be perfused.


**Figure 32. The barbed end of the tubing is inserted into the aorta of the native heart. The tubing must be secured with hose clamps or zip ties above the aortic valve to ensure perfusion through the coronary arteries.**

1.6 Use a 30 or 60 mL syringe to fill the tubing with Type I water. Insert the tubing within the cartridge of a Masterflex roller pump at its approximate midpoint. Submerge the inflow end of the tubing in the bottom of a 4L beaker filled with 2.5L of water and secure the tubing.

1.7 Place the heart in the beaker filled with water, and prime the pump to remove air bubbles. If bubbles are observed coming from the aorta where the tubing is inserted, the aorta may need to

be repositioned or secured with additional ties. An airtight seal is important to maintain adequate pressure during the decellularization process.

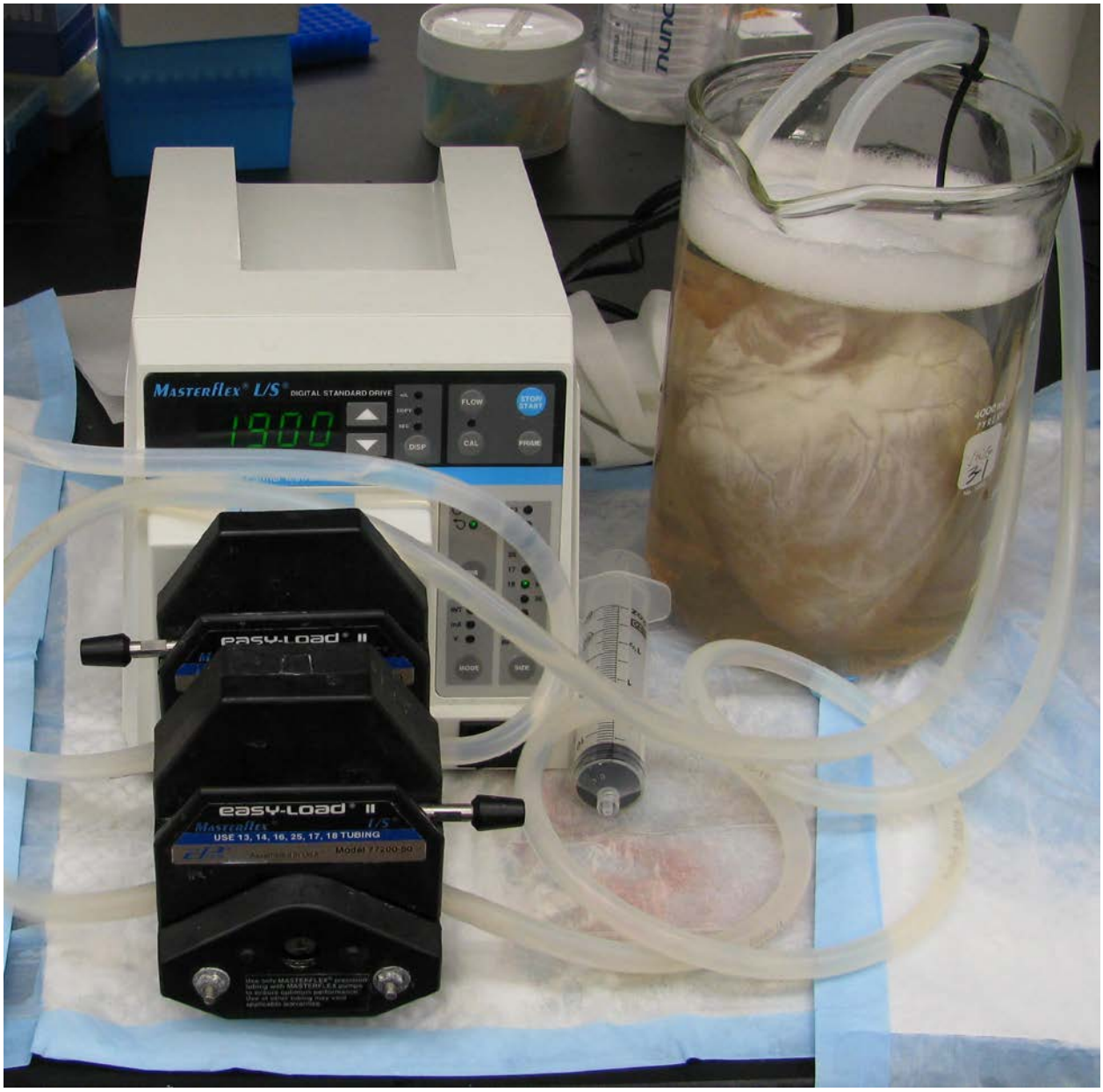


**Figure 33. The heart is submerged in water in a 4L beaker and air bubbles must be removed from the tubing. If bubbles are observed emerging from the aorta near the tubing, additional ties must be used to secure the tubing to the aorta in order to maintain adequate pressure in the tissue.**

1.8 Place the 4L beaker containing 3L of a 0.2% Trypsin/0.05% EDTA/0.05% $NaN_3$ solution on stir plate and warm it to 37°C in preparation of the decellularization process.

**2. Tissue Rinses**

2.1 Set the pump to a flow rate of 400 mL/min, ensuring that the correct tubing size is selected. Flush the heart with Type I water for 15-25 minutes. As the pump is started, the heart should swell and effuse blood from the ventricles. Fresh solution should be substituted every 5-10 minutes, or as needed based on the amount of blood removed from the heart. If blood is not effused from the heart, adjust the tubing and clamps as necessary.

2.2 Stop the pump and transfer the heart to a separate beaker filled with 2X Phosphate Buffered Saline (PBS). After the tubing is submerged in solution, start the pump and increase the flow rate to 700 mL/min. The heart should remain in solution for 15 minutes, changing the solution every 5 minutes. Each solution change requires the pump to be stopped temporarily while the tissue and tubing is moved to the new beaker.

2.3 Transfer the heart to Type I water for 10 minutes and increase the flow rate to 750 mL/min.

**3. Decellularization and Solution Perfusion**

3.1 Transfer the heart to the beaker containing 0.2% Trypsin/0.05% EDTA/0.05% $NaN_3$ at 37°C. Increase the pump speed to 1200 mL/min and start the pump. Use a stir bar placed at the bottom of the beaker to circulate solution in the beaker. The heart should remain in the 0.2% Trypsin/0.05% EDTA/0.05% $NaN_3$ solution at 37°C for a total of three hours. After 1 hour,

increase the pump speed to 1500 mL/min. After an additional hour, increase the pump speed to 1800 mL/min. The tissue is slowly subjected to increased perfusion speeds to condition the tissue and prevent rupture of the vessels. The heart will swell and nearly double in size during this step of the protocol. The tissue will lose its natural color, progressing from the atria to the apex throughout the protocol.

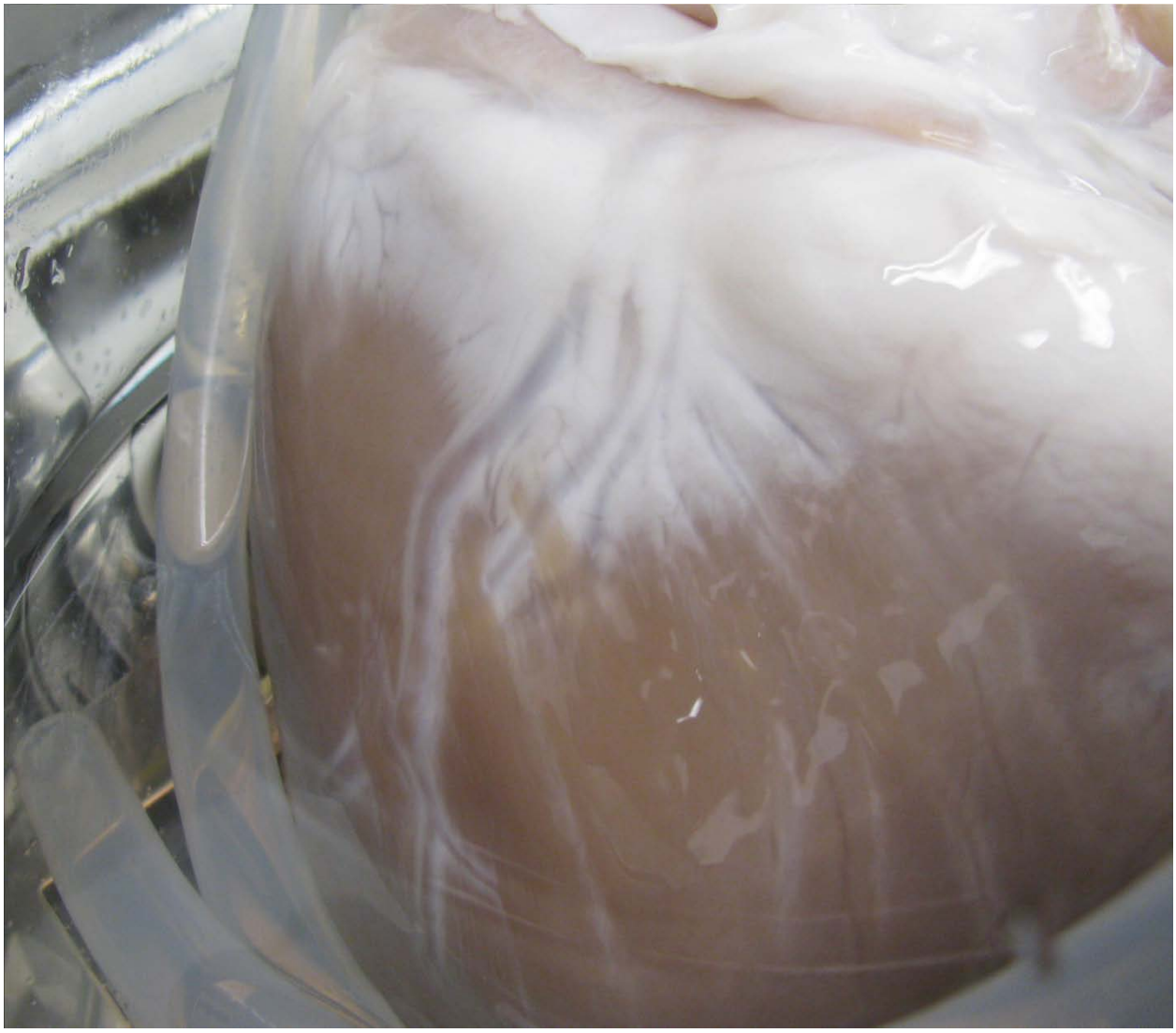

**Figure 34. As solutions are perfused through the coronary arteries, the heart will lose its native color, progressing from the atria to the apex of the heart and localized around the coronaries.**

3.2 After each solution perfusion, a two step rinse is performed to remove cellular debris, chemical residue, and aid cell lysis. Each rinse consists of a ten minute rinse in Type I water followed by a ten minute rinse with 2X PBS solution at room temperature. Each wash consists of removal of solution from the original beaker, adding rinse solutions, and circulating the perfusate

within the beaker containing the submerged heart. After the 0.2% Trypsin/0.05% EDTA/0.05% $NaN_3$ solution, perfuse water at 1900 mL/min and then perfuse 2X PBS at 1950 mL/min.

3.3 Transfer the heart to a solution of 3% Triton X-100/0.05% EDTA/0.05% $NaN_3$ at room temperature. Increase the pump speed to 2000 mL/min and perfuse solution for one hour. Remove the solution from the beaker and replace with fresh solution, increase the pump speed to 2100 mL/min, and perfuse the fresh solution for an additional hour and a half, bringing the total time in 3% Triton X-100/0.05% EDTA/0.05% $NaN_3$ to 2.5 hours.

3.4 Rinse the tissue in Type I water at 2150 mL/min and 2X PBS at 2180 mL/min for ten minutes each.

3.5 Transfer the heart to a 4% Sodium Deoxycholate solution at room temperature. Increase the pump speed to 2200 mL/min and perfuse solution for three hours.

3.6 Rinse the tissue in Type I water at and 2X PBS at 2200 mL/min for 15 minutes each, changing the solutions after 5-10 minutes for each solution. The described perfusion steps may be split over multiple days by performing the rinse step twice and storing the heart with attached tubing overnight at 4°C and submerged in Type I water.

3.7 The following day, perform a 5 minute rinse with Type I water at 750 mL/min, followed by a 5 minute rinse in 1X PBS at 1500mL/min. The protocol may then be continued at the described flow rate in the proper solution.

## 4. Disinfection and Final Processing

4.1 Transfer the heart to a 0.1% peracetic acid/4% ethanol solution and perfuse solution for 1.5 hours at 2200 mL/min.

4.2 The final rinses for the tissue are all performed at 2200 mL/min. Perfuse the tissue with 1X PBS for 15 minutes, followed by two 5 minute washes in Type I water. This series of rinses is repeated once more in order to complete the solution perfusion procedure.

4.3 Turn the pump off and remove the heart from solution to drain the heart. Cut the ties from the aorta, remove all tubing, and place the heart in an empty beaker to drain for 1 hour. Excess liquid will need to be drained periodically. Lay the heart on an absorbent pad to fully drain the heart.


**Figure 35. After completion of the disinfection and rinse steps of the protocol, the tubing is removed and the heart is placed on an absorbent pad to allow the excess water to drain out of the heart. This ensures an accurate measurement when weighing the tissue and also allows the tissue to relax before sectioning.**

4.4 After most of the water is removed, record the weight of the cardiac extracellular matrix (C-ECM). The heart can be expected to lose approximately 20-25% of its initial weight during the decellularization process.

4.5 Dissect the right and left ventricles, as well as the ventricular septum for DNA quantification and histological processing in order to confirm complete decellularization of the tissue.

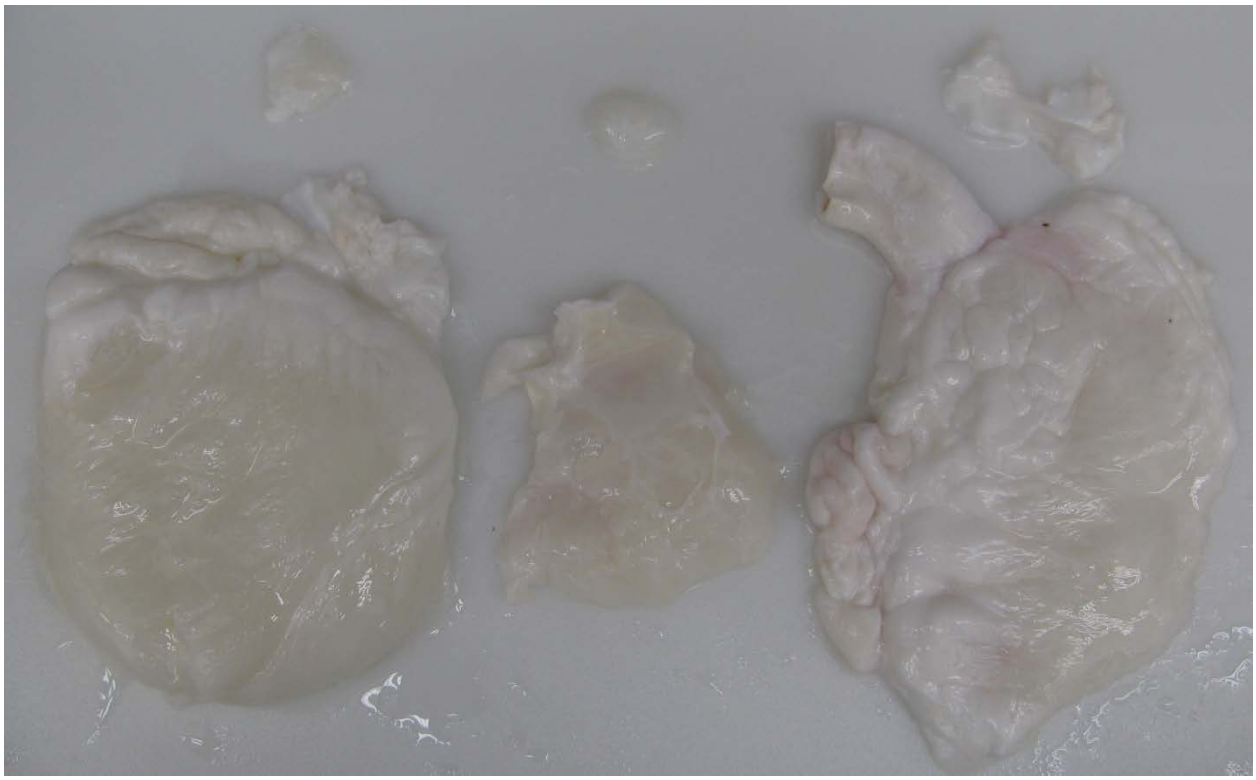

**Figure 36. The left ventricle (LV), right ventricle (RV), and ventricular septum are all removed from the decellularized heart for histologic processing, freezing and lyophilization, and DNA quantification.**

4.6 Freeze the C-ECM at -80°C for at least 2 hours before lyophilization.

## RESULTS

The effects of the decellularization process on whole porcine hearts naturally varies due to differences in size, pressures, and vessel arrangement. Therefore, the exact composition of the derived extracellular matrix scaffolds will not be the same from heart to heart. The completion of the described protocol will yield a heart that appears white or translucent, indicating the loss of cellular material. However, it is widely accepted that a tissue can be considered "decellularized" based on the combination of a few more quantitative parameters [8]. A successful decellularization protocol will produce a matrix with less than 50 ng of double stranded DNA per mg of tissue.

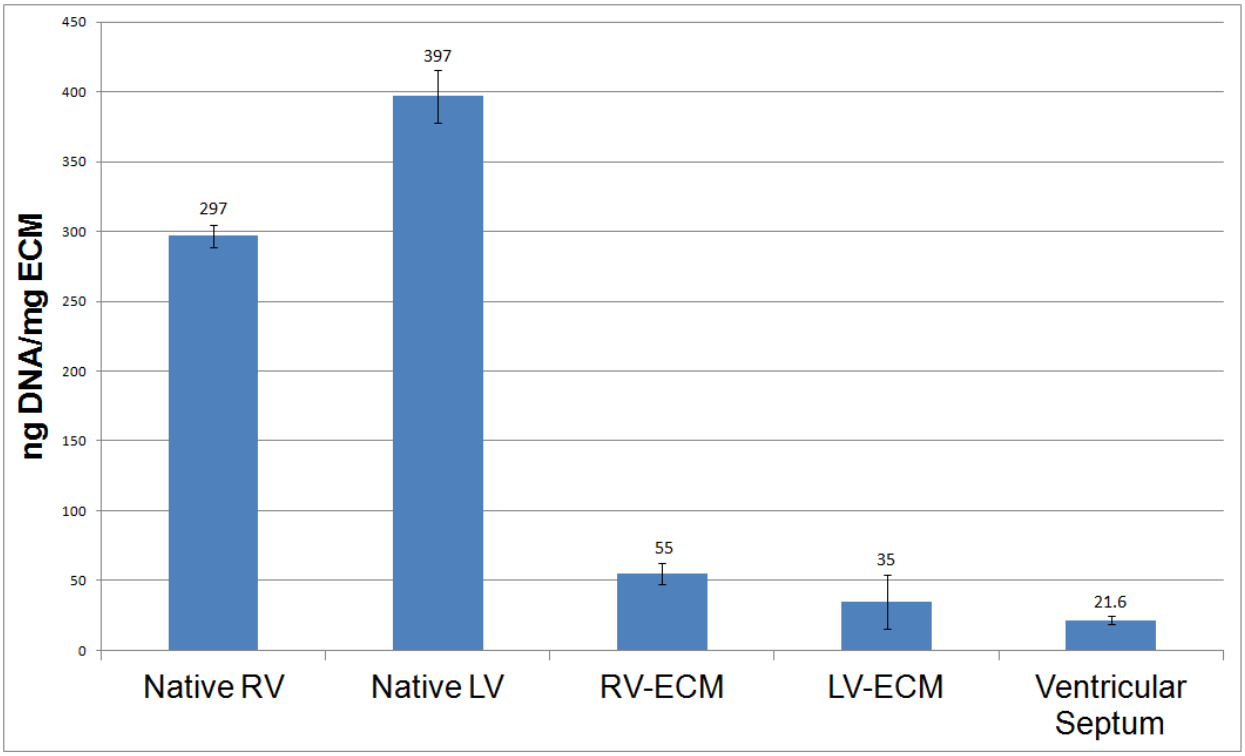


**Figure 37. Quantitative analysis of DNA content using a Pico Green assay. The ventricles from cECM hearts show a significant decrease in DNA content when compared to native ventricles. The DNA values observed from this protocol are observed at or below the 50 ng/mg standard for decellularized tissues.**

In order to avoid a host immune response upon implantation of the matrix, the remaining DNA should also contain less than 200 base pairs.

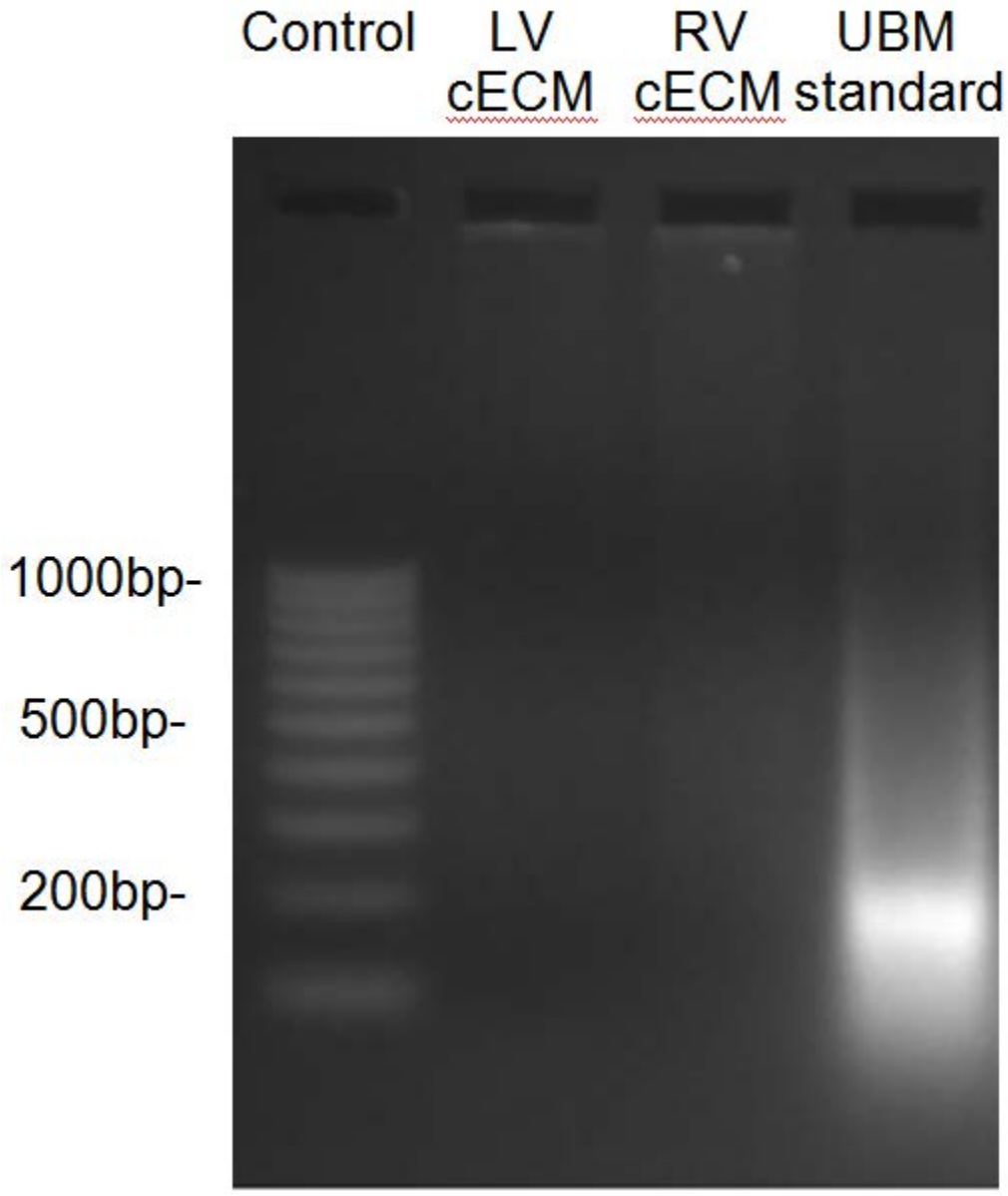


**Figure 38. DNA fragment size, as determined by ethidium bromide gel, showed little residual DNA in the decellularized ventricles when compared to a urinary bladder matrix (UBM) standard.**

To confirm these findings, Hematoxylin and Eosin staining should reveal the absence of nuclear staining in representative sections of the ventricles and ventricular septum.

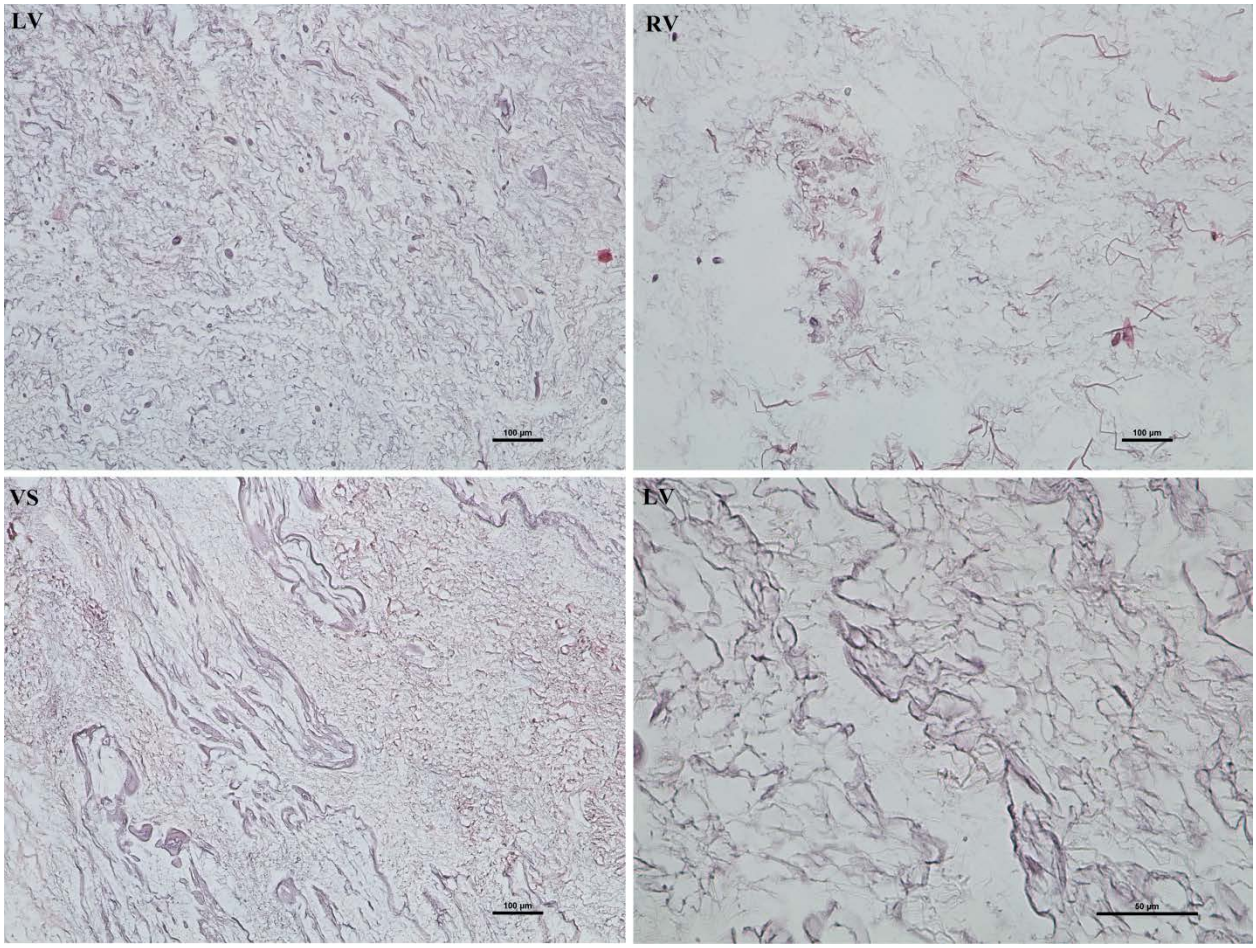


**Figure 39. Hematoxylin and Eosin staining showed complete removal of nuclear material from the ventricles following completion of the decellularization protocol.**

## DISCUSSION

The current study described methodology for consistent and efficient decellularization of a porcine heart. The protocol was a modification to a previously published report [1], and included longer exposure to flow and increased pressure, which provided more repeatable results. The resulting decellularized tissue met all of the published criteria for successful decellularization of tissue [2].

Frequent solution changes were performed to limit the reintroduction of cellular material to the tissue, and the duration of exposure to each decellularization agent was minimized to reduce adverse effects on the ECM. During the beginning stages of the protocol, the perfusion rate was gradually increased to condition the tissue and allow for higher flow rates during the later stages of the protocol. Without conditioning the tissue in the early stages, the vasculature of the heart can rupture, making perfusion of the heart impossible. The protocol was used due to its efficiency, and no claims are made to its superiority over other protocols. The precise composition of decellularization agents and rates of perfusion may conceivably be varied to yield a protocol with better mechanical or biologic characteristics, but the general principles for delivery of the agents to the heart are applicable.

The preservation of the native three-dimensional structure of the heart was attributed to several procedures performed throughout the decellularization protocol. First, the tissue was trimmed and frozen upon arrival. Freezing promoted cell lysis and was important for pre-conditioning the tissue for the perfusion cycles. The tissue was thoroughly inspected for cuts and 2 cm intact intact aorta superior to the aortic valve. If any pericardium or epicardium was cut, the organ was discarded because the perfusate did not reach downstream regions of the heart, and the heart was not fully decellularized. Next, the tissue was fully thawed in type I water before use. The water allowed the tissue to relax as it thawed and also aided the removal of residual blood clots within the heart. Finally, as the tubing was inserted, care was taken to ensure that the aortic valve remained intact so that it formed a water-tight seal around the tubing, so that a proper pressure was maintained and that the solution entered the coronary arteries.

After each decellularization protocol was completed, a series of quality control measures were completed to ensure complete removal of cellular material. The current study verified that

the protocol eliminated histologic staining for cell nuclei, showed that less than 50 ng of DNA was present per mg of dry weight of the tissue, and that any DNA was less than 200 bp in size [131]. Previously published methods for cardiac decellularization showed similar levels of decellularization in DNA staining and quantification [127, 130, 195, 196]. Complete decellularization was accomplished in these studies using similar treatments of enzymes and detergents. However, in the present study, the length of exposure to each chemical was increased, there were more solution changes, and the flow rates were increased. The present protocol also increased the length of chemical rinses, potentially leading to more efficient removal of chemical residues from the extracellular matrix.

In conclusion, porcine heart decellularization is possible and the methods are straight-forward. Continued investigation of this material will provide insight into its potential for clinical use and future studies will be performed in vitro to examine the ability of the scaffold to support cardiac cells seeded and cultured on the matrix. The methods described herein may also be applicable to decellularization of human hearts.

# APPENDIX B

## HYDRATED XENOGENEIC DECELLULARIZED TRACHEAL MATRIX AS A SCAFFOLD FOR TRACHEAL RECONSTRUCTION

## ABSTRACT

Tracheal injury is a rare but complex problem. Primary tracheal reconstructions are commonly performed, but complications such as tension and inadequate vascular supply limit the length of surgical resection. The objective of the present study was to determine whether a hydrated, decellularized porcine tracheal extracellular matrix showed the potential to serve as a functional tracheal replacement graft. Porcine tracheas were decellularized and evaluated to characterize their biochemical composition and biomechanical behavior. Hydrated decellularized tracheal matrix (HDTM) grafts (>5cm) were implanted heterotopically beneath the strap muscle and wrapped in the omentum in a canine model for 2 and 8 weeks followed by histologic and mechanical analysis. HDTM patches (2x3cm) were also used in a patch tracheoplasty model. The repair site was evaluated bronchoscopically and radiographically, and the grafts were analyzed by histologic methods to evaluate epithelialization and persistence of the cartilage rings. The present study showed that HDTM maintains mechanical characteristics necessary for function under physiologic loading conditions even after 8 weeks of heterotopic implantation. After orthotopic implantation, the grafts were shown to support development of a columnar, pseudostratified, ciliated epithelium,

but the cartilage structures showed histologic evidence of degradation and limited new cartilage formation. The results of the study showed tracheal ECM scaffolds support the formation of site-specific epithelium and provide sufficient mechanical integrity withstand physiologic pressures in the short-term. However, for long-term success, it appears that pre-implantation to allow vascularization or preseeding of the graft with chondrocytes will be necessary.

## INTRODUCTION

Tracheal lesions and injury, including post-intubation stenosis, tumor, and iatrogenic, may require tracheal resection with primary reconstruction [197]. Although reconstruction can be performed in most cases with successful outcome, anastomotic complications are associated with morbidity and mortality [197, 198]. Reoperation, long resections (>4 cm), and poor wound healing (e.g., diabetes) are among the risk factors that predict for anastomotic complications, and are all typically associated with increased anastomotic tension and poor vascular supply [198]. The generally accepted limit for tracheal resection is a length of approximately 6 cm in adults, or approximately 50% of the original tracheal length, with a smaller percentage available for resection in the pediatric population [199, 200]. When primary reconstruction is not possible after tracheal resection, patients receive palliative treatment such as irradiation, stents, and T tubes [197]. An effective tracheal replacement could mitigate the risk of anastomotic complications associated with long resections, and could provide an alternative for patients for which resection is not an option.

Biologic scaffolds derived from tracheal tissue have been investigated for use in tracheal replacement due to their mechanical and biochemical similarity to the native trachea. Macchiarini et al. recently used a decellularized allogeneic trachea that was recellularized with autologous

epithelial and bone marrow cells to show the first successful reconstruction of a bronchus using a tissue engineered construct [139]. A recent preclinical study showed that scaffolds derived from porcine urinary bladder matrix (UBM) were able to reconstitute a pseudostratified, columnar, ciliated epithelium in a patch tracheoplasty in a canine model [201]. In contrast, a lyophilized form of porcine decellularized tracheal matrix (DTM) showed mostly squamous epithelium with scattered ciliated cells. Neither UBM nor DTM showed regeneration of cartilaginous tissue. The results for DTM were surprising in light of previous studies that showed successful reconstruction of intrathoracic trachea with a decellularized allogeneic tracheal graft in a canine model [202, 203]. Aside from the tissue source, the primary difference between the two tracheal scaffolds was the state of hydration as the DTM was lyophilized prior to implantation. Therefore, the objective of the present study was to determine whether hydrated DTM (HDTM) from a porcine source has the potential to serve as a functional scaffold for tracheal reconstruction in a canine model. Since full-circumferential orthotopic tracheal reconstruction carries with it substantial morbidity and mortality for animals if implanted grafts lose functionality, three feasibility studies posing less severe complications were performed. First, HDTM was evaluated for effectiveness of decellularization and changes in biochemical composition and mechanical behavior as compared to the native trachea. Second, the host response and mechanical behavior of the HDTM were assessed after heterotopic implantation in the neck and abdomen of dogs for periods of 2 and 8 weeks. Finally, HDTM scaffolds were used for repair in an orthotopic patch tracheoplasty model and evaluated 8 weeks after repair to determine whether the scaffold promoted formation of mechanically functional cartilage and site-specific epithelium.

## METHODS

*Study Design*

Twelve mongrel dogs weighing 19.5 ± 0.3 kg were subjected to heterotopic surgical implantation of two 5 cm long HDTM scaffolds, one inserted beneath the strap muscle adjacent to the native trachea and one wrapped in the omentum within the abdominal cavity. Two sites were evaluated to determine whether the remodeling was site dependent. Six animals were euthanized at 2 or 8 weeks and the HDTM scaffolds from the neck and abdominal cavity were resected along with the native canine tracheas (≥5cm). A portion of each specimen was prepared for histology, and the remainder was wrapped in saline-soaked gauze and stored at -80°C until mechanical testing.

A second group of 6 dogs underwent surgical resection of a 1-cm-wide x 2-cm-long defect (about 30% of circumference and 3 rings long) of the ventral cervical trachea. The HDTM patches were examined bronchoscopically and radiographically at 4 weeks after surgery and just prior to sacrifice. All dogs were euthanized 8 weeks after surgery, at which time explanted tissue was evaluated for gross morphology, standard histology, and immunohistochemistry.

All animal procedures were performed in compliance with the *Guide for the Care and Use of Laboratory Animals* (National Institutes of Health Publication No. 88-23, revised 1996) and approved by the Institutional Animal Care and Use Committee at the University of Pittsburgh.

*HDTM Scaffold Preparation*

Whole tracheas (>6cm) were harvested from market-weight pigs (approximately 110 to 130 kg) after slaughter from an abattoir and transported on ice to laboratory facilities. Tracheas

were cleaned by repeated rinses in deionized water. Larynx, bronchi, and residual external connective tissues were then discarded. Tissue was frozen at -80°C until time for decellularization. For decellularization, each trachea was thawed at room temperature in di$H_20$ and subjected to 48 hours immersion in 3% Triton X-100 solution at 4°C on a rocker plate, changing solution after 24 hours. After 48 hours, a 0.1% (v/v) peracetic acid, 4% (v/v) ethanol, 96% (v/v) deionized water (di$H_20$) wash was administered for 2 hours at 300 rpm on a mechanical shaker to decellularize and disinfect tissue. The tissues were then rinsed 15-min in 0.9% NaCl and di$H_20$ on a mechanical shaker to remove residual solutions. Each trachea was trimmed to 5cm length, packaged to retain hydrated state in 0.9% NaCl, and subjected to terminal sterilization via gamma irradiation (2 MRad). Hydrated, sterilized grafts were stored at 4$^o$C until use (usually less than two weeks.)

*Analysis of HDTM Grafts*

HDTM grafts were fixed in 10% neutral buffered formalin and prepared for paraffin processing. Five micron sections were stained with Hematoxylin and Eosin to evaluate removal of cellular material and Alcian Blue to evaluate the presence of glycosaminoglycans (GAGs) in the cartilage rings.

The amount of GAGs within the HDTM was quantified and compared to native trachea using a Blyscan Sulfated Glycosaminoglycan assay kit (Biocolor, B1000) per the manufacturer's instructions. Briefly, 0.05g hydrated samples of intact porcine trachea, isolated tracheal mucosa, and isolated tracheal cartilage from both native and decellularized tracheas were obtained. Samples were incubated at 37$^o$C on rocker in 2.5mL of Pronase buffer (1.5mg/mL Type XIV Protease, 0.1M Tris (pH 7.5), and 10mM $CaCl_2$) for 48 hours with vortexing after 12 hours. Digested samples were centrifuged at 1000rpm for 10min. 25µL of supernatant from each sample was

aliquotted to a 1.5mL Eppendorf, to which 75µL deionized water was added. 1mL Blyscan dye reagent was added to each tube and the tubes were stirred at 300rpm for 30min at room temperature. Tubes were then centrifuged at 20,000rpm at room temperature for 10min, the supernatant was removed, and 1mL dissociation reagent was added to each tube. After vortexing, tubes were left at room temperature to react for 15minutes, then vortexed and left to react for an additional 15min. Three sets of 200µL aliquots were placed into a transparent 96-well plate, the absorbance was measured at 656nm, and the results were compared to the standard curve ($R^2 > 0.99$).

The presence of the basement membrane within the HDTM grafts was investigated immunohistochemically using ABC elite (Vector Labs, PK-6100) and DAB detection kits (Vector Labs, SK-4100) for Collagen VII (Chemicon, MAB1345) and Laminin (Sigma, L-9393). Frozen sections were fixed in acetone and incubated with 1.5% normal horse serum (Vector Labs, S-2000) for 30 minutes. Samples were then incubated with the aforementioned primary antibodies (1:500, 1:100 dilutions respectively) for 30-60 minutes, then secondary antibodies (Vector, BA-2001 at 1:200; and Vector, BA-1000 at 1:200 respectively) for 30 minutes. ABC was applied for 30 minutes, then DAB for 3-10 minutes before serial alcohol and xylene dehydration and coverslipping.

*Surgical Procedure*

All animals were sedated with acepromazine (0.1 mg/kg intramuscular), followed by intravenous administration of thiopental (12 to 25 mg/kg), intubation and isoflurane (1.5–3%) maintenance of surgical place anesthesia. Cefazolin (15 mg/kg intravenous) was administered before surgical preparation and skin incision.

For heterotopic implantation of HDTM, aseptic technique was used to make an incision between the strap muscles in the neck, approximately 2-3 cm in length. A sterilized, 5cm long PTFE rod was inserted through the lumen of the graft and sutured in place using non-resorbable Prolene suture (Ethicon) to prevent collapse of the graft after implantation. The constructs (graft and PTFE rod) were then placed beneath the strap muscle, adjacent to the native trachea. A second incision was made in the abdominal cavity and another HDTM/PTFE construct was wrapped in the omentum. At 2 and 8 week time points, animals were sacrificed and native tracheas were harvested along with remodeled HDTM grafts from the neck and abdominal cavity.


**Figure 40. Full circumferential scaffolds of HDTM were implanted heteropically in both the neck beneath strap muscles adjacent to the native trachea (A) and wrapped with omentum in the abdominal cavity (B). Patches of HDTM (2 cm x 3 cm) were used for patch tracheoplasty of a ventral tracheal defect (1 cm x 2 cm) (C).**

For orthotopic patch tracheoplasty, aseptic technique was used to expose the proximal cervical trachea through a midline neck incision. A 1-cm-wide x 2-cm-long portion of the ventral tracheal wall was surgically removed. The defect was then repaired with a HDTM device with at least 5mm overlap around the edges of the defect (~ 2cm x 3cm). All grafts were secured using absorbable 4–0 polydioxanone suture (PDS; Ethicon, Somerville, NJ). Non-resorbable Prolene suture (Ethicon) were used to mark the corners of the repair site. The scaffold placement site was

tested for air leaks by submerging in saline while applying a Valsalva maneuver. The repair was examined by bronchoscopy to verify graft placement and airway patency [201].

*Postoperative Care*

Dogs were recovered from anesthesia, extubated, and monitored until resting comfortably in a sternal position. The dogs were housed in cages overnight and returned to their larger run housing (3.05 x 4.27 m) on postoperative day 1. Oral prophylactic antibiotics were administered (cephalothin/cephalexin, 35 mg/kg, twice daily) for 7 to 9 days. The dogs received intravenous acepromazine (0.1 mg/kg) and butorphanol (0.05 mg/kg) for 2 days, followed by subcutaneous or intramuscular buprenorphine (0.01 to 0.02 mg/kg) every 12 hours thereafter for analgesia as needed.

*Clinical, Bronchoscopic, and Radiographic Assessment*

Animals that were subjected to heterotopic implantation of HDTM grafts had a predetermined follow-up period of 2 or 8 weeks, at which time the dog was euthanized. Likewise, animals that were subjected to patch tracheoplasty had predetermined follow-up periods of 8 weeks, at which time the dogs were also euthanized. Bronchoscopic examinations and radiographs of patch reconstructions were conducted at 4 and 8 weeks after the procedure to evaluate scaffold remodeling. Airway stenosis was evaluated using a flexible bronchoscope, and visually quantified as a percentage decrease in the ventrodorsal diameter of the trachea. Strictures were classified as mild (< 25%), moderate (25% to 50%) or severe (> 50%). Documented bronchoscopic data included appearance of the graft surface and its relationship to the native trachea, signs of inflammation (eg, exudate, granulation tissue), presence or absence of tracheomalacia, and

stricture formation. Radiographs (Vetel Diagnostics, San Luis Obispo, CA) were obtained of the sagittal plane to determine whether cartilage rings from the graft were present.

*Histologic Evaluation*

Cross-sectional tissue specimens were cut from the ends of the heterotopic implants, and the specimen was fixed in 10% NBF for histologic analysis and stained with Masson's Trichrome and Alcian Blue. For the patch tracheoplasty implants, approximately six cross-sectional tissue specimens were cut along the longitudinal length of the graft. Two of the specimens were fixed in 10% NBF for histologic analysis and stained with Masson's Trichrome, Alcian Blue, or Periodic Acid-Schiff. Two additional specimens were fixed in 2% paraformaldehyde for 1 hour and frozen in OCT. Frozen sections were analyzed by fluorescent staining for β-tubulin for cilia (Santa Cruz Biotech, sc-12462-R, 1:1000 dilution), F-actin for microvilli (Invitrogen, A22287, 1:250 dilution), and DAPI for nuclear staining. The final two specimens were fixed in 2.5% glutaraldehyde, treated with 1% (w/v) osmium tetroxide, and dehydrated via a gradient of alcohol washes for use in scanning electron microscopy to determine the extent of cilia coverage on the epithelium.

*Pressure Diameter Assessment*

The effects of decellularization on the mechanical behavior of the HDTM graft was determined by performing pressure-diameter response testing of 5 porcine tracheas both before and after decellularization. In a separate experiment, the passive pressure-diameter response of remodeled HDTM grafts implanted heterotopically in a canine model was compared to that of native canine trachea. In both experiments, a custom built system that was modified based on previously published methodology was used to evaluate the pressure-diameter response [204-206].

Each trachea was first secured inside a modified *in vitro* pressure-diameter testing system controlled via a custom designed LabVIEW program (National Instruments v8.6.1, Austin, TX).

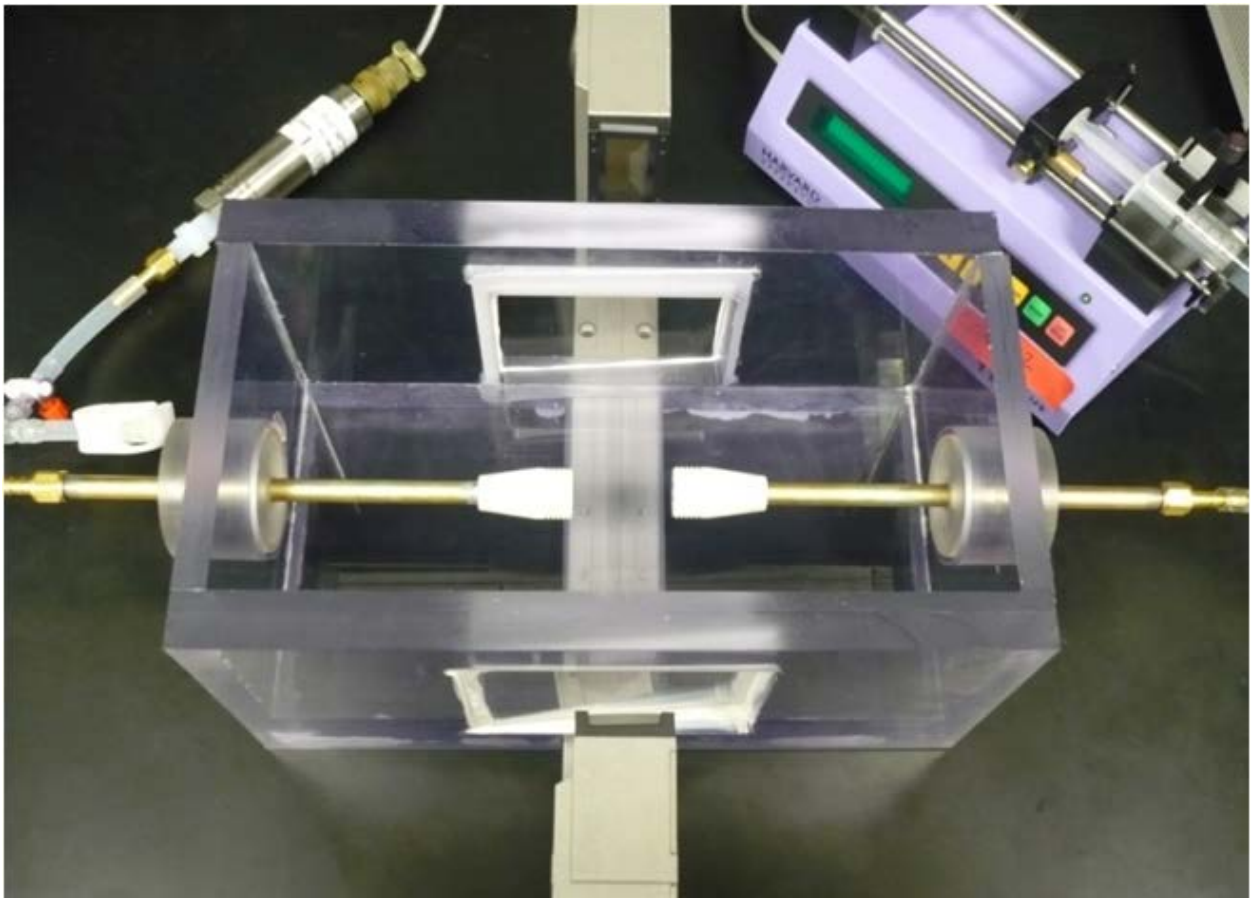

**Figure 41. A custom built mechanical testing device was used to test the pressure diameter response of tracheas.**

Communication of a pressure sensor (Honeywell Sensotec Model FPA, Columbus, OH) located downstream of the sample was initiated through a DAQ card (National Instruments USB 6009, Austin, TX). A hydrostatic pressure head was created by pumping saline into or out of the trachea using a 60cc syringe connected to a pump (Harvard Apparatus, Model 11 Plus, Philadelphia, PA). The mounted trachea was enclosed within a 3L bathing chamber and submerged in saline. An optical LED micrometer (Keyence Model LS 7070MT, Wood Dale, IL) positioned

orthogonal to the sample was used to measure the outer diameter (OD) of the trachea continuously as the pressure was varied. Diameter measurements were made in the center region of the tracheal tissue in two orthogonal directions (ventral-dorsal and transverse) due to the anisotropic behavior of the trachea in the membranous portion. Upon mounting, a small tension was placed on the tissue along the length of the graft to simulate physiologic tension. Pressure-diameter response was determined by cycling the intraluminal pressure between -10 and 60 mm Hg to simulate physiologic breathing patterns. The grafts were pre-cycled for approximately ten cycles to ensure uniform hysteresis before the final response curve was saved for analysis. The two OD measurements for each 5 mmHg pressure increment were converted to a cross sectional area, assuming an elliptical tracheal cross-section shape.

*Statistical Analysis*

A two-way independent ANOVA was run at each 10 mmHg pressure increment to analyze differences between cross sectional areas of heterotopically implanted tracheas within and between groups of the pressure diameter tests. A repeated measures ANOVA was also performed on porcine tracheas that were tested in the pressure diameter system before and after decellularization. All analyses were performed using the SPSS package (version 16.0; SPSS, Inc, Chicago, Ill). Statistical significance was set at $p < 0.05$.

# RESULTS

*Characterization of Decellularized Tracheal Matrix*

Hematoxylin and Eosin (H&E) staining confirmed the removal of cellular and nuclear material in the mucosal layers of the HDTM. However, nuclear staining persisted within the cartilage rings of the grafts. In addition, Alcian Blue staining of HDTM scaffolds showed positive staining for glycosaminoglycans within the cartilage. HDTM showed positive staining for collagen VII and laminin (data not shown) localized on the luminal surface of the material, confirming maintenance of the basement membrane of the HDTM grafts after the decellularization process. Pressure-diameter testing of the tracheas before and after decellularization showed that decellularization had little effect on the biomechanical behavior. The decellularization process tended to show increased tissue compliance, but significant differences in the pressure-diameter response were only shown at 50 mmHg and 60 mmHg. At negative pressure, the tracheas behaved very similarly to the native trachea with no statistical difference detected in the cross-sectional area.

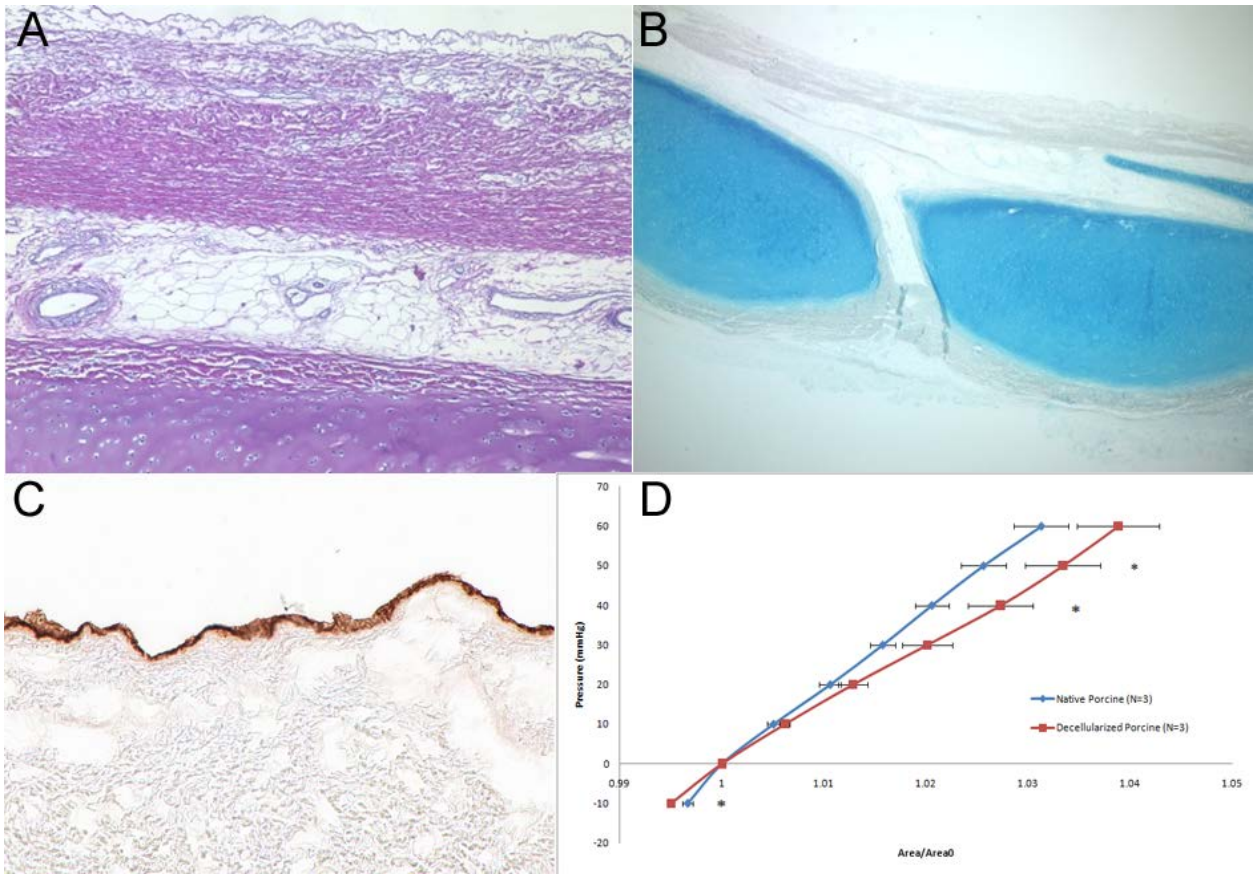


**Figure 42. (A) Hematoxylin and eosin staining of the HDTM shows no cellular material in the mucosal layers of the tissue, however nuclear staining persists within the cartilaginous tissue. (B) Alcian Blue staining of HDTM shows that the process does not remove glycosaminoglycans from the cartilage that are necessary for maintenance of biomechanical behavior. (C) The decellularization process also preserves the basement membrane as shown by positive staining for collagen VII on the luminal surface of the HDTM. (D) Graph of pressure vs. the change in cross sectional area for native porcine tracheas and HDTM of the same samples after decellularization. There is little difference in the mechanical properties of the grafts at the time of implantation. (* denotes statistical significance, $p \leq 0.05$)**

The glycosaminoglycan content was further quantified showing that the concentration of glycosaminoglycans decreased by about 50% in the intact HDTM, predominantly due to a loss of glycosaminoglycans in the cartilage tissue.

**Table 3. Glycosaminoglycan content with percent change due to the decellularization process.**

| µg GAG/mg tissue | Native (n=3) | Decellularized (n=3) | % Change |
|---|---|---|---|
| Intact | 22.25 | 10.61 | -52.31 |
| Mucosa | 1.77 | 7.34 | 314.69 |
| Cartilage | 81.8 | 44.16 | -46.01 |

*Evaluation of Heterotopic Implants*

All treated dogs recovered without complications from the surgical procedure and had an uneventful early postoperative course. Seroma formation occurred in the heterotopic neck position within the first three days after implantation in two animals and was associated with rapid degradation of the implanted scaffolds and loss of mechanical integrity. These animals were replaced in the study. All other animals had uneventful postsurgical courses until planned euthanasia at either 2 or 8 weeks after the procedure.

Remodeled grafts were recovered from dogs immediately after euthanasia. Grafts generally retained the original size and shape, and showed evidence of vascularization, and qualitatively showed mechanical resistance in response to external load. The abluminal surface of the grafts isolated from the omentum showed coverage with adipose tissue that could not be easily removed.

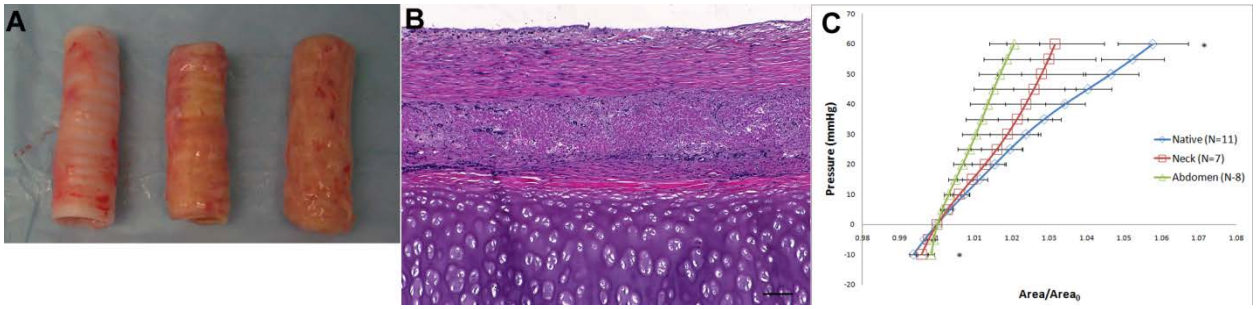


**Figure 43. (A) Comparison of native canine trachea with remodeled HDTM grafts (t = 8 weeks) from neck and abdomen. (B) Cellular presence is abundant in the epithelial layers of remodeled grafts at 8 weeks after implantation in the neck. Little nuclear staining is shown in the cartilage tissue. (10x, Scale = 100µm) (C) Graph of pressure vs. the change in cross sectional area for remodeled HDTM and native canine trachea. Grafts implanted in the neck and abdomen had smaller changes in area over physiologic pressure range than native canine trachea. (* denotes statistical significance, $p \leq 0.05$)**

Histologic analysis of the explanted grafts showed abundant cellular infiltration of rounded and spindle shaped mononuclear cells throughout the connective tissue surrounding, but not including, the cartilage rings at both 2 and 8 weeks after implantation. There was evidence of vascularization throughout the graft, but particularly near the abluminal surface. Cells lining the basement membrane in some areas formed a monolayer, but there was no morphologic evidence of ciliated cells present on the luminal surface in any heterotopic grafts.

The general shape of the pressure-diameter response curves for the heterotopically implanted grafts from both the neck and the abdomen were similar to that of native canine trachea from the recipients. The compliance of the grafts tended to be lower than for the native canine trachea, with the grafts implanted in the abdomen showing lowest compliance. However, the only statistically significant differences in the pressure diameter response were detected at -10 mmHg and 60 mmHg ($p < 0.05$).

*Evaluation of Patch Tracheoplasty Implants*

All animals recovered from surgery without complication and survived until scheduled euthanasia. One animal showed signs of seroma below the incision by day 3, but it resolved spontaneously by day 7. Bronchoscopic evaluation of the grafts showed the formation of whitish, connective tissue replacing the implant. The grafts were generally smooth and shiny, suggesting epithelial coverage. In two dogs, the surface was interrupted by a protrusion into the lumen, which appeared to be a cartilage ring present with graft. Radiographic analysis showed the persistence of cartilage rings in 4 of the 6 animals.

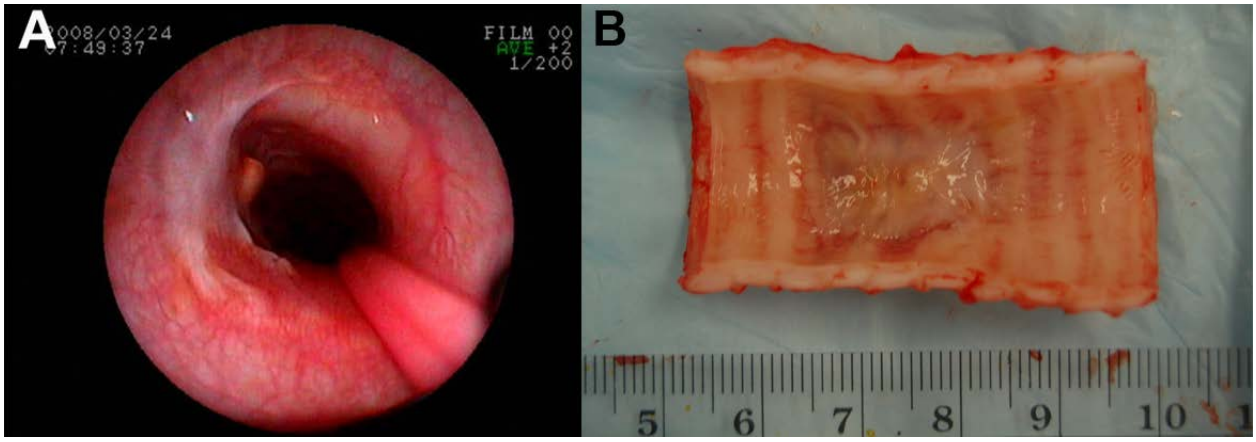


**Figure 44. (A) Bronchoscopic view of the remodeled HDTM scaffold 8 weeks after patch tracheoplasty. The remodeled HDTM appears whitish in appearance with limited reduction in the luminal diameter of the trachea. (B) Gross view of remodeled HDTM patch after tracheoplasty. The shiny surface suggests development of an epithelial layer and blood vessel formation is evident within the patch.**

Morphologic analysis of the remodeled graft showed deposition of new host tissue that was well vascularized. There was limited contracture of the graft that led to a reduction in luminal diameter of less than 10%. Cartilage rings from within the graft protruded into the lumen by approximately 2-3 mm in two animals. When the rings were present they largely retained their

circumferential geometry and there was no evidence of tracheomalacia. In the two cases in which cartilage rings were not observed, the resulting remodeling response led to the replacement of the graft with a thin layer of connective tissue with no inherent rigidity. In all cases, the remodeled lumen was shiny, suggesting epithelial coverage.

Histologic examination of HDTM patches showed persistence of cartilage rings that were surrounded by new host connective tissue in 4 of 6 animals. The cartilage rings showed the presence of GAGs in sections stained with Alcian Blue, but there was no evidence of cellular infiltration into the cartilage.

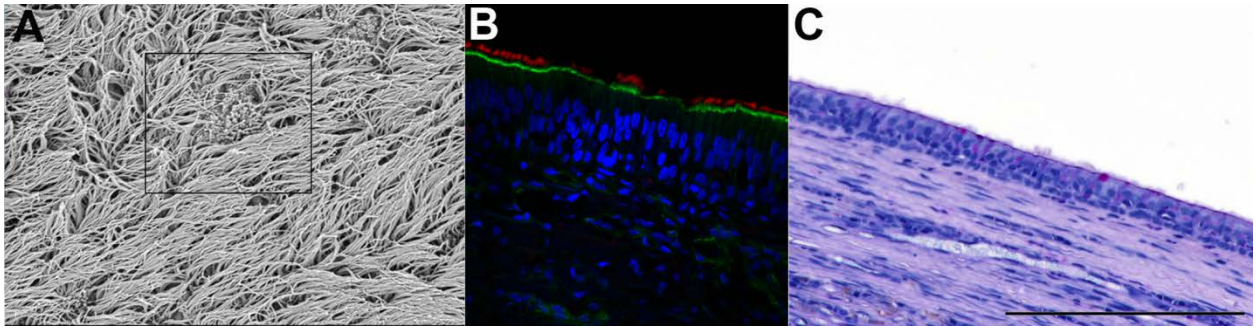


**Figure 45. The cartilaginous rings within the HDTM persist for at least 2 months as shown by (A) X-Ray, (B) Alcian Blue staining , and (C) Periodic Acid-Schiff staining (4x, Scale = 100µm). The arrows point to cartilage that was part of the HDTM patch and the asterisks denote newly formed cartilage.**

There was histologic evidence of degradation of the cartilage rings in two of the animals, with only one animal showing evidence of new cartilage formation that was localized and did not bridge the gap of cartilage formed by the defect. The new host connective tissue showed increased cellular density compared to normal tracheal mucosa. Histologic analysis showed the presence of a columnar, pseudostratified, ciliated epithelium with secretory cells in all animals.

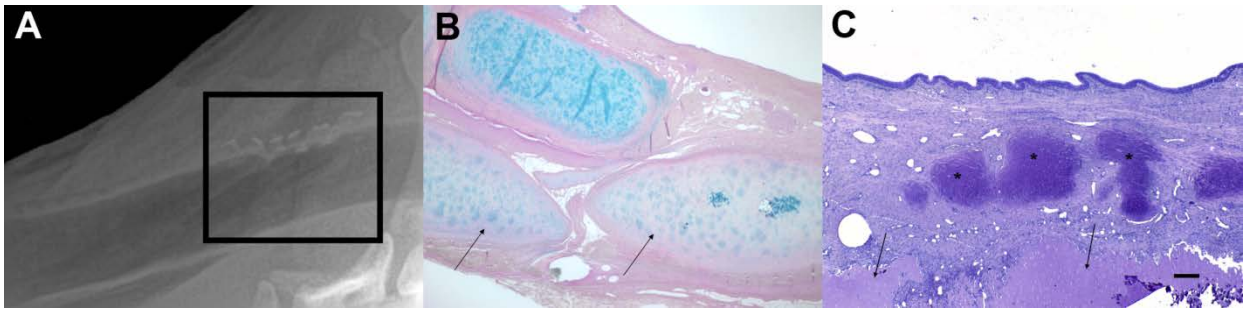


**Figure 46. (A) Scanning electron microscopy shows mature cilia covering the middle region of the remodeled HDTM, although the density of the cilia appear to be slighly less than for the normal trachea. There are also regions of microvilli observed (box). (B) Immunofluorescent staining confirms the presence of cilia and microvilli with positive staining of alpha tubulin (red) in the cilia and F-actin (green) in the microvilli. (C) Periodic Acid-Schiff staining (40x, Scale = 100μm) shows the organization of the epithelial layer containing abundant secretory cells and complete coverage with cilia.**

Cilia were observed morphologically in Masson's trichrome stained sections and in SEM images. Immunofluorsecent staining confirmed the presence of acetylated tubulin, which is indicative of cilia, and F-actin, which is indicative of microvillus. PAS staining confirmed the presence of scattered secretory cells near the apical surface of the epithelium that appeared in greater numbers near the edges of the defect and more sparsely in the middle. In the two animals that lacked cartilage rings, there was no apparent difference in the morphology of the mucosal tissue or the epithelium.

## DISCUSSION

The present study showed that tracheal ECM supports the formation of site-specific epithelium and provide sufficient mechanical integrity withstand physiologic pressures in the short-term. Heterotopic implantation of full circumferential grafts showed cellular infiltration and vascular

development within the graft. The cartilage structures within the heterotopic implants persisted for up to 8 weeks and showed comparable mechanical integrity to the native trachea. Orthotopic implantation in a patch tracheoplasty model showed that the HDTM also promoted re-epithelialization with a columnar, pseudostratified, ciliated epithelium with scattered secretory cells. In the majority of the animals, cartilage rings from the graft persisted within the repair site.

The present study described a decellularization protocol for tracheal tissue with duration of three days as opposed to recently published protocols that take 45 days or longer [139, 207, 208]. The protocol is effective at decellularizing the connective tissue surrounding the cartilage rings, but does not fully decellularize the cartilage, which is also similar to previous reports [139, 207, 208]. Previous studies have shown that chondrocytes lack MHC complexes [209], but the biologic significance of these remnant host cells in a xenogeneic recipient is unknown. The present decellularization method showed retention of GAGs within the cartilage comparable with native cartilage [210], and preserved a basement membrane structure on the lumen of the graft [211]. The present study also showed that the HDTM grafts have a pressure-diameter response that is similar to native tracheas at the time of implantation. Although previous reports have shown similar mechanical strength of native tracheas and decellularized tracheal grafts [208], the tests were performed in uniaxial tension, so the results only verify that the grafts did not experience detectable collagen damage due to the decellularization process, while the present results confirm that the HDTM graft will tolerate physiologic loading.

The orthotopic remodeling results of the present study are in contrast to the results of a previous study that showed that lyophilized decellularized tracheal matrix resulted in the formation of fibrous connective tissue with squamous epithelial formation and no persistence of cartilage in the same patch tracheoplasty model after 8 weeks of remodeling [201]. The epithelial formation in

the present study was similar to that observed on urinary bladder matrix, a different form of xenogeneic ECM, which showed complete coverage with ciliated cells and scattered secretory cells. The presence of these differentiated cells is thought to be due to the proliferation of basal cells on the scaffold that have been shown to be the progenitor cells of the tracheal epithelium [212-215]. Several studies have shown that the presence of a basement membrane promotes proliferation and differentiation of basal cells in vitro [216, 217].

The persistence of cartilage in the present study as compared to our previous study appears to be directly dependent on the hydration of the cartilage within the scaffold. Cartilage is rich in GAGs that retain water, thereby giving cartilage its ability to resist compressive stress [218-220]. It is possible that dehydration of the matrix alters the conformation of the GAGs such that they no longer maintain a strong affinity for water. Previous studies of ECM scaffolds derived from porcine small intestine showed that after lyophilization, tissues were only able to take up approximately 70% of their original water content [221].

The in vivo remodeling results of the present study are similar to those that describe the use of a decellularized canine tracheal allograft that was used to reconstruct the intrathoracic trachea [203, 222]. The previous study utilized a similar decellularization protocol to the one used in the present study, but the grafts were not sterilized. The previous study claimed that the protocol yielded a hybrid scaffold with decellularized mucosal tissue and viable chondrocytes that participated in the remodeling response [222]. The protocol used in the present study was unlikely to preserve viable chondrocytes within the cartilage due to prolonged freezing time and terminal sterilization. The present study showed that HDTM can provide mechanical support necessary for respiration for a period approaching 8 weeks. However, implantation at the orthotopic site showed that 8 weeks is likely the limit for persistence of functional cartilage since two of the orthotopic

grafts showed histologic evidence of cartilage degradation and two other showed complete loss of the cartilaginous structures. Only one of the grafts showed histologic evidence of newly formed cartilage within the graft, however the cartilage formation was very localized and did not bridge the gap created by the defect. It is possible that the lack of vascularization at the time of orthotopic implantation led to the more rapid remodeling response, and that a period of pre-implantation at a heterotopic site may provide the vascular supply necessary for the cartilage grafts to eventually be remodeled into viable tissue [223-226]. Another option would be to seed the scaffold with mesenchymal cells that would form cartilage either [139, 227-229]. Recent studies have shown that cartilage tubes formed after heterotopic implantation do not adequately support epithelialization [230], so a combination of combination of seeded chondrocytes on an ECM scaffold may address the limitations of both approaches.

Degradation is an important aspect of the remodeling of extracellular matrix scaffolds. Several reports have shown that non-crosslinked scaffolds derived from mucosal tissues (e.g., porcine small intestinal submucosa) are completely degraded within 90 days after implantation [114, 115], while scaffolds derived from dermis may take longer to degrade. Chemical crosslinking is known to delay or prevent ECM scaffold degradation [182, 231], and cellular remnants within the scaffold have been shown to delay the degradation process [176]. In the present study, the tracheal scaffold appears to follow a two phase degradation profile, with the mucosal connective tissue degrading quickly and being replaced by new host tissue, and the cartilage degrading more slowly. This unique degradation profile has important implications for the host remodeling response since delayed degradation is associated with a pro-inflammatory response that can lead to either scar tissue formation or a foreign body response [232]. Conversely, rapid degradation of ECM scaffolds is associated with the release of matricryptic peptides that have innate bioactivity, including

chemotaxis for progenitor cells and bacteriostasis [118, 124, 180], and replacement of the scaffold with site-appropriate tissue. The constructive tracheal remodeling observed in the present study is more typical of the response to a degrading scaffold.

There are several limitations to the present study. First, the study utilized a heterotopic implant model and an orthotopic patch tracheoplasty model to assess the potential for HDTM to serve as a full circumferential tracheal replacement. Given the possibility of respiratory distress if the approach failed, we deemed it appropriate to take a conservative approach by avoiding full circumferential replacement. Based on the present results, future studies will evaluate HDTM in a model of full circumferential tracheal reconstruction with and without pre-implantation in the neck. In addition, the study is limited in that the source of cells that populated the remodeled tissue is unknown, particularly for the epithelial formation. Future studies including sacrifice at earlier time points will be required to determine if local cells migrate onto the ECM scaffold, and if so, which populations of cells are involved. As a third limitation, the present study specifically excluded any investigation of cell seeding so that the role of the HDTM alone might be better understood. However, it is likely that appropriate seeding of epithelial cells and chondrocytes in an appropriate bioreactor system may improve the remodeling outcome. Despite these limitations, the present study supports further investigation of decellularized tracheal matrix. Although the findings suggest that a mesenchymal cell population is probably necessary to promote cartilaginous formation, the HDTM should provide sufficient mechanical strength to sustain physiologic loading immediately after implantation and supports the development of mature airway epithelium.

# APPENDIX C

## ACKNOWLDEDGEMENTS AND FUNDING SOURCES

Funding for all research described was provided by NIH Grant R03EB009237 (TWG), the support of the William G. McGowan Charitable Fund's support to the McGowan Institute for Regenerative Medicine, and Children's Hospital of Pittsburgh of UPMC; as well as NIH Training Grants T32EB001026-06 from the National Institute of Biomedical Imaging And Bioengineering and T32HL076124-05 entitled "Cardiovascular Bioengineering Training Program".

**Acknowledgements for Specific Aim 1:**

The authors would like to recognize contributions from Dr. Lei Yang at Children's Hospital of Pittsburgh as well as Dr. John Wainwright.

**Acknowledgements for Specific Aim 2:**

The authors would like to recognize contributions from Dr. Glenn Gaudette and John Favreau at the Worchester Polytechnic Institute in assistance with strain analysis data.

**Acknowledgments for Appendix A:**

The authors would like to acknowledge Brogan Guest and Kristen Lippert for their contributions to this work.

**Acknowledgements for Appendix B:**

The authors would like to acknowledge funding from the Commonwealth of Pennsylvania. The authors would also like to thank Susan D. Reynolds for scientific review of the manuscript prior to submission.

## BIBLIOGRAPHY


1. Hoffman, J.I. and S. Kaplan, *The incidence of congenital heart disease.* J Am Coll Cardiol, 2002. **39**(12): p. 1890-900.

2. Roger, V.L., et al., *Executive summary: heart disease and stroke statistics--2012 update: a report from the American Heart Association.* Circulation. **125**(1): p. 188-97.

3. Gilbert, T.W., et al., *Repair of the thoracic wall with an extracellular matrix scaffold in a canine model.* J Surg Res, 2008. **147**(1): p. 61-7.

4. Brown, B.N., et al., *Macrophage phenotype as a predictor of constructive remodeling following the implantation of biologically derived surgical mesh materials.* Acta Biomater. **8**(3): p. 978-87.

5. Cortiella, J., et al., *Influence of acellular natural lung matrix on murine embryonic stem cell differentiation and tissue formation.* Tissue Eng Part A, 2010. **16**(8): p. 2565-80.

6. Nieponice, A., et al., *An extracellular matrix scaffold for esophageal stricture prevention after circumferential EMR.* Gastrointest Endosc, 2009. **69**(2): p. 289-96.

7. Ozawa, T., et al., *Histologic changes of nonbiodegradable and biodegradable biomaterials used to repair right ventricular heart defects in rats.* J Thorac Cardiovasc Surg, 2002. **124**(6): p. 1157-64.

8. Ozawa, T., et al., *Optimal biomaterial for creation of autologous cardiac grafts.* Circulation, 2002. **106**(12 Suppl 1): p. I176-82.

9. Eschenhagen, T., et al., *3D engineered heart tissue for replacement therapy.* Basic Res Cardiol, 2002. **97 Suppl 1**: p. I146-52.

10. Zimmermann, W.H., et al., *Cardiac grafting of engineered heart tissue in syngenic rats.* Circulation, 2002. **106**(12 Suppl 1): p. I151-7.

11. Hata, H., et al., *Engineering a novel three-dimensional contractile myocardial patch with cell sheets and decellularised matrix.* Eur J Cardiothorac Surg. **38**(4): p. 450-5.

12. Masuda, S., et al., *Cell sheet engineering for heart tissue repair.* Adv Drug Deliv Rev, 2008. **60**(2): p. 277-85.

13. Shimizu, T., et al., *Fabrication of pulsatile cardiac tissue grafts using a novel 3-dimensional cell sheet manipulation technique and temperature-responsive cell culture surfaces.* Circ Res, 2002. **90**(3): p. e40.

14. Zimmermann, W.H., et al., *Three-dimensional engineered heart tissue from neonatal rat cardiac myocytes.* Biotechnol Bioeng, 2000. **68**(1): p. 106-14.

15. Zimmermann, W.H., et al., *Tissue engineering of a differentiated cardiac muscle construct.* Circ Res, 2002. **90**(2): p. 223-30.

16. Didie, M., et al., *Parthenogenetic stem cells for tissue-engineered heart repair.* J Clin Invest. **123**(3): p. 1285-98.

17. Johnson, S.L., *The history of cardiac surgery, 1896-1955*. 1970, Baltimore,: Johns Hopkins Press. xv, 201 p.

18. Absolon, K.B. and M.A. Naficy, *First successful cardiac operation in a human, 1896 : a documentation : the life, the times, and the work of Ludwig Rehn (1849-1930)*. 2002, Rockville, MD: Kabel. 246 p.

19. Go, A.S., et al., *Heart disease and stroke statistics--2013 update: a report from the American Heart Association.* Circulation. **127**(1): p. e6-e245.

20. *Report of the New England Regional Infant Cardiac Program.* Pediatrics, 1980. **65**(2 Pt 2): p. 375-461.

21. Rosamond, W., et al., *Heart disease and stroke statistics--2008 update: a report from the American Heart Association Statistics Committee and Stroke Statistics Subcommittee.* Circulation, 2008. **117**(4): p. e25-146.

22. Hoffman, J.I., S. Kaplan, and R.R. Liberthson, *Prevalence of congenital heart disease.* Am Heart J, 2004. **147**(3): p. 425-39.

23. Ford, E.S., et al., *Explaining the decrease in U.S. deaths from coronary disease, 1980-2000.* N Engl J Med, 2007. **356**(23): p. 2388-98.

24. Chiong, M., et al., *Cardiomyocyte death: mechanisms and translational implications.* Cell Death Dis. **2**: p. e244.

25. Freytes, D.O., L. Santambrogio, and G. Vunjak-Novakovic, *Optimizing dynamic interactions between a cardiac patch and inflammatory host cells.* Cells Tissues Organs. **195**(1-2): p. 171-82.

26. Child, J.S., *Fallot's tetralogy and pregnancy: prognostication and prophesy.* J Am Coll Cardiol, 2004. **44**(1): p. 181-3.

27. Martins, P. and E. Castela, *Transposition of the great arteries.* Orphanet J Rare Dis, 2008. **3**: p. 27.

28. Bondy, C.A., *Hypoplastic left heart syndrome.* N Engl J Med. **362**(21): p. 2026-8.

29. Pignone, M., et al., *Aspirin, statins, or both drugs for the primary prevention of coronary heart disease events in men: a cost-utility analysis.* Ann Intern Med, 2006. **144**(5): p. 326-36.

30. Heran, B.S., et al., *Angiotensin receptor blockers for heart failure.* Cochrane Database Syst Rev. **4**: p. CD003040.

31. Hunt, S.A., et al., *2009 focused update incorporated into the ACC/AHA 2005 Guidelines for the Diagnosis and Management of Heart Failure in Adults: a report of the American College of Cardiology Foundation/American Heart Association Task Force on Practice Guidelines: developed in collaboration with the International Society for Heart and Lung Transplantation.* Circulation, 2009. **119**(14): p. e391-479.

32. Boron, W.F. and E.L. Boulpaep, *Medical physiology : a cellular and molecular approach*. 1st ed. 2003, Philadelphia, PA: W.B. Saunders. xiii, 1319 p.

33. Freemantle, N., et al., *beta Blockade after myocardial infarction: systematic review and meta regression analysis.* BMJ, 1999. **318**(7200): p. 1730-7.

34. Tuttle, R.R. and J. Mills, *Dobutamine: development of a new catecholamine to selectively increase cardiac contractility.* Circ Res, 1975. **36**(1): p. 185-96.

35. Al-Khatib, S.M., et al., *Implantable cardioverter defibrillators and cardiac resynchronization therapy in patients with left ventricular dysfunction: randomized trial evidence through 2004.* Am Heart J, 2005. **149**(6): p. 1020-34.

36. Osaki, S., et al., *Improved survival in patients with ventricular assist device therapy: the University of Wisconsin experience.* Eur J Cardiothorac Surg, 2008. **34**(2): p. 281-8.

37. Hijikata, W., et al., *A magnetically levitated centrifugal blood pump with a simple-structured disposable pump head.* Artif Organs, 2008. **32**(7): p. 531-40.

38. Qian, K.X., et al., *Permanent magnetic-levitation of rotating impeller: a decisive breakthrough in the centrifugal pump.* J Med Eng Technol, 2002. **26**(1): p. 36-8.

39. Schulman, A.R., et al., *Comparisons of infection complications between continuous flow and pulsatile flow left ventricular assist devices.* J Thorac Cardiovasc Surg, 2007. **133**(3): p. 841-2.

40. Almond, C.S., et al., *Berlin Heart EXCOR Pediatric Ventricular Assist Device for Bridge to Heart Transplantation in US Children.* Circulation. **127**(16): p. 1702-11.

41. Antaki, J.F., et al., *PediaFlow Maglev Ventricular Assist Device: A Prescriptive Design Approach.* Cardiovasc Eng. **1**(1): p. 104-121.

42. Maul, T.M., et al., *Pre-clinical Implants of the Levitronix PediVAS Pediatric Ventricular Assist Device - Strategy for Regulatory Approval.* Cardiovasc Eng Technol. **2**(4): p. 263-275.

43. Wearden, P.D., et al., *The PediaFlow pediatric ventricular assist device.* Semin Thorac Cardiovasc Surg Pediatr Card Surg Annu, 2006: p. 92-8.

44. Ashbrook, M., et al., *Left Ventricular Assist Device-Induced Coagulation and Platelet Activation and Effect of the Current Anticoagulant Therapy Regimen.* Clin Appl Thromb Hemost.

45. Samuels, L.E., et al., *Argatroban as a primary or secondary postoperative anticoagulant in patients implanted with ventricular assist devices.* Ann Thorac Surg, 2008. **85**(5): p. 1651-5.

46. Schulman, A.R., et al., *Effect of left ventricular assist device infection on post-transplant outcomes.* J Heart Lung Transplant, 2009. **28**(3): p. 237-42.

47. Adachi, I., et al., *Ventricular assist device infection necessitating device exchange following extensive myocardial resection.* J Artif Organs, 2009. **12**(4): p. 271-3.

48. Stehlik, J., et al., *ISHLT International Registry for Heart and Lung Transplantation - three decades of scientific contributions.* Transplant Rev (Orlando). **27**(2): p. 38-42.

49. de Jonge, N., et al., *Guidelines for heart transplantation.* Neth Heart J, 2008. **16**(3): p. 79-87.

50. Hertz, M.I., *The Registry of the International Society for Heart and Lung Transplantation--Introduction to the 2012 annual reports: new leadership, same vision.* J Heart Lung Transplant. **31**(10): p. 1045-51.

51. Zandonella, C., *Tissue engineering: The beat goes on.* Nature, 2003. **421**(6926): p. 884-6.

52. Holtzer, H., J. Abbott, and M.W. Cavanaugh, *Some properties of embryonic cardiac myoolasts.* Exp Cell Res, 1959. **16**(3): p. 595-601.

53. McDonald, T.F., H.G. Sachs, and R.L. DeHaan, *Development of sensitivity to tetrodotoxin in beating chick embryo hearts, single cells, and aggregates.* Science, 1972. **176**(4040): p. 1248-50.

54. Hobo, K., et al., *Therapeutic angiogenesis using tissue engineered human smooth muscle cell sheets.* Arterioscler Thromb Vasc Biol, 2008. **28**(4): p. 637-43.

55. Kanzaki, M., et al., *Tissue engineered epithelial cell sheets for the creation of a bioartificial trachea.* Tissue Eng, 2006. **12**(5): p. 1275-83.

56. Kanzaki, M., et al., *Dynamic sealing of lung air leaks by the transplantation of tissue engineered cell sheets.* Biomaterials, 2007. **28**(29): p. 4294-302.

57. Eschenhagen, T. and W.H. Zimmermann, *Engineering myocardial tissue.* Circ Res, 2005. **97**(12): p. 1220-31.

58. Vandenburgh, H.H., P. Karlisch, and L. Farr, *Maintenance of highly contractile tissue-cultured avian skeletal myotubes in collagen gel.* In Vitro Cell Dev Biol, 1988. **24**(3): p. 166-74.

59. Vandenburgh, H.H., *A computerized mechanical cell stimulator for tissue culture: effects on skeletal muscle organogenesis.* In Vitro Cell Dev Biol, 1988. **24**(7): p. 609-19.

60. Vandenburgh, H.H., S. Swasdison, and P. Karlisch, *Computer-aided mechanogenesis of skeletal muscle organs from single cells in vitro.* FASEB J, 1991. **5**(13): p. 2860-7.

61. Simpson, D.G., et al., *Modulation of cardiac myocyte phenotype in vitro by the composition and orientation of the extracellular matrix.* J Cell Physiol, 1994. **161**(1): p. 89-105.

62. McDevitt, T.C., et al., *Spatially organized layers of cardiomyocytes on biodegradable polyurethane films for myocardial repair.* J Biomed Mater Res A, 2003. **66**(3): p. 586-95.

63. Sacks, M.S. and D.C. Gloeckner, *Quantification of the fiber architecture and biaxial mechanical behavior of porcine intestinal submucosa.* J Biomed Mater Res, 1999. **46**(1): p. 1-10.

64. Gilbert, T.W., et al., *Collagen fiber alignment and biaxial mechanical behavior of porcine urinary bladder derived extracellular matrix.* Biomaterials, 2008. **29**(36): p. 4775-82.

65. Menasche, P., *Cardiac cell therapy: lessons from clinical trials.* J Mol Cell Cardiol. **50**(2): p. 258-65.

66. Quyyumi, A.A., et al., *CD34(+) cell infusion after ST elevation myocardial infarction is associated with improved perfusion and is dose dependent.* Am Heart J. **161**(1): p. 98-105.

67. Hare, J.M., *Translational development of mesenchymal stem cell therapy for cardiovascular diseases.* Tex Heart Inst J, 2009. **36**(2): p. 145-7.

68. Hare, J.M., et al., *A randomized, double-blind, placebo-controlled, dose-escalation study of intravenous adult human mesenchymal stem cells (prochymal) after acute myocardial infarction.* J Am Coll Cardiol, 2009. **54**(24): p. 2277-86.

69. Kehat, I., et al., *Human embryonic stem cells can differentiate into myocytes with structural and functional properties of cardiomyocytes.* J Clin Invest, 2001. **108**(3): p. 407-14.

70. Yang, L., et al., *Human cardiovascular progenitor cells develop from a KDR+ embryonic-stem-cell-derived population.* Nature, 2008. **453**(7194): p. 524-8.

71. Laflamme, M.A. and C.E. Murry, *Regenerating the heart.* Nat Biotechnol, 2005. **23**(7): p. 845-56.

72. Sheridan, C., *Cardiac stem cell therapies inch toward clinical litmus test.* Nat Biotechnol. **31**(1): p. 5-6.

73. Payne, W.S. and J.W. Kirklin, *Late complications after plastic reconstruction of outflow tract in tetralogy of Fallot.* Ann Surg, 1961. **154**: p. 53-7.

74. Untersinger, F., B. Koch, and G. Simonis, *[Aneurysmal complication of a dacron vascular prosthesis]*. J Chir (Paris), 1982. **119**(12): p. 731-3.

75. Lane-Smith, D.M., D.A. Gillis, and P.D. Roy, *Repair of pectus excavatum using a Dacron vascular graft strut.* J Pediatr Surg, 1994. **29**(9): p. 1179-82.

76. Merendino, K.A., G.W. Girvin, and G.I. Thomas, *The clinical use of Teflon tubes as a vascular substitute for major arteries.* Surgery, 1958. **43**(6): p. 959-68.

77. Honigman, F.H., D.E. Wagner, and P. Nemir, Jr., *The fate of Teflon vascular grafts.* J Thorac Cardiovasc Surg, 1969. **57**(2): p. 255-68.

78. Oku, H., et al., *Right ventricular outflow tract prosthesis in total correction of tetralogy of Fallot.* Circulation, 1980. **62**(3): p. 604-9.

79. Yoshida, M., et al., *Right ventricular outflow tract reconstruction with bicuspid valved polytetrafluoroethylene conduit.* Ann Thorac Surg. **91**(4): p. 1235-8; discussion 1239.

80. Alvarez-Cordero, R., et al., *Evaluation of polyglycolic acid sutures in vascular surgery.* J Surg Res, 1973. **15**(1): p. 35-44.

81. Hagiwara, H., et al., *Vascular responses to a biodegradable polymer (polylactic acid) based biolimus A9-eluting stent in porcine models.* EuroIntervention. **8**(6): p. 743-51.

82. Zong, X., et al., *Electrospun fine-textured scaffolds for heart tissue constructs.* Biomaterials, 2005. **26**(26): p. 5330-8.

83. Canton, I., et al., *Development of an Ibuprofen-releasing biodegradable PLA/PGA electrospun scaffold for tissue regeneration.* Biotechnol Bioeng. **105**(2): p. 396-408.

84. Guan, J., J.J. Stankus, and W.R. Wagner, *Biodegradable elastomeric scaffolds with basic fibroblast growth factor release.* J Control Release, 2007. **120**(1-2): p. 70-8.

85. Xu, H., et al., *Rapid prototyped PGA/PLA scaffolds in the reconstruction of mandibular condyle bone defects.* Int J Med Robot. **6**(1): p. 66-72.

86. Zwingmann, J., et al., *Chondrogenic differentiation of human articular chondrocytes differs in biodegradable PGA/PLA scaffolds.* Tissue Eng, 2007. **13**(9): p. 2335-43.

87. Freed, L.E., et al., *Biodegradable polymer scaffolds for tissue engineering.* Biotechnology (N Y), 1994. **12**(7): p. 689-93.

88. Fujimoto, K.L., et al., *An elastic, biodegradable cardiac patch induces contractile smooth muscle and improves cardiac remodeling and function in subacute myocardial infarction.* J Am Coll Cardiol, 2007. **49**(23): p. 2292-300.

89. Fujimoto, K.L., et al., *In vivo evaluation of a porous, elastic, biodegradable patch for reconstructive cardiac procedures.* Ann Thorac Surg, 2007. **83**(2): p. 648-54.

90. Guan, J., et al., *Synthesis, characterization, and cytocompatibility of elastomeric, biodegradable poly(ester-urethane)ureas based on poly(caprolactone) and putrescine.* J Biomed Mater Res, 2002. **61**(3): p. 493-503.

91. Fujimoto, K.L., et al., *Synthesis, characterization and therapeutic efficacy of a biodegradable, thermoresponsive hydrogel designed for application in chronic infarcted myocardium.* Biomaterials, 2009. **30**(26): p. 4357-68.

92. Breymann, T., et al., *European Contegra multicentre study: 7-year results after 165 valved bovine jugular vein graft implantations.* Thorac Cardiovasc Surg, 2009. **57**(5): p. 257-69.

93. Rajani, B., R.B. Mee, and N.B. Ratliff, *Evidence for rejection of homograft cardiac valves in infants.* J Thorac Cardiovasc Surg, 1998. **115**(1): p. 111-7.

94. Konuma, T., et al., *Performance of CryoValve SG decellularized pulmonary allografts compared with standard cryopreserved allografts.* Ann Thorac Surg, 2009. **88**(3): p. 849-54; discussion 554-5.

95. Hickey, E.J., et al., *Late risk of outcomes for adults with repaired tetralogy of Fallot from an inception cohort spanning four decades.* Eur J Cardiothorac Surg, 2009. **35**(1): p. 156-64; discussion 164.

96. Cardis, B.M., D.A. Fyfe, and W.T. Mahle, *Elastic properties of the reconstructed aorta in hypoplastic left heart syndrome.* Ann Thorac Surg, 2006. **81**(3): p. 988-91.

97. Hooper, D.K., et al., *Panel-reactive antibodies late after allograft implantation in children.* Ann Thorac Surg, 2005. **79**(2): p. 641-4; discussion 645.

98. Feingold, B., et al., *Tolerance to incompatible ABO blood group antigens is not observed following homograft implantation.* Hum Immunol. **72**(10): p. 835-40.

99. Feingold, B., et al., *Expression of A and B blood group antigens on cryopreserved homografts.* Ann Thorac Surg, 2009. **87**(1): p. 211-4.

100. Elkins, R.C., et al., *Decellularized human valve allografts.* Ann Thorac Surg, 2001. **71**(5 Suppl): p. S428-32.

101. Hopkins, R.A., et al., *Decellularization reduces calcification while improving both durability and 1-year functional results of pulmonary homograft valves in juvenile sheep.* J Thorac Cardiovasc Surg, 2009. **137**(4): p. 907-13, 913e1-4.

102. Sievers, H.H., et al., *Decellularized pulmonary homograft (SynerGraft) for reconstruction of the right ventricular outflow tract: first clinical experience.* Z Kardiol, 2003. **92**(1): p. 53-9.

103. Miller, D.V., W.D. Edwards, and K.J. Zehr, *Endothelial and smooth muscle cell populations in a decellularized cryopreserved aortic homograft (SynerGraft) 2 years after implantation.* J Thorac Cardiovasc Surg, 2006. **132**(1): p. 175-6.

104. Badylak, S.F., et al., *Comparison of the resistance to infection of intestinal submucosa arterial autografts versus polytetrafluoroethylene arterial prostheses in a dog model.* J Vasc Surg, 1994. **19**(3): p. 465-72.

105. Badylak, S.F., et al., *Small intestinal submucosa as a large diameter vascular graft in the dog.* J Surg Res, 1989. **47**(1): p. 74-80.

106. Badylak, S.F., et al., *Extracellular matrix for myocardial repair.* Heart Surg Forum, 2003. **6**(2): p. E20-6.

107. Kochupura, P.V., et al., *Tissue-engineered myocardial patch derived from extracellular matrix provides regional mechanical function.* Circulation, 2005. **112**(9 Suppl): p. I144-9.

108. Lantz, G.C., et al., *Small intestinal submucosa as a small-diameter arterial graft in the dog.* J Invest Surg, 1990. **3**(3): p. 217-27.

109. Lantz, G.C., et al., *Small intestinal submucosa as a superior vena cava graft in the dog.* J Surg Res, 1992. **53**(2): p. 175-81.

110. Ota, T., et al., *A fusion protein of hepatocyte growth factor enhances reconstruction of myocardium in a cardiac patch derived from porcine urinary bladder matrix.* J Thorac Cardiovasc Surg, 2008. **136**(5): p. 1309-17.

111. Robinson, K.A., et al., *Extracellular matrix scaffold for cardiac repair.* Circulation, 2005. **112**(9 Suppl): p. I135-43.

112. Sandusky, G.E., Jr., et al., *Histologic findings after in vivo placement of small intestine submucosal vascular grafts and saphenous vein grafts in the carotid artery in dogs.* Am J Pathol, 1992. **140**(2): p. 317-24.

113. Sandusky, G.E., G.C. Lantz, and S.F. Badylak, *Healing comparison of small intestine submucosa and ePTFE grafts in the canine carotid artery.* J Surg Res, 1995. **58**(4): p. 415-20.

114. Gilbert, T.W., et al., *Degradation and remodeling of small intestinal submucosa in canine Achilles tendon repair.* J Bone Joint Surg Am, 2007. **89**(3): p. 621-30.

115. Record, R.D., et al., *In vivo degradation of $^{14}$C-labeled small intestinal submucosa (SIS) when used for urinary bladder repair.* Biomaterials, 2001. **22**(19): p. 2653-9.

116. Gilbert, T.W., A.M. Stewart-Akers, and S.F. Badylak, *A quantitative method for evaluating the degradation of biologic scaffold materials.* Biomaterials, 2007. **28**(2): p. 147-50.

117. Badylak, S.F., et al., *Host protection against deliberate bacterial contamination of an extracellular matrix bioscaffold versus Dacron mesh in a dog model of orthopedic soft tissue repair.* J Biomed Mater Res B Appl Biomater, 2003. **67**(1): p. 648-54.

118. Brennan, E.P., et al., *Antibacterial activity within degradation products of biological scaffolds composed of extracellular matrix.* Tissue Eng, 2006. **12**(10): p. 2949-55.

119. Jernigan, T.W., et al., *Small intestinal submucosa for vascular reconstruction in the presence of gastrointestinal contamination.* Ann Surg, 2004. **239**(5): p. 733-8; discussion 738-40.

120. Shell, D.H., 4th, et al., *Comparison of small-intestinal submucosa and expanded polytetrafluoroethylene as a vascular conduit in the presence of gram-positive contamination.* Ann Surg, 2005. **241**(6): p. 995-1001; discussion 1001-4.

121. Medberry, C.J., et al., *Resistance to Infection of Five Different Materials in a Rat Body Wall Model.* J Surg Res.

122. Badylak, S.F., et al., *Marrow-derived cells populate scaffolds composed of xenogeneic extracellular matrix.* Exp Hematol, 2001. **29**(11): p. 1310-8.

123. Zantop, T., et al., *Extracellular matrix scaffolds are repopulated by bone marrow-derived cells in a mouse model of Achilles tendon reconstruction.* J Orthop Res, 2006. **24**(6): p. 1299-309.

124. Reing, J.E., et al., *Degradation products of extracellular matrix affect cell migration and proliferation.* Tissue Eng Part A, 2009. **15**(3): p. 605-14.

125. Badylak, S.F., D.O. Freytes, and T.W. Gilbert, *Extracellular matrix as a biological scaffold material: Structure and function.* Acta Biomaterialia, 2009. **5**(1): p. 1-13.

126. Ott, H.C., et al., *Regeneration and orthotopic transplantation of a bioartificial lung.* Nat Med, 2010. **16**(8): p. 927-33.

127. Ott, H.C., et al., *Perfusion-decellularized matrix: using nature's platform to engineer a bioartificial heart.* Nat Med, 2008.

128. Petersen, T.H., et al., *Tissue-engineered lungs for in vivo implantation.* Science, 2010. **329**(5991): p. 538-41.

129. Uygun, B.E., et al., *Organ reengineering through development of a transplantable recellularized liver graft using decellularized liver matrix.* Nat Med, 2010.

130. Wainwright, J.M., et al., *Preparation of cardiac extracellular matrix from an intact porcine heart.* Tissue Eng Part C Methods, 2010. **16**(3): p. 525-32.

131. Crapo, P.M., T.W. Gilbert, and S.F. Badylak, *An overview of tissue and whole organ decellularization processes.* Biomaterials, 2011. **32**(12): p. 3233-43.

132. Gilbert, T.W., *Strategies for tissue and organ decellularization.* J Cell Biochem, 2012.

133. Gilbert, T.W., T.L. Sellaro, and S.F. Badylak, *Decellularization of tissues and organs.* Biomaterials, 2006. **27**(19): p. 3675-83.

134. Calle, E.A., T.H. Petersen, and L.E. Niklason, *Procedure for lung engineering.* J Vis Exp, (49).

135. Soto-Gutierrez, A., et al., *A whole-organ regenerative medicine approach for liver replacement.* Tissue Eng Part C Methods. **17**(6): p. 677-86.

136. Uygun, B.E., et al., *Organ reengineering through development of a transplantable recellularized liver graft using decellularized liver matrix.* Nat Med. **16**(7): p. 814-20.

137. Ott, H.C., et al., *Regeneration and orthotopic transplantation of a bioartificial lung.* Nat Med. **16**(8): p. 927-33.

138. Elliott, M.J., et al., *Tracheal reconstruction in children using cadaveric homograft trachea.* Eur J Cardiothorac Surg, 1996. **10**(9): p. 707-12.

139. Macchiarini, P., et al., *Clinical transplantation of a tissue-engineered airway.* Lancet, 2008. **372**(9655): p. 2023-30.

140. Remlinger, N.T., et al., *Hydrated xenogeneic decellularized tracheal matrix as a scaffold for tracheal reconstruction.* Biomaterials. **31**(13): p. 3520-3526.

141. Sellaro, T.L., et al., *Maintenance of hepatic sinusoidal endothelial cell phenotype in vitro using organ-specific extracellular matrix scaffolds.* Tissue Eng, 2007. **13**(9): p. 2301-10.

142. Cortiella, J., et al., *Influence of acellular natural lung matrix on murine embryonic stem cell differentiation and tissue formation.* Tissue Eng Part A. **16**(8): p. 2565-80.

143. Soto-Gutierrez, A., et al., *Perspectives on whole-organ assembly: moving toward transplantation on demand.* J Clin Invest. **122**(11): p. 3817-23.

144. Crapo, P.M., T.W. Gilbert, and S.F. Badylak, *An overview of tissue and whole organ decellularization processes.* Biomaterials. **32**(12): p. 3233-43.

145. Gilbert, T.W., *Strategies for tissue and organ decellularization.* J Cell Biochem. **113**(7): p. 2217-22.

146. Wainwright, J.M., et al., *Right ventricular outflow tract repair with a cardiac biologic scaffold.* Cells Tissues Organs. **195**(1-2): p. 159-70.

147. Ott, H.C., et al., *Perfusion-decellularized matrix: using nature's platform to engineer a bioartificial heart.* Nat Med, 2008. **14**(2): p. 213-21.

148. Wainwright, J.M., et al., *Right ventricular outflow tract repair with a cardiac biologic scaffold.* Cells Tissues Organs, 2012. **195**(1-2): p. 159-70.

149. Ota, T., et al., *Electromechanical characterization of a tissue-engineered myocardial patch derived from extracellular matrix.* J Thorac Cardiovasc Surg, 2007. **133**(4): p. 979-85.

150. Kelly, D.J., et al., *Increased myocyte content and mechanical function within a tissue-engineered myocardial patch following implantation.* Tissue Eng Part A, 2009. **15**(8): p. 2189-201.

151. Andree, B., et al., *Small Intestinal Submucosa Segments as Matrix for Tissue Engineering: Review.* Tissue Eng Part B Rev.

152. Fujimoto, K.L., et al., *Engineered fetal cardiac graft preserves its cardiomyocyte proliferation within postinfarcted myocardium and sustains cardiac function.* Tissue Eng Part A. **17**(5-6): p. 585-96.

153. Turner, W.S., et al., *Cardiac tissue development for delivery of embryonic stem cell-derived endothelial and cardiac cells in natural matrices.* J Biomed Mater Res B Appl Biomater. **100**(8): p. 2060-72.

154. Jin, C.Z., et al., *In vivo cartilage tissue engineering using a cell-derived extracellular matrix scaffold.* Artif Organs, 2007. **31**(3): p. 183-92.

155. Brown, B.N., et al., *Surface characterization of extracellular matrix scaffolds.* Biomaterials. **31**(3): p. 428-37.

156. Gilbert, T.W., et al., *Fiber kinematics of small intestinal submucosa under biaxial and uniaxial stretch.* J Biomech Eng, 2006. **128**(6): p. 890-8.

157. Gilbert, T.W., et al., *Gene expression by fibroblasts seeded on small intestinal submucosa and subjected to cyclic stretching.* Tissue Eng, 2007. **13**(6): p. 1313-23.

158. von der Mark, K., et al., *Nanoscale engineering of biomimetic surfaces: cues from the extracellular matrix.* Cell Tissue Res. **339**(1): p. 131-53.

159. Chen, Z.G., et al., *Electrospun collagen-chitosan nanofiber: a biomimetic extracellular matrix for endothelial cell and smooth muscle cell.* Acta Biomater. **6**(2): p. 372-82.

160. Eschenhagen, T., et al., *Three-dimensional reconstitution of embryonic cardiomyocytes in a collagen matrix: a new heart muscle model system.* FASEB J, 1997. **11**(8): p. 683-94.

161. Dora, C.D., et al., *Time dependent variations in biomechanical properties of cadaveric fascia, porcine dermis, porcine small intestine submucosa, polypropylene mesh and autologous fascia in the rabbit model: implications for sling surgery.* J Urol, 2004. **171**(5): p. 1970-3.

162. Butler, C.E., H.N. Langstein, and S.J. Kronowitz, *Pelvic, abdominal, and chest wall reconstruction with AlloDerm in patients at increased risk for mesh-related complications.* Plast Reconstr Surg, 2005. **116**(5): p. 1263-75; discussion 1276-7.

163. Chen, S.G., Y.S. Tzeng, and C.H. Wang, *Treatment of severe burn with DermACELL((R)), an acellular dermal matrix.* Int J Burns Trauma. **2**(2): p. 105-9.

164. Freedman, B.E., *Full incorporation of Strattice Reconstructive Tissue Matrix in a reinforced hiatal hernia repair: a case report.* J Med Case Rep. **6**(1): p. 234.

165. Petersen, T.H., et al., *Tissue-engineered lungs for in vivo implantation.* Science. **329**(5991): p. 538-41.

166. Quarti, A., et al., *Preliminary experience in the use of an extracellular matrix to repair congenital heart diseases.* Interact Cardiovasc Thorac Surg. **13**(6): p. 569-72.

167. Badylak, S.F., et al., *The use of extracellular matrix as an inductive scaffold for the partial replacement of functional myocardium.* Cell Transplant, 2006. **15 Suppl 1**: p. S29-40.

168. Singelyn, J.M., et al., *Naturally derived myocardial matrix as an injectable scaffold for cardiac tissue engineering.* Biomaterials, 2009. **30**(29): p. 5409-16.

169. Lehr, E.J., et al., *Decellularization reduces immunogenicity of sheep pulmonary artery vascular patches.* J Thorac Cardiovasc Surg. **141**(4): p. 1056-62.

170. Xiong, Y., et al., *Decellularized Porcine Saphenous Artery for Small-Diameter Tissue-Engineered Conduit Graft.* Artif Organs.

171. Lofland, G.K., et al., *Initial pediatric cardiac experience with decellularized allograft patches.* Ann Thorac Surg. **93**(3): p. 968-71.

172. Singelyn, J.M., J.A. DeQuach, and K.L. Christman, *Injectable myocardial matrix as a scaffold for myocardial tissue engineering.* Conf Proc IEEE Eng Med Biol Soc, 2009. **2009**: p. 2406-8.

173. Wainwright, J.M., et al., *Preparation of cardiac extracellular matrix from an intact porcine heart.* Tissue Eng Part C Methods. **16**(3): p. 525-32.

174. Remlinger, N.T., Wearden, P.D., Gilbert, T.W. , *Procedure for Decellularization of Porcine Heart by Retrograde Coronary Perfusion.* J Vis Exp, 2012.

175. Remlinger, N.T., P.D. Wearden, and T.W. Gilbert, *Procedure for decellularization of porcine heart by retrograde coronary perfusion.* J Vis Exp, (70).

176. Brown, B.N., et al., *Macrophage phenotype and remodeling outcomes in response to biologic scaffolds with and without a cellular component.* Biomaterials, 2009. **30**(8): p. 1482-91.

177. Sellaro, T.L., et al., *Maintenance of human hepatocyte function in vitro by liver-derived extracellular matrix gels.* Tissue Eng Part A. **16**(3): p. 1075-82.

178. Gilbert, T.W., et al., *Morphologic assessment of extracellular matrix scaffolds for patch tracheoplasty in a canine model.* Ann Thorac Surg, 2008. **86**(3): p. 967-74; discussion 967-74.

179. Keane, T.J., et al., *Consequences of ineffective decellularization of biologic scaffolds on the host response.* Biomaterials. **33**(6): p. 1771-81.

180. Beattie, A.J., et al., *Chemoattraction of progenitor cells by remodeling extracellular matrix scaffolds.* Tissue Eng Part A, 2009. **15**(5): p. 1119-25.

181. Silva, K.D., R.L. Gamelli, and R. Shankar, *Bone marrow stem cell and progenitor response to injury.* Wound Repair Regen, 2001. **9**(6): p. 495-500.

182. Valentin, J.E., et al., *Macrophage participation in the degradation and remodeling of extracellular matrix scaffolds.* Tissue Eng Part A, 2009. **15**(7): p. 1687-94.

183. Badylak, S.F., et al., *Macrophage phenotype as a determinant of biologic scaffold remodeling.* Tissue Eng Part A, 2008. **14**(11): p. 1835-42.

184. Mantovani, A., et al., *The chemokine system in diverse forms of macrophage activation and polarization.* Trends Immunol, 2004. **25**(12): p. 677-86.

185. Mosser, D.M. and J.P. Edwards, *Exploring the full spectrum of macrophage activation.* Nat Rev Immunol, 2008. **8**(12): p. 958-69.

186. Malliaras, K., et al., *Cardiomyocyte proliferation and progenitor cell recruitment underlie therapeutic regeneration after myocardial infarction in the adult mouse heart.* EMBO Mol Med. **5**(2): p. 191-209.

187. Porrello, E.R., et al., *Transient regenerative potential of the neonatal mouse heart.* Science. **331**(6020): p. 1078-80.

188. Hodde, J.P., et al., *Retention of endothelial cell adherence to porcine-derived extracellular matrix after disinfection and sterilization.* Tissue Eng, 2002. **8**(2): p. 225-34.

189. Clause, K.C., et al., *A three-dimensional gel bioreactor for assessment of cardiomyocyte induction in skeletal muscle-derived stem cells.* Tissue Eng Part C Methods. **16**(3): p. 375-85.

190. Courtney, T., et al., *Design and analysis of tissue engineering scaffolds that mimic soft tissue mechanical anisotropy.* Biomaterials, 2006. **27**(19): p. 3631-8.

191. Karlon, W.J., et al., *Automated measurement of myofiber disarray in transgenic mice with ventricular expression of ras.* Anat Rec, 1998. **252**(4): p. 612-25.

192. Sacks, M.S., D.B. Smith, and E.D. Hiester, *A small angle light scattering device for planar connective tissue microstructural analysis.* Ann Biomed Eng, 1997. **25**(4): p. 678-89.

193. Shreiber, D.I., P.A. Enever, and R.T. Tranquillo, *Effects of pdgf-bb on rat dermal fibroblast behavior in mechanically stressed and unstressed collagen and fibrin gels.* Exp Cell Res, 2001. **266**(1): p. 155-66.

194. Albers, A.M., *An Investigation into Cellular Attachment and Contraction in Collagen-GAG Scaffolds with Characterized Pore Sizes.* 2004.

195. Akhyari, P., et al., *The quest for an optimized protocol for whole-heart decellularization: a comparison of three popular and a novel decellularization technique and their diverse effects on crucial extracellular matrix qualities.* Tissue Eng Part C Methods, 2011. **17**(9): p. 915-26.

196. Weymann, A., et al., *Development and evaluation of a perfusion decellularization porcine heart model--generation of 3-dimensional myocardial neoscaffolds.* Circ J, 2011. **75**(4): p. 852-60.

197. Grillo, H.C., *Tracheal replacement: a critical review.* Ann Thorac Surg, 2002. **73**(6): p. 1995-2004.

198. Wright, C.D., et al., *Anastomotic complications after tracheal resection: prognostic factors and management.* J Thorac Cardiovasc Surg, 2004. **128**(5): p. 731-9.

199. Macchiarini, P., et al., *Laryngotracheal resection and reconstruction for postintubation subglottic stenosis. Lessons learned.* Eur J Cardiothorac Surg, 1993. **7**(6): p. 300-5.

200. Wright, C.D., et al., *Pediatric tracheal surgery.* Ann Thorac Surg, 2002. **74**(2): p. 308-13; discussion 314.

201. Gilbert, T.W., et al., *Morphologic assessment of extracellular matrix scaffolds for patch tracheoplasty in a canine model.* Ann Thorac Surg, 2008. **86**(3): p. 967-73; discussion 973-74.

202. Liu, Y., et al., *Experimental study of blood typing in immunosuppressant-free tracheal transplantation in dogs.* Thorac Cardiovasc Surg, 2003. **51**(4): p. 216-20.

203. Liu, Y., et al., *A new tracheal bioartificial organ: evaluation of a tracheal allograft with minimal antigenicity after treatment by detergent.* Asaio J, 2000. **46**(5): p. 536-9.

204. Badylak, S.F., et al., *Esophageal reconstruction with ECM and muscle tissue in a dog model.* J Surg Res, 2005. **128**(1): p. 87-97.

205. Jankowski, R.J., et al., *Development of an experimental system for the study of urethral biomechanical function.* Am J Physiol Renal Physiol, 2004. **286**(2): p. F225-32.

206. Santelices, L.C., et al., *Experimental system for ex vivo measurement of murine aortic stiffness.* Physiol Meas, 2007. **28**(8): p. N39-49.

207. Conconi, M.T., et al., *Tracheal matrices, obtained by a detergent-enzymatic method, support in vitro the adhesion of chondrocytes and tracheal epithelial cells.* Transpl Int, 2005. **18**(6): p. 727-34.

208. Jungebluth, P., et al., *Structural and morphologic evaluation of a novel detergent-enzymatic tissue-engineered tracheal tubular matrix.* J Thorac Cardiovasc Surg, 2009. **138**(3): p. 586-93.

209. Liu, Y., et al., *Immunosuppressant-free allotransplantation of the trachea: the antigenicity of tracheal grafts can be reduced by removing the epithelium and mixed glands from the graft by detergent treatment.* J Thorac Cardiovasc Surg, 2000. **120**(1): p. 108-14.

210. Kojima, K., et al., *A composite tissue-engineered trachea using sheep nasal chondrocyte and epithelial cells.* FASEB J, 2003. **17**(8): p. 823-8.

211. Brown, B., et al., *The basement membrane component of biologic scaffolds derived from extracellular matrix.* Tissue Eng, 2006. **12**(3): p. 519-26.

212. Hajj, R., et al., *Basal cells of the human adult airway surface epithelium retain transit-amplifying cell properties.* Stem Cells, 2007. **25**(1): p. 139-48.

213. Hong, K.U., et al., *Basal cells are a multipotent progenitor capable of renewing the bronchial epithelium.* Am J Pathol, 2004. **164**(2): p. 577-88.

214. Hong, K.U., et al., *In vivo differentiation potential of tracheal basal cells: evidence for multipotent and unipotent subpopulations.* Am J Physiol Lung Cell Mol Physiol, 2004. **286**(4): p. L643-9.

215. Rock, J.R., et al., *Basal cells as stem cells of the mouse trachea and human airway epithelium.* Proc Natl Acad Sci U S A, 2009. **106**(31): p. 12771-5.

216. Boers, J.E., A.W. Ambergen, and F.B. Thunnissen, *Number and proliferation of basal and parabasal cells in normal human airway epithelium.* Am J Respir Crit Care Med, 1998. **157**(6 Pt 1): p. 2000-6.

217. Hosokawa, T., et al., *Differentiation of tracheal basal cells to ciliated cells and tissue reconstruction on the synthesized basement membrane substratum in vitro.* Connect Tissue Res, 2007. **48**(1): p. 9-18.

218. Rains, J.K., et al., *Mechanical properties of human tracheal cartilage.* J Appl Physiol, 1992. **72**(1): p. 219-25.

219. Roberts, C.R. and P.D. Pare, *Composition changes in human tracheal cartilage in growth and aging, including changes in proteoglycan structure.* Am J Physiol, 1991. **261**(2 Pt 1): p. L92-101.

220. Mathews, M.B. and L. Decker, *Comparative studies of water sorption of hyaline cartilage.* Biochim Biophys Acta, 1977. **497**(1): p. 151-9.

221. Whitson, B.A., et al., *Multilaminate resorbable biomedical device under biaxial loading.* J Biomed Mater Res, 1998. **43**(3): p. 277-81.

222. Liu, Y., et al., *New type of tracheal bioartificial organ treated with detergent: maintaining cartilage viability is necessary for successful immunosuppressant free allotransplantation.* Asaio J, 2002. **48**(1): p. 21-5.

223. Chue, W.L., et al., *Dog peritoneal and pleural cavities as bioreactors to grow autologous vascular grafts.* J Vasc Surg, 2004. **39**(4): p. 859-67.

224. Li, J., P. Xu, and H. Chen, *Successful tracheal autotransplantation with two-stage approach using the greater omentum.* Ann Thorac Surg, 1997. **64**(1): p. 199-202.

225. Walles, T., *Bioartificial tracheal grafts: can tissue engineering keep its promise?* Expert Rev Med Devices, 2004. **1**(2): p. 241-50.

226. Walles, T., et al., *Experimental generation of a tissue-engineered functional and vascularized trachea.* J Thorac Cardiovasc Surg, 2004. **128**(6): p. 900-6.

227. Asnaghi, M.A., et al., *A double-chamber rotating bioreactor for the development of tissue-engineered hollow organs: from concept to clinical trial.* Biomaterials, 2009. **30**(29): p. 5260-9.

228. Kaneshiro, N., et al., *Cultured articular chondrocytes sheets for partial thickness cartilage defects utilizing temperature-responsive culture dishes.* Eur Cell Mater, 2007. **13**: p. 87-92.

229. Weidenbecher, M., et al., *Fabrication of a neotrachea using engineered cartilage.* Laryngoscope, 2008. **118**(4): p. 593-8.

230. Weidenbecher, M., et al., *Tissue-engineered trachea for airway reconstruction.* Laryngoscope, 2009. **119**(11): p. 2118-23.

231. Valentin, J.E., et al., *Extracellular matrix bioscaffolds for orthopaedic applications. A comparative histologic study.* J Bone Joint Surg Am, 2006. **88**(12): p. 2673-86.

232. Badylak, S.F., et al., *Macrophage phenotype as a determinant of biologic scaffold remodeling.* Tissue Eng Part A, 2008. **14**(11): p. 1835-1842.